

Appendix G Examples of Probabilistic Seismic Hazard Analysis

Section I

Example 1

Simplified Calculation of Probabilistic Seismic Hazard

G1-1. Introduction

a. This example presents a simplified seismic hazard analysis illustrating the steps involved in computing the frequency of exceedance of a peak ground acceleration of 0.2 g at a site, $v(0.2)$. The frequency of exceedance is computed using the equation

$$v(z) = \sum_N \left[\sum_M \lambda(m_i) \cdot \sum_R P(R = r_j | m_i) \cdot P(Z > z | m_i, r_j) \right]_n \quad (G1-1)$$

The calculation involves the following steps:

- (1) Computing the frequency of occurrence of events of magnitude m_i on source n , ($\lambda(m_i)$).
- (2) Calculating the probability distribution for distances from the site to events of magnitude m_i on source n , ($P(R = r_j | m_i)$).
- (3) For each source-to-site distance, computing the probability that an event of magnitude m_i will exceed the specified ground motion level z , ($P(Z > z | m_i, r_j)$).

The total rate of exceedance is then obtained by summing over all distances for a given event magnitude, and then over all event magnitudes.

The example calculation presented in this section is performed using the input parameters for the two seismic sources defined in Figure G1-1.

G1-2. Computation of Event Rates, $\lambda(m_i)$

a. The first step is the computation of the rate of occurrence of events of magnitude m_i , $\lambda(m_i)$. These are obtained by discretizing the cumulative recurrence relationship at a specified discretization step size, Δm . The cumulative earthquake recurrence relationship is given by the truncated exponential form of the Gutenberg and Richter recurrence law

$$N(M > m) = \alpha(m^0) \cdot \frac{10^{-b(m-m^0)} - 10^{-b(m^u-m^0)}}{1.0 - 10^{-b(m^u-m^0)}} \quad (G1-2)$$

where

m^0 = lower bound magnitude of interest to the calculation

m^u = maximum magnitude event that can occur on the source

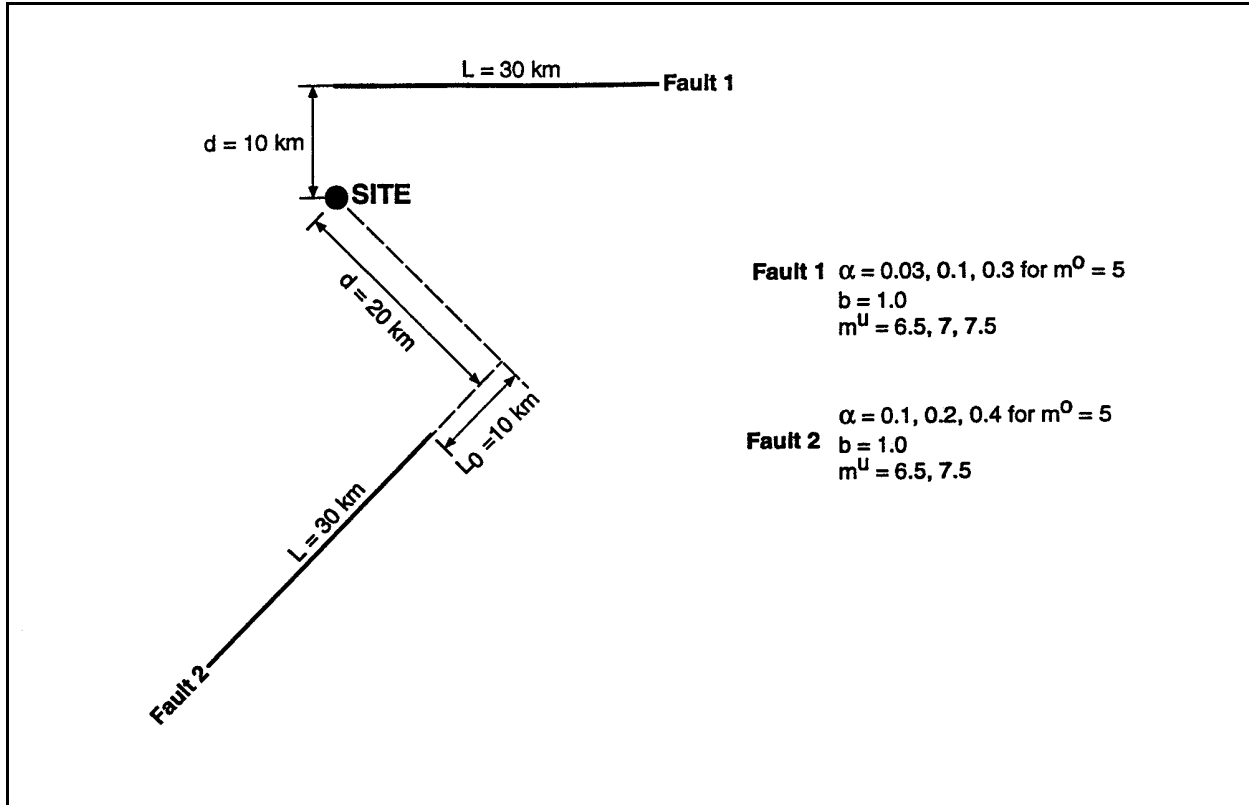


Figure G1-1. Example problem

b = slope or b -value of the recurrence curve

$\alpha(m^0)$ = frequency of occurrence of events of magnitude m^0 and larger

b. The computation of the event rate is given by the expression

$$\lambda(m_i) = N(m > m_i - \Delta m/2) - N(m > m_i + \Delta m/2) \quad (\text{G1-3})$$

Using a discretization step, $\Delta m = 0.5$, gives $\lambda(m_i)$ for Fault 1 using the following parameters (see Figure G1-1):

$$m^0 = 5.0, \alpha(m^0) = 0.1, b = 1.0, m^u = 6.5, 7.0, 7.5.$$

c. The calculation procedure is illustrated in Figure G1-2 for the specific case of computing $\lambda(m = 5.5)$ given $\alpha(m^0) = 0.1$, $b = 1.0$, and $m^u = 6.5$. Using Equation G1-2, the computed cumulative number of events of magnitude greater than $m - \Delta m/2 = 5.25$ is 0.0548 and the cumulative number of events of magnitude greater than $m + \Delta m/2 = 5.75$ is 0.0151. Using Equation G1-3, $\lambda(m = 5.5) = 0.0548 - 0.0151 = 0.0397$. This calculation is repeated for all of the events that are considered for a given maximum magnitude. These calculations are tabulated in Table G1-1 for the three maximum magnitude values.

d. The earthquake recurrence rates for $\alpha(m^0) = 0.03$ and 0.3 are equal to 0.3 and 3.0 times the values in Table G1-1. Similarly, $\lambda(m_i)$ for Fault 2 is obtained using the following parameters (Figure G1-1):

$$m^0 = 5.0, \alpha(m^0) = 0.2, b = 1.0, m^u = 6.5, 7.5 \text{ (Table G1-2).}$$

Table G1-1
Earthquake Recurrence Frequencies for Fault 1

m_i	$m^u = 6.5$			$m^u = 7$			$m^u = 7.5$		
	$N(m > m_i - \Delta m/2)$	$N(m > m_i + \Delta m/2)$	$\lambda(m_i)$	$N(m > m_i - \Delta m/2)$	$N(m > m_i + \Delta m/2)$	$\lambda(m_i)$	$N(m > m_i - \Delta m/2)$	$N(m > m_i + \Delta m/2)$	$\lambda(m_i)$
5	0.10000	0.05480	0.04520	0.10000	0.05579	0.04421	0.10000	0.05610	0.04390
5.5	0.05480	0.01510	0.03971	0.05579	0.01695	0.03884	0.05610	0.01752	0.03857
6	0.01510	0.00254	0.01256	0.01695	0.00467	0.01228	0.01752	0.00532	0.01220
6.5	0.00254	0.00000	0.00254	0.00467	0.00079	0.00388	0.00532	0.00147	0.00386
7				0.00079	0.00000	0.00079	0.00147	0.00025	0.00122
7.5							0.00025	0.00000	0.00025

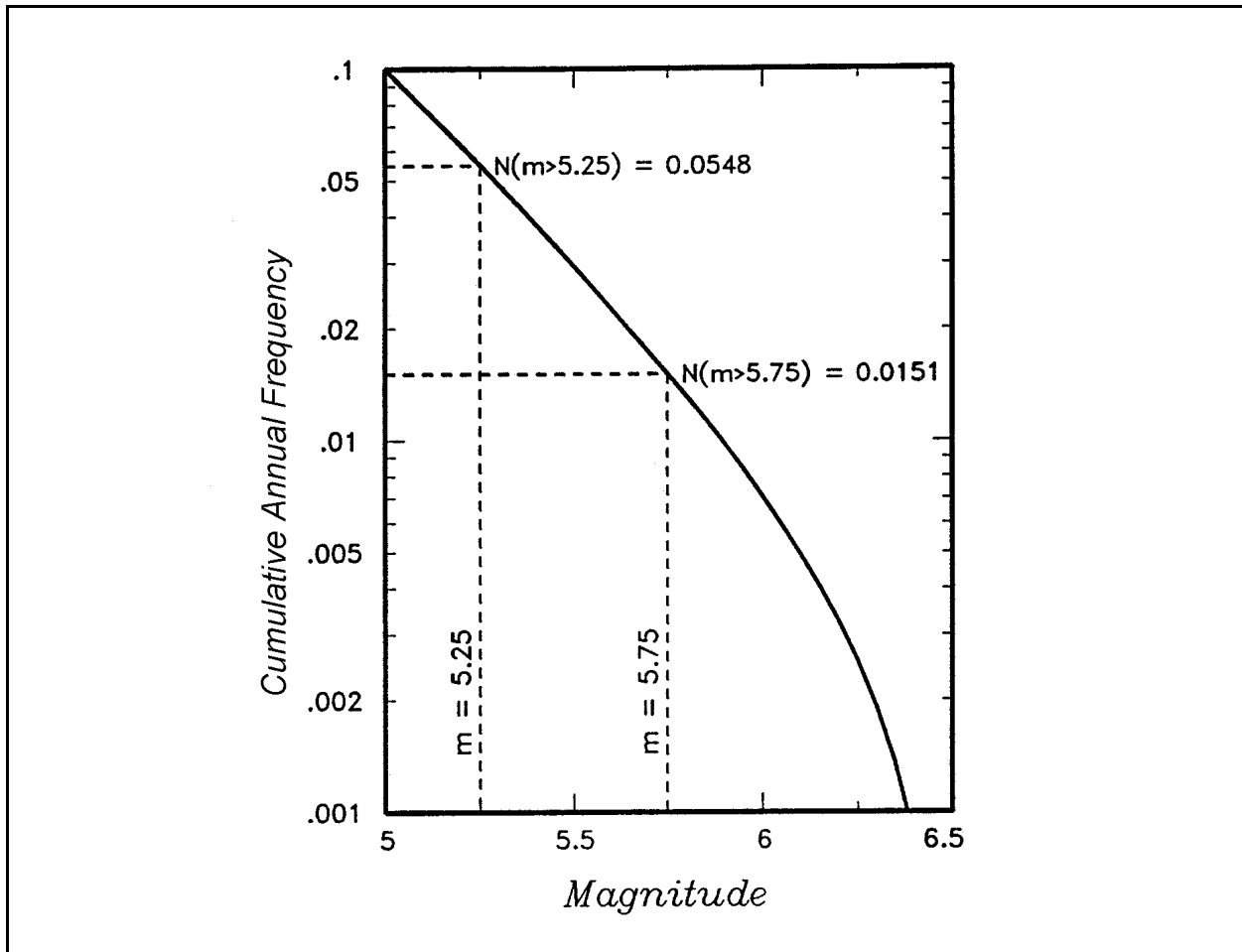


Figure G1-2. Example recurrence rate calculation

Table G1-2
Earthquake Recurrence Frequencies for Fault 2

m_i	$m^u = 6.5$			$m^u = 7.5$		
	$N(m > m_i - \Delta m/2)$	$N(m > m_i + \Delta m/2)$	$\lambda(m_i)$	$N(m > m_i - \Delta m/2)$	$N(m > m_i + \Delta m/2)$	$\lambda(m_i)$
5	0.20000	0.10961	0.09039	0.20000	0.11219	0.08781
5.5	0.10961	0.03020	0.07941	0.11219	0.03504	0.07715
6	0.03020	0.00508	0.02511	0.03504	0.01065	0.02440
6.5	0.00508	0.00000	0.00508	0.01065	0.00293	0.00771
7				0.00293	0.00049	0.00244
7.5				0.00049	0.00000	0.00049

The earthquake occurrence rates for $\alpha(m^0) = 0.1$ and 0.4 are obtained by multiplying the rates in Table G1-2 by 0.5 and 2.0 .

G1-3. Computation of the Conditional Probability Distribution for Source-to-Site Distance

a. The probability distribution for distance from the site to earthquake rupture on the source is computed conditionally on the earthquake magnitude because it is affected by the rupture size of the earthquake rupture.

b. Der Kiureghian and Ang (1977) give the following expression for the cumulative probability distribution to a linear rupture segment uniformly distributed along a linear fault

$$\begin{aligned}
 P(R < r) &= 0 && \text{for } R < (d^2 + L_0^2)^{1/2} \\
 P(R < r) &= \frac{(r^2 - d^2)^{1/2} - L_0}{L - X(m_i)} && \text{for } (d^2 + L_0^2)^{1/2} \leq R < \{d^2 + [L + L_0 - X(m_i)]^2\}^{1/2} \quad (\text{G1-4}) \\
 P(R < r) &= 1 && \text{for } R > \{d^2 + [L + L_0 - X(m_i)]^2\}^{1/2}
 \end{aligned}$$

where $X(m_i)$ = rupture length, km, for magnitude m_i given by the equation $X(m_i) = \text{MIN} [\exp (-4.654 + 1.189m_i), \text{fault length}]$. The MIN function is used to confine the rupture to the fault length. Occasionally, the expected length of rupture, given a magnitude, will exceed the fault length for maximum magnitude estimated by techniques other than rupture length.

c. The conditional distance probability function $P(R = r_j | m_i)$ is obtained by discretizing the cumulative distance probability relationship using a suitable step size.

d. Using a discretization step $\Delta r = 5.0$ km and the fault geometries shown in Figure G1-1, the discrete distance distributions are obtained for the two faults. The calculation procedure is illustrated in Figure G1-3 for the specific case of computing $P(r = 15)$ given $d = 10$ km, $L_0 = 0$, $L = 30$ km, and $X(m = 5) = 3.64$ km for Fault 1. Using Equation G1-4, the cumulative probability that $R < 15 - \Delta r/2 = 12.5$ km is 0.2845 and the cumulative probability that $R < 15 + \Delta r/2 = 17.5$ km is 0.5447 . The difference between these two cumulative probabilities is the probability that $R = 15$ km, and is $0.5447 - 0.2845 = 0.2602$. This calculation is repeated for all of the distances that are possible for the fault. These calculations are tabulated in Table G1-3 for the two faults.

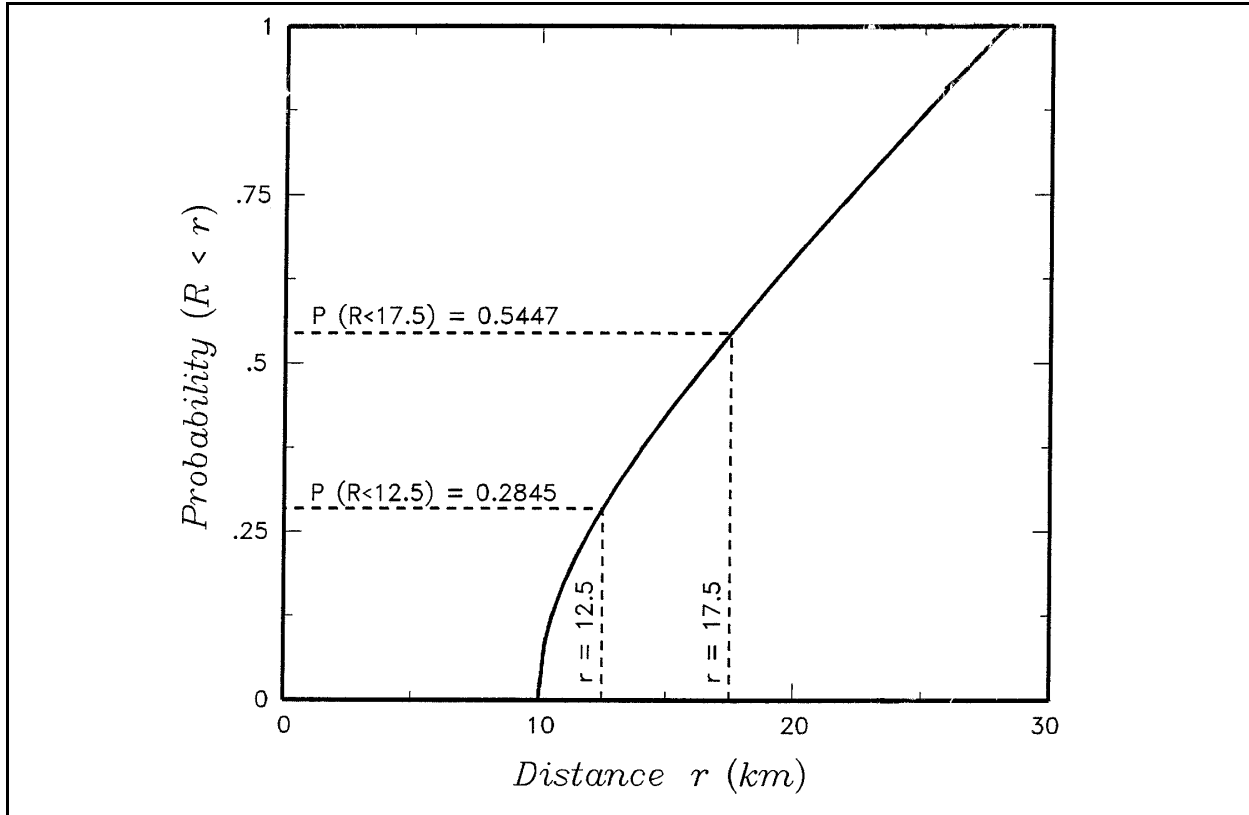


Figure G1-3. Example distance probability calculation

G1-4. Computation of Attenuation Conditional Probability of Exceedance

a. The attenuation conditional probability distribution $P(Z > z | m_i, r_j)$ is computed using a lognormal distribution

$$P(Z > z | m_i, r_j) = 1.0 - F' \left\{ \frac{\ln(z) - E[\ln(Z)]}{S[\ln(Z)]} \right\} \quad (G1-5)$$

where $E[\ln(Z)]$ is the mean log ground motion level given by the attenuation relationship. For this example, the ground motion attenuation relationship for peak acceleration is given by the relationship of Sadigh, Egan, and Youngs (1986):

$$E[\ln(Z)] = -2.611 + 1.1 \cdot m_i - 1.750 \cdot \ln(r_j + 0.8217 \cdot e^{0.4814 \cdot m_i}) \quad \text{for } m \leq 6.5$$

$$E[\ln(Z)] = -2.611 + 1.1 \cdot m_i - 1.75 \cdot \ln(r_j + 0.3157 \cdot e^{0.6286 \cdot m_i}) \quad \text{for } m > 6.5 \quad (G1-6)$$

where r_j is in km and Z is in g, and $S[\ln(Z)]$ is the standard error of the log ground motion level given by the relationship

$$S[\ln(Z)] = 1.26 - 0.14 \cdot m_i \quad \text{for } m \leq 6.5$$

$$S[\ln(Z)] = 0.35 \quad \text{for } m > 6.5 \quad (G1-7)$$

Table G1-3
Discrete Distance Distributions for Faults 1 and 2

m_i	$X(m_i)$	r_j	$P(R < r_j + \Delta r/2 m_i)$	$P(R = r_j m_i)$
For Fault 1: $d = 10$ km, $L_0 = 0$ km, and $L = 30$ km				
5	3.64	5	0.0000	0.0000
		10	0.2845	0.2845
		15	0.5447	0.2603
		20	0.7645	0.2198
		25	0.9717	0.2072
		30	1.0000	0.0283
5.5	6.59	5	0.0000	0.0000
		10	0.3204	0.3204
		15	0.6135	0.2931
		20	0.8610	0.2475
		25	1.0000	0.1390
		30	1.0000	0.0000
6	11.94	5	0.0000	0.0000
		10	0.4153	0.4153
		15	0.7953	0.3799
		20	1.0000	0.2047
		25	1.0000	0.0000
		30	1.0000	0.0000
6.5	21.64	5	0.0000	0.0000
		10	0.8970	0.8970
		15	1.0000	0.1030
		20	1.0000	0.0000
		25	1.0000	0.0000
		30	1.0000	0.0000
7	30.00	5	0.0000	0.0000
		10	1.0000	1.0000
		15	1.0000	0.0000
		20	1.0000	0.0000
		25	1.0000	0.0000
		30	1.0000	0.0000
7.5	30.00	5	0.0000	0.0000
		10	1.0000	1.0000
		15	1.0000	0.0000
		20	1.0000	0.0000
		25	1.0000	0.0000
		30	1.0000	0.0000
For Fault 2: $d = 20$ km, $L_0 = 10$ km, and $L = 30$ km				
5	3.64	15	0.0000	0.0000
		20	0.0117	0.0117
		25	0.3366	0.3249
(Continued)				

Table G1-3 (Concluded)

m_i	$X(m_i)$	r_j	$P(R < r_j + \Delta r/2 m_i)$	$P(R = r_j m_i)$
For Fault 2: $d = 20$ km, $L_o = 10$ km, and $L = 30$ km				
5 (Cont.)	3.64	30	0.5924	0.2558
		35	0.8239	0.2315
		40	1.0000	0.1761
5.5	6.59	15	0.0000	0.0000
		20	0.0131	0.0131
		25	0.3791	0.3659
		30	0.6671	0.2880
		35	0.9279	0.2607
		40	1.0000	0.0721
6	11.94	15	0.0000	0.0000
		20	0.0170	0.0170
		25	0.4914	0.4744
		30	0.8648	0.3734
		35	1.0000	0.1352
		40	1.0000	0.0000
6.5	21.64	15	0.0000	0.0000
		20	0.0368	0.0368
		25	1.0000	0.9632
		30	1.0000	0.0000
		35	1.0000	0.0000
		40	1.0000	0.0000
7	30.00	15	0.0000	0.0000
		20	1.0000	1.0000
		25	1.0000	0.0000
		30	1.0000	0.0000
		35	1.0000	0.0000
		40	1.0000	0.0000
7.5	30.00	15	0.0000	0.0000
		20	1.0000	1.0000
		25	1.0000	0.0000
		30	1.0000	0.0000
		35	1.0000	0.0000
		40	1.0000	0.0000

The distribution is truncated at the 3σ level so that $F'()$ represents the cumulative of a truncated normal distribution

$$F'(U) = \frac{F(U) - F(-3)}{1.0 - 2 \cdot F(-3)} \quad (G1-8)$$

where $F(U)$ is the standard cumulative normal distribution, $U = \{\ln(z) - E[\ln(Z)]\}/S[\ln(Z)]$, and $F(-3)$ is 0.00135. A table of standard normal cumulative probability values is provided in Table G1-4.

Table G1-4
Cumulative Probabilities for Unit Normal Variable

<i>U</i>	<i>F(U)</i>								
-4.00	0.000032	-3.99	0.000033	-3.98	0.000034	-3.97	0.000036	-3.96	0.000037
-3.95	0.000039	-3.94	0.000041	-3.93	0.000042	-3.92	0.000044	-3.91	0.000046
-3.90	0.000048	-3.89	0.000050	-3.88	0.000052	-3.87	0.000054	-3.86	0.000057
-3.85	0.000059	-3.84	0.000062	-3.83	0.000064	-3.82	0.000067	-3.81	0.000069
-3.80	0.000072	-3.79	0.000075	-3.78	0.000078	-3.77	0.000082	-3.76	0.000085
-3.75	0.000088	-3.74	0.000092	-3.73	0.000096	-3.72	0.000100	-3.71	0.000104
-3.70	0.000108	-3.69	0.000112	-3.68	0.000117	-3.67	0.000121	-3.66	0.000126
-3.65	0.000131	-3.64	0.000136	-3.63	0.000142	-3.62	0.000147	-3.61	0.000153
-3.60	0.000159	-3.59	0.000165	-3.58	0.000172	-3.57	0.000178	-3.56	0.000185
-3.55	0.000193	-3.54	0.000200	-3.53	0.000208	-3.52	0.000216	-3.51	0.000224
-3.50	0.000233	-3.49	0.000242	-3.48	0.000251	-3.47	0.000260	-3.46	0.000270
-3.45	0.000280	-3.44	0.000291	-3.43	0.000302	-3.42	0.000313	-3.41	0.000325
-3.40	0.000337	-3.39	0.000349	-3.38	0.000362	-3.37	0.000376	-3.36	0.000390
-3.35	0.000404	-3.34	0.000419	-3.33	0.000434	-3.32	0.000450	-3.31	0.000466
-3.30	0.000483	-3.29	0.000501	-3.28	0.000519	-3.27	0.000538	-3.26	0.000557
-3.25	0.000577	-3.24	0.000598	-3.23	0.000619	-3.22	0.000641	-3.21	0.000664
-3.20	0.000687	-3.19	0.000711	-3.18	0.000736	-3.17	0.000762	-3.16	0.000789
-3.15	0.000816	-3.14	0.000845	-3.13	0.000874	-3.12	0.000904	-3.11	0.000935
-3.10	0.000968	-3.09	0.001001	-3.08	0.001035	-3.07	0.001070	-3.06	0.001107
-3.05	0.001144	-3.04	0.001183	-3.03	0.001223	-3.02	0.001264	-3.01	0.001306
-3.00	0.001350	-2.99	0.001395	-2.98	0.001441	-2.97	0.001489	-2.96	0.001538
-2.95	0.001589	-2.94	0.001641	-2.93	0.001695	-2.92	0.001750	-2.91	0.001807
-2.90	0.001866	-2.89	0.001926	-2.88	0.001988	-2.87	0.002052	-2.86	0.002118
-2.85	0.002186	-2.84	0.002256	-2.83	0.002327	-2.82	0.002401	-2.81	0.002477
-2.80	0.002555	-2.79	0.002635	-2.78	0.002718	-2.77	0.002803	-2.76	0.002890
-2.75	0.002980	-2.74	0.003072	-2.73	0.003167	-2.72	0.003264	-2.71	0.003364
-2.70	0.003467	-2.69	0.003573	-2.68	0.003681	-2.67	0.003793	-2.66	0.003907
-2.65	0.004025	-2.64	0.004145	-2.63	0.004269	-2.62	0.004396	-2.61	0.004527
-2.60	0.004661	-2.59	0.004799	-2.58	0.004940	-2.57	0.005085	-2.56	0.005234
-2.55	0.005386	-2.54	0.005543	-2.53	0.005703	-2.52	0.005868	-2.51	0.006037
-2.50	0.006210	-2.49	0.006387	-2.48	0.006569	-2.47	0.006756	-2.46	0.006947
-2.45	0.007143	-2.44	0.007344	-2.43	0.007549	-2.42	0.007760	-2.41	0.007976
-2.40	0.008198	-2.39	0.008424	-2.38	0.008656	-2.37	0.008894	-2.36	0.009137
-2.35	0.009387	-2.34	0.009642	-2.33	0.009903	-2.32	0.010170	-2.31	0.010444
-2.30	0.010724	-2.29	0.011011	-2.28	0.011304	-2.27	0.011604	-2.26	0.011911
-2.25	0.012224	-2.24	0.012545	-2.23	0.012874	-2.22	0.013209	-2.21	0.013553
-2.20	0.013903	-2.19	0.014262	-2.18	0.014629	-2.17	0.015003	-2.16	0.015386
-2.15	0.015778	-2.14	0.016177	-2.13	0.016586	-2.12	0.017003	-2.11	0.017429
-2.10	0.017864	-2.09	0.018309	-2.08	0.018763	-2.07	0.019226	-2.06	0.019699
-2.05	0.020182	-2.04	0.020675	-2.03	0.021178	-2.02	0.021692	-2.01	0.022216
-2.00	0.022750	-1.99	0.023295	-1.98	0.023852	-1.97	0.024419	-1.96	0.024998

(Sheet 1 of 4)

Table G1-4 (Continued)

<i>U</i>	<i>F(U)</i>								
-1.95	0.025588	-1.94	0.026190	-1.93	0.026803	-1.92	0.027429	-1.91	0.028067
-1.90	0.028717	-1.89	0.029379	-1.88	0.030054	-1.87	0.030742	-1.86	0.031443
-1.85	0.032157	-1.84	0.032884	-1.83	0.033625	-1.82	0.034380	-1.81	0.035148
-1.80	0.035930	-1.79	0.036727	-1.78	0.037538	-1.77	0.038364	-1.76	0.039204
-1.75	0.040059	-1.74	0.040930	-1.73	0.041815	-1.72	0.042716	-1.71	0.043633
-1.70	0.044565	-1.69	0.045514	-1.68	0.046479	-1.67	0.047460	-1.66	0.048457
-1.65	0.049471	-1.64	0.050503	-1.63	0.051551	-1.62	0.052616	-1.61	0.053699
-1.60	0.054799	-1.59	0.055917	-1.58	0.057053	-1.57	0.058208	-1.56	0.059380
-1.55	0.060571	-1.54	0.061780	-1.53	0.063008	-1.52	0.064255	-1.51	0.065522
-1.50	0.066807	-1.49	0.068112	-1.48	0.069437	-1.47	0.070781	-1.46	0.072145
-1.45	0.073529	-1.44	0.074934	-1.43	0.076359	-1.42	0.077804	-1.41	0.079270
-1.40	0.080757	-1.39	0.082264	-1.38	0.083793	-1.37	0.085343	-1.36	0.086915
-1.35	0.088508	-1.34	0.090123	-1.33	0.091759	-1.32	0.093418	-1.31	0.095098
-1.30	0.096800	-1.29	0.098525	-1.28	0.100273	-1.27	0.102042	-1.26	0.103835
-1.25	0.105650	-1.24	0.107488	-1.23	0.109349	-1.22	0.111232	-1.21	0.113139
-1.20	0.115070	-1.19	0.117023	-1.18	0.119000	-1.17	0.121000	-1.16	0.123024
-1.15	0.125072	-1.14	0.127143	-1.13	0.129238	-1.12	0.131357	-1.11	0.133500
-1.10	0.135666	-1.09	0.137857	-1.08	0.140071	-1.07	0.142310	-1.06	0.144572
-1.05	0.146859	-1.04	0.149170	-1.03	0.151505	-1.02	0.153864	-1.01	0.156248
-1.00	0.158655	-0.99	0.161087	-0.98	0.163543	-0.97	0.166023	-0.96	0.168528
-0.95	0.171056	-0.94	0.173609	-0.93	0.176186	-0.92	0.178786	-0.91	0.181411
-0.90	0.184060	-0.89	0.186733	-0.88	0.189430	-0.87	0.192150	-0.86	0.194895
-0.85	0.197663	-0.84	0.200454	-0.83	0.203269	-0.82	0.206108	-0.81	0.208970
-0.80	0.211855	-0.79	0.214764	-0.78	0.217695	-0.77	0.220650	-0.76	0.223627
-0.75	0.226627	-0.74	0.229650	-0.73	0.232695	-0.72	0.235762	-0.71	0.238852
-0.70	0.241964	-0.69	0.245097	-0.68	0.248252	-0.67	0.251429	-0.66	0.254627
-0.65	0.257846	-0.64	0.261086	-0.63	0.264347	-0.62	0.267629	-0.61	0.270931
-0.60	0.274253	-0.59	0.277595	-0.58	0.280957	-0.57	0.284339	-0.56	0.287740
-0.55	0.291160	-0.54	0.294599	-0.53	0.298056	-0.52	0.301532	-0.51	0.305026
-0.50	0.308538	-0.49	0.312067	-0.48	0.315614	-0.47	0.319178	-0.46	0.322758
-0.45	0.326355	-0.44	0.329969	-0.43	0.333598	-0.42	0.337243	-0.41	0.340903
-0.40	0.344578	-0.39	0.348268	-0.38	0.351973	-0.37	0.355691	-0.36	0.359424
-0.35	0.363169	-0.34	0.366928	-0.33	0.370700	-0.32	0.374484	-0.31	0.378280
-0.30	0.382089	-0.29	0.385908	-0.28	0.389739	-0.27	0.393580	-0.26	0.397432
-0.25	0.401294	-0.24	0.405165	-0.23	0.409046	-0.22	0.412936	-0.21	0.416834
-0.20	0.420740	-0.19	0.424655	-0.18	0.428576	-0.17	0.432505	-0.16	0.436441
-0.15	0.440382	-0.14	0.444330	-0.13	0.448283	-0.12	0.452242	-0.11	0.456205
-0.10	0.460172	-0.09	0.464144	-0.08	0.468119	-0.07	0.472097	-0.06	0.476078
-0.05	0.480061	-0.04	0.484047	-0.03	0.488034	-0.02	0.492022	-0.01	0.496011
0.00	0.500000	0.01	0.503989	0.02	0.507978	0.03	0.511966	0.04	0.515953
0.05	0.519939	0.06	0.523922	0.07	0.527903	0.08	0.531881	0.09	0.535856

(Sheet 2 of 4)

EM 1110-2-6050
30 Jun 99

Table G1-4 (Continued)

<i>U</i>	<i>F(U)</i>								
0.10	0.539828	0.11	0.543795	0.12	0.547758	0.13	0.551717	0.14	0.555670
0.15	0.559618	0.16	0.563559	0.17	0.567495	0.18	0.571424	0.19	0.575345
0.20	0.579260	0.21	0.583166	0.22	0.587064	0.23	0.590954	0.24	0.594835
0.25	0.598706	0.26	0.602568	0.27	0.606420	0.28	0.610261	0.29	0.614092
0.30	0.617911	0.31	0.621720	0.32	0.625516	0.33	0.629300	0.34	0.633072
0.35	0.636831	0.36	0.640576	0.37	0.644309	0.38	0.648027	0.39	0.651732
0.40	0.655422	0.41	0.659097	0.42	0.662757	0.43	0.666402	0.44	0.670031
0.45	0.673645	0.46	0.677242	0.47	0.680822	0.48	0.684386	0.49	0.687933
0.50	0.691462	0.51	0.694974	0.52	0.698468	0.53	0.701944	0.54	0.705401
0.55	0.708840	0.56	0.712260	0.57	0.715661	0.58	0.719043	0.59	0.722405
0.60	0.725747	0.61	0.729069	0.62	0.732371	0.63	0.735653	0.64	0.738914
0.65	0.742154	0.66	0.745373	0.67	0.748571	0.68	0.751748	0.69	0.754903
0.70	0.758036	0.71	0.761148	0.72	0.764238	0.73	0.767305	0.74	0.770350
0.75	0.773373	0.76	0.776373	0.77	0.779350	0.78	0.782305	0.79	0.785236
0.80	0.788145	0.81	0.791030	0.82	0.793892	0.83	0.796731	0.84	0.799546
0.85	0.802337	0.86	0.805106	0.87	0.807850	0.88	0.810570	0.89	0.813267
0.90	0.815940	0.91	0.818589	0.92	0.821214	0.93	0.823814	0.94	0.826391
0.95	0.828944	0.96	0.831472	0.97	0.833977	0.98	0.836457	0.99	0.838913
1.00	0.841345	1.01	0.843752	1.02	0.846136	1.03	0.848495	1.04	0.850830
1.05	0.853141	1.06	0.855428	1.07	0.857690	1.08	0.859929	1.09	0.862143
1.10	0.864334	1.11	0.866500	1.12	0.868643	1.13	0.870762	1.14	0.872857
1.15	0.874928	1.16	0.876976	1.17	0.879000	1.18	0.881000	1.19	0.882977
1.20	0.884930	1.21	0.886861	1.22	0.888768	1.23	0.890651	1.24	0.892512
1.25	0.894350	1.26	0.896165	1.27	0.897958	1.28	0.899727	1.29	0.901475
1.30	0.903199	1.31	0.904902	1.32	0.906582	1.33	0.908241	1.34	0.909877
1.35	0.911492	1.36	0.913085	1.37	0.914657	1.38	0.916207	1.39	0.917736
1.40	0.919243	1.41	0.920730	1.42	0.922196	1.43	0.923642	1.44	0.925066
1.45	0.926471	1.46	0.927855	1.47	0.929219	1.48	0.930563	1.49	0.931888
1.50	0.933193	1.51	0.934478	1.52	0.935745	1.53	0.936992	1.54	0.938220
1.55	0.939429	1.56	0.940620	1.57	0.941792	1.58	0.942947	1.59	0.944083
1.60	0.945201	1.61	0.946301	1.62	0.947384	1.63	0.948449	1.64	0.949497
1.65	0.950529	1.66	0.951543	1.67	0.952540	1.68	0.953521	1.69	0.954486
1.70	0.955435	1.71	0.956367	1.72	0.957284	1.73	0.958185	1.74	0.959071
1.75	0.959941	1.76	0.960796	1.77	0.961636	1.78	0.962462	1.79	0.963273
1.80	0.964070	1.81	0.964852	1.82	0.965621	1.83	0.966375	1.84	0.967116
1.85	0.967843	1.86	0.968557	1.87	0.969258	1.88	0.969946	1.89	0.970621
1.90	0.971283	1.91	0.971933	1.92	0.972571	1.93	0.973197	1.94	0.973810
1.95	0.974412	1.96	0.975002	1.97	0.975581	1.98	0.976148	1.99	0.976705
2.00	0.977250	2.01	0.977784	2.02	0.978308	2.03	0.978822	2.04	0.979325
2.05	0.979818	2.06	0.980301	2.07	0.980774	2.08	0.981237	2.09	0.981691
2.10	0.982136	2.11	0.982571	2.12	0.982997	2.13	0.983414	2.14	0.983823
2.15	0.984222	2.16	0.984614	2.17	0.984997	2.18	0.985371	2.19	0.985738

(Sheet 3 of 4)

Table G1-4 (Concluded)

<i>U</i>	<i>F(U)</i>								
2.20	0.986097	2.21	0.986447	2.22	0.986791	2.23	0.987126	2.24	0.987455
2.25	0.987776	2.26	0.988089	2.27	0.988396	2.28	0.988696	2.29	0.988989
2.30	0.989276	2.31	0.989556	2.32	0.989830	2.33	0.990097	2.34	0.990358
2.35	0.990613	2.36	0.990863	2.37	0.991106	2.38	0.991344	2.39	0.991576
2.40	0.991802	2.41	0.992024	2.42	0.992240	2.43	0.992451	2.44	0.992656
2.45	0.992857	2.46	0.993053	2.47	0.993244	2.48	0.993431	2.49	0.993613
2.50	0.993790	2.51	0.993963	2.52	0.994132	2.53	0.994297	2.54	0.994457
2.55	0.994614	2.56	0.994766	2.57	0.994915	2.58	0.995060	2.59	0.995201
2.60	0.995339	2.61	0.995473	2.62	0.995604	2.63	0.995731	2.64	0.995855
2.65	0.995975	2.66	0.996093	2.67	0.996207	2.68	0.996319	2.69	0.996427
2.70	0.996533	2.71	0.996636	2.72	0.996736	2.73	0.996833	2.74	0.996928
2.75	0.997020	2.76	0.997110	2.77	0.997197	2.78	0.997282	2.79	0.997365
2.80	0.997445	2.81	0.997523	2.82	0.997599	2.83	0.997673	2.84	0.997744
2.85	0.997814	2.86	0.997882	2.87	0.997948	2.88	0.998012	2.89	0.998074
2.90	0.998134	2.91	0.998193	2.92	0.998250	2.93	0.998305	2.94	0.998359
2.95	0.998411	2.96	0.998462	2.97	0.998511	2.98	0.998559	2.99	0.998605
3.00	0.998650	3.01	0.998694	3.02	0.998736	3.03	0.998777	3.04	0.998817
3.05	0.998856	3.06	0.998893	3.07	0.998930	3.08	0.998965	3.09	0.998999
3.10	0.999032	3.11	0.999065	3.12	0.999096	3.13	0.999126	3.14	0.999155
3.15	0.999184	3.16	0.999211	3.17	0.999238	3.18	0.999264	3.19	0.999289
3.20	0.999313	3.21	0.999336	3.22	0.999359	3.23	0.999381	3.24	0.999402
3.25	0.999423	3.26	0.999443	3.27	0.999462	3.28	0.999481	3.29	0.999499
3.30	0.999517	3.31	0.999534	3.32	0.999550	3.33	0.999566	3.34	0.999581
3.35	0.999596	3.36	0.999610	3.37	0.999624	3.38	0.999638	3.39	0.999651
3.40	0.999663	3.41	0.999675	3.42	0.999687	3.43	0.999698	3.44	0.999709
3.45	0.999720	3.46	0.999730	3.47	0.999740	3.48	0.999749	3.49	0.999758
3.50	0.999767	3.51	0.999776	3.52	0.999784	3.53	0.999792	3.54	0.999800
3.55	0.999807	3.56	0.999815	3.57	0.999821	3.58	0.999828	3.59	0.999835
3.60	0.999841	3.61	0.999847	3.62	0.999853	3.63	0.999858	3.64	0.999864
3.65	0.999869	3.66	0.999874	3.67	0.999879	3.68	0.999883	3.69	0.999888
3.70	0.999892	3.71	0.999896	3.72	0.999900	3.73	0.999904	3.74	0.999908
3.75	0.999912	3.76	0.999915	3.77	0.999918	3.78	0.999922	3.79	0.999925
3.80	0.999928	3.81	0.999931	3.82	0.999933	3.83	0.999936	3.84	0.999938
3.85	0.999941	3.86	0.999943	3.87	0.999946	3.88	0.999948	3.89	0.999950
3.90	0.999952	3.91	0.999954	3.92	0.999956	3.93	0.999958	3.94	0.999959
3.95	0.999961	3.96	0.999963	3.97	0.999964	3.98	0.999966	3.99	0.999967
4.00	0.999968								

(Sheet 4 of 4)

b. For ground motion level $z = 0.2$ g, $\ln(z) = -1.6094$. Considering a magnitude 5 earthquake occurring at a distance of 10 km from the site, the median ground motions that this event will produce, from Equation G1-6, is 0.103 g, and the standard error of $\ln(z)$, from Equation G1-7, is 0.56. The probability that this event will produce a peak acceleration in excess of 0.2 g is computed using

Equation G1-8. The normalized deviate, U , is computed by $[\ln(0.2) - \ln(0.103)]/0.56 = 1.188$. The probability that ground motions produced by this event will be less than or equal to 0.2 g, assuming a truncated lognormal distribution, is $F'(1.188) = [F(1.188) - F(-3)]/[1 - 2F(-3)] = [0.88258 - 0.00135]/[1 - 0.0027] = 0.88369$. Therefore, the probability of exceeding 0.2 g is $1 - 0.88369 = 0.11631$. The computed values of $P(Z > z | m_i, r_j)$ are tabulated in Table G1-5 for the range of magnitudes and distances considered.

m_i	r_j	$E[\ln(Z)]$	$S[\ln(Z)]$	U	$P(Z > z m_i, r_j)$
5	10	-2.275	0.56	1.188	0.11631
	15	-2.681	0.56	1.914	0.02652
	20	-3.011	0.56	2.503	0.00482
	25	-3.288	0.56	2.998	0.000001
	30	-3.528	0.56	3.425	0
5.5	10	-1.939	0.49	0.672	0.25025
	15	-2.303	0.49	1.415	0.07738
	20	-2.604	0.49	2.03	0.01987
	25	-2.861	0.49	2.555	0.00397
	30	-3.085	0.49	3.012	0
6	10	-1.627	0.42	0.042	0.48304
	15	-1.949	0.42	0.809	0.20853
	20	-2.221	0.42	1.456	0.07156
	25	-2.456	0.42	2.016	0.02062
	30	-2.663	0.42	2.509	0.00471
6.5	10	-1.341	0.35	-0.768	0.77954
	15	-1.621	0.35	0.033	0.48689
	20	-1.862	0.35	0.723	0.23415
	25	-2.075	0.35	1.329	0.09078
	30	-2.264	0.35	1.87	0.02948
7	10	-1.168	0.35	-1.26	0.89723
	15	-1.398	0.35	-0.605	0.72799
	20	-1.6	0.35	-0.026	0.51032
	25	-1.782	0.35	0.493	0.31045
	30	-1.947	0.35	0.963	0.16682
7.5	10	-1.031	0.35	-1.652	0.95200
	15	-1.215	0.35	-1.128	0.87135
	20	-1.381	0.35	-0.653	0.74392
	25	-1.532	0.35	-0.22	0.58731
	30	-1.672	0.35	0.179	0.42886

G1-5. Computation of Frequency of Exceedance

a. Computation of $\nu(0.2)$ from Equation G1-1 is performed by multiplying the values of $\lambda(m_i)$ by the probability of a specific distance, $P(R = r_j | m_i)$, and the conditional probability of ground motion exceedance for the specified magnitude and distance, $P(Z > z | m_i, r_j)$, then summing over all distances and magnitudes. For example, the frequency of magnitude 5 events on Fault 1, $\lambda(m = 5)$, is given in

Table G1-1 (for $m^u = 6.5$) as 0.04520. From Table G1-3, the probability that a magnitude 5 earthquake on Fault 1 will occur at 10 km from the site is 0.2845. From Table G1-5, the probability that a magnitude 5 earthquake at a distance of 10 km will produce a peak acceleration in excess of 0.2 g is 0.11631. Thus the frequency of those magnitude 5 earthquakes occurring on Fault 1 at 10 km from the site that contribute to the hazard of exceeding 0.2 g is $\nu(0.2) = 0.04520 \times 0.2845 \times 0.11631 = 0.00150$. Table G1-6 summarizes the calculations for $\nu(0.2)$ for the two faults for one earthquake recurrence rate.

b. In the same manner that the event rates for $\alpha(m^0) = 0.03$ and 0.3 for Fault 1 were simple multiples of the event rates for $\alpha(m^0) = 0.1$, the values of $\nu(0.2)$ for Fault 1 for $\alpha(m^0) = 0.03$ and 0.3 are obtained by multiplying the values of $\nu(0.2)$ for $\alpha(m^0) = 0.1$ listed in Table G1-6 by 0.3 and 3, respectively. The values of $\nu(0.2)$ for Fault 2 for $\alpha(m^0) = 0.1$ and 0.4 are obtained by multiplying the values of $\nu(0.2)$ for $\alpha(m^0) = 0.2$ listed in Table G1-6 by 0.5 and 2, respectively.

G1-6. Logic Tree Analysis

a. The example problem in Figure G1-1 contains alternative values for the frequency of earthquake occurrence on each of the faults $\alpha(m^0)$ and maximum magnitude m^u . These alternative values are represented in logic trees shown in Figure G1-4. The probabilities assigned to each of the branches on the logic trees represent subjective assessments of the relative credibility of each of the parameters. The logic trees shown in the figure are abbreviated, in that they do not show all of the branches possible, but only those branches corresponding to the computations listed in Table G1-6. Table G1-7 lists the exceedance frequencies for all of the branches of the logic trees. Note the maximum magnitude distributions shown on the logic trees are repeated for each value of activity rate $\alpha(m^0)$.

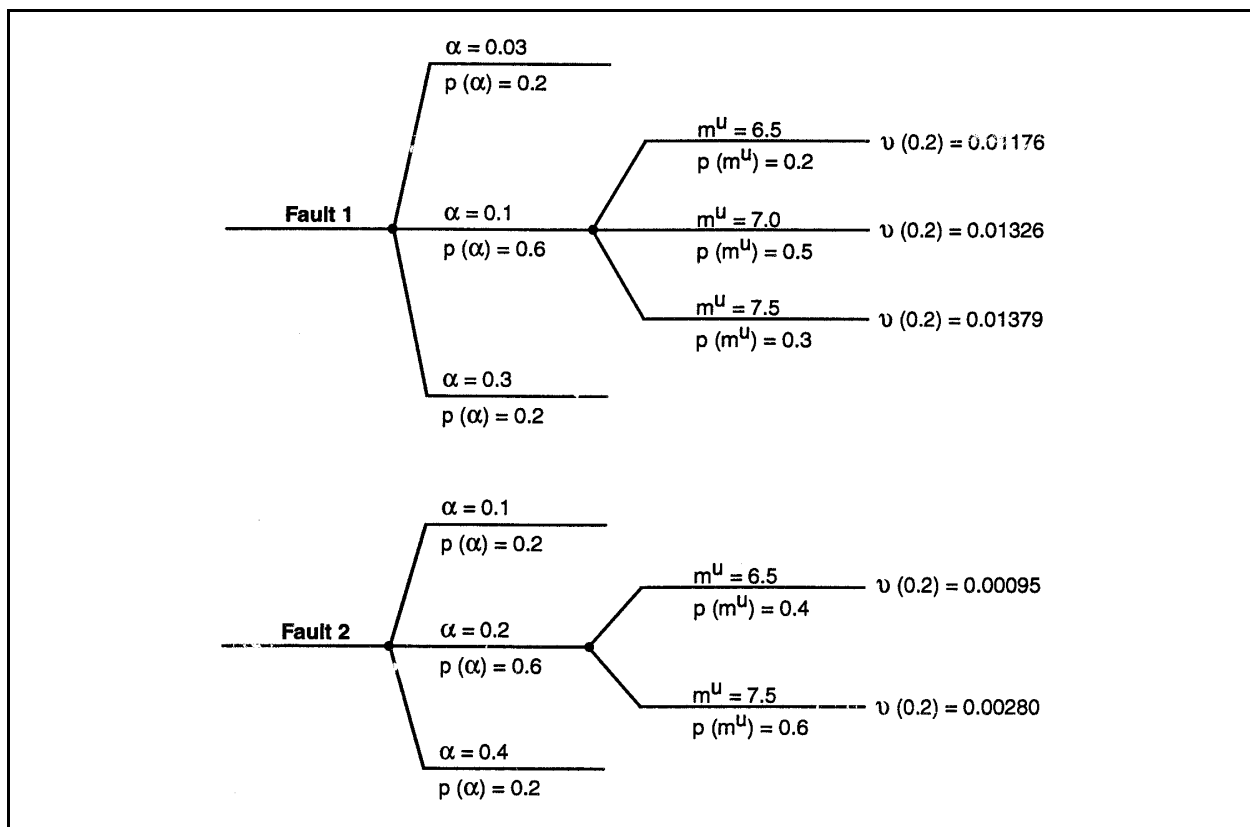


Figure G1-4. Logic trees

Table G1-6
Computation of Frequency of Exceeding 0.2 g, $\nu(0.2)$

m_i	$\lambda(m_i)$	$m^u = 6.5$				$m^u = 7$					$m^u = 7.5$				
		r_i	$P(r_i)$	$P(Z > 0.2)$	$\nu(0.2)$	$\lambda(m_i)$	r_i	$P(r_i)$	$P(Z > 0.2)$	$\nu(0.2)$	$\lambda(m_i)$	r_i	$P(r_i)$	$P(Z > 0.2)$	$\nu(0.2)$
For Fault 1 and $\alpha(m^u) = 0.1$															
5	0.04520	10	0.2845	0.11631	0.00150	0.04421	10	0.2845	0.11631	0.00146	0.04391	10	0.2845	0.11631	0.00145
		15	0.2603	0.02652	0.00031		15	0.2603	0.02652	0.00031		15	0.2603	0.02652	0.00030
		20	0.2198	0.00482	0.00005		20	0.2198	0.00482	0.00005		20	0.2198	0.00482	0.00005
		25	0.2072	0.00001	0.00000		25	0.2072	0.00001	0.00000		25	0.2072	0.00001	0.00000
		30	0.0283	0	0.00000		30	0.0283	0	0.00000		30	0.0283	0	0.00000
5.5	0.03971	10	0.3204	0.25025	0.00318	0.03884	10	0.3204	0.25025	0.00311	0.03857	10	0.3204	0.25025	0.00309
		15	0.2931	0.07738	0.00090		15	0.2931	0.07738	0.00088		15	0.2931	0.07738	0.00087
		20	0.2475	0.01987	0.00020		20	0.2475	0.01987	0.00019		20	0.2475	0.01987	0.00019
		25	0.1390	0.00397	0.00002		25	0.1390	0.00397	0.00002		25	0.1390	0.00397	0.00002
		30	0.0000	0	0.00000		30	0.0000	0	0.00000		30	0.0000	0	0.00000
6	0.01256	10	0.4153	0.48304	0.00252	0.01228	10	0.4153	0.48304	0.00246	0.01220	10	0.4153	0.48304	0.00245
		15	0.3799	0.20853	0.00099		15	0.3799	0.20853	0.00097		15	0.3799	0.20853	0.00097
		20	0.2047	0.07156	0.00018		20	0.2047	0.07156	0.00018		20	0.2047	0.07156	0.00018
		25	0.0000	0.02062	0.00000		25	0.0000	0.02062	0.00000		25	0.0000	0.02062	0.00000
6.5	0.00254	10	0.8970	0.77954	0.00178	0.00388	10	0.8970	0.77954	0.00272	0.00386	10	0.8970	0.77954	0.00270
		15	0.1030	0.48689	0.00013		15	0.1030	0.48689	0.00019		15	0.1030	0.48689	0.00019
		20	0.0000	0.23415	0.00000		20	0.0000	0.23415	0.00000		20	0.0000	0.23415	0.00000
7						0.000786	10	1.0000	0.89723	0.00071	0.00122	10	1.0000	0.89723	0.00109
							15	0.0000	0.72799	0.00000		15	0.0000	0.72799	0.00000
7.5											0.00025	10	1.0000	0.95200	0.00024
												15	0.0000	0.87135	0.00000
					$\Sigma = 0.01176$					$\Sigma = 0.01326$					$\Sigma = 0.01379$
For Fault 2 and $\alpha(m^u) = 0.2$															
5	0.09039	20	0.0117	0.00482	0.00001	--	--	--	--	--	0.08781	20	0.0117	0.00482	0.00000
		25	0.3249	0.00001	0.00000	--	--	--	--	--		25	0.3249	0.00001	0.00000
		30	0.2558	0	0.00000	--	--	--	--	--		30	0.2558	0	0.00000
		35	0.2315	0	0.00000	--	--	--	--	--		35	0.2315	0	0.00000
		40	0.1761	0	0.00000	--	--	--	--	--		40	0.1761	0	0.00000
5.5	0.07941	20	0.0131	0.01987	0.00002	--	--	--	--	--	0.07715	20	0.0131	0.01987	0.00002
		25	0.3659	0.00397	0.00012	--	--	--	--	--		25	0.3659	0.00397	0.00011
		30	0.2880	0	0.00000	--	--	--	--	--		30	0.2880	0	0.00000
		35	0.2607	0	0.00000	--	--	--	--	--		35	0.2607	0	0.00000
		40	0.0721	0	0.00000	--	--	--	--	--		40	0.0721	0	0.00000
6	0.02511	20	0.0170	0.07156	0.00003	--	--	--	--	--	0.02440	20	0.0170	0.07156	0.00003
		25	0.4744	0.02062	0.00025	--	--	--	--	--		25	0.4744	0.02062	0.00024
		30	0.3734	0.00471	0.00004	--	--	--	--	--		30	0.3734	0.00471	0.00004
		35	0.1352	0.00024	0.00000	--	--	--	--	--		35	0.1352	0.00024	0.00000
		40	0.0000	0	0.00000	--	--	--	--	--		40	0.0000	0	0.00000
6.5	0.00508	20	0.0368	0.23415	0.00004	--	--	--	--	--	0.00772	20	0.0368	0.23415	0.00007
		25	0.9632	0.09078	0.00044	--	--	--	--	--		25	0.9632	0.09078	0.00067
		30	0.0000	0.02948	0.00000	--	--	--	--	--		30	0.0000	0.02948	0.00000
7						--	--	--	--	--	0.00244	20	1.0000	0.51032	0.00124
						--	--	--	--	--		25	0.0000	0.31045	0.00000
7.5						--	--	--	--	--	0.00050	20	1.0000	0.74392	0.00037
						--	--	--	--	--		25	0.0000	0.58731	0.00000
					$\Sigma = 0.000951$										$\Sigma = 0.002803$

Table G1-7
Frequencies of Exceeding 0.2 g, $v(0.2)$, for Faults 1 and 2 Computed for Parameters Shown in Figure G1-4.

$\alpha(m^a)$	$P(\alpha)$	m^u	$P(m^u)$	$v(0.2)$	$P(v)$
Fault 1					
0.03	0.2	6.5	0.2	0.00353	0.04
0.03	0.2	7.0	0.5	0.00398	0.10
0.03	0.2	7.5	0.3	0.00414	0.06
0.10	0.6	6.5	0.2	0.01176	0.12
0.10	0.6	7.0	0.5	0.01326	0.30
0.10	0.6	7.5	0.3	0.01379	0.18
0.30	0.2	6.5	0.2	0.03528	0.04
0.30	0.2	7.0	0.5	0.03978	0.10
0.30	0.2	7.5	0.3	0.04138	0.06
					$\Sigma P(v) = 1.00$
Fault 2					
0.1	0.2	6.5	0.4	0.00048	0.08
0.1	0.2	7.5	0.6	0.00140	0.12
0.2	0.6	6.5	0.4	0.00095	0.24
0.2	0.6	7.5	0.6	0.00280	0.36
0.4	0.2	6.5	0.4	0.00190	0.08
0.4	0.2	7.5	0.6	0.00560	0.12
					$\Sigma P(v) = 1.00$

b. The mean exceedance frequency for Fault 1 is computed as follows:

$$E[v(0.2)]_{Fault 1} = \sum_k P[v(0.2)_k] \cdot v_k(0.2) = 0.0165 \quad (G1-9)$$

c. The mean exceedance frequency for Fault 2 is

$$E[v(0.2)]_{Fault 2} = \sum_k P[v(0.2)_k] \cdot v_k(0.2) = 0.0023 \quad (G1-10)$$

d. The total hazard is found by summing the contributions from the two faults:

$$E[v(0.2)] = \sum_n E[v(0.2)]_n = 0.0188 \quad (G1-11)$$

The distribution in the computed hazard is found by computing the sum of all possible combinations of the end branches of the two logic trees. That is

$$v(0.2)_{ij} = v(0.2)_i + v(0.2)_j \quad (G1-12)$$

$$P[v(0.2)_{ij}] = P[v(0.2)_i] \cdot P[v(0.2)_j] \quad (G1-13)$$

where $v(0.2)_i$ refers to hazard from Fault 1 and $v(0.2)_j$ refers to hazard from Fault 2.

e. Computing the 54 combinations of possible hazard values and ordering the result in increasing exceedance frequency gives the discrete distribution for the exceedance frequency from the two faults listed in Table G1-8. Various percentiles of the distribution are listed in the right column. The resulting distribution is plotted in Figure G1-5.

Table G1-8
Distribution for Exceedance Frequency

$\nu(0.2)$	$P[\nu(0.2)]$	$\Sigma P[\nu(0.2)]$	
0.00401	0.00320	0.00320	
0.00446	0.00800	0.01120	
0.00448	0.00960	0.02080	
0.00462	0.00480	0.02560	
0.00493	0.02400	0.04960	
0.00493	0.00480	0.05440	5 th percentile
0.00509	0.01440	0.06880	
0.00538	0.01200	0.08080	
0.00543	0.00320	0.08400	
0.00554	0.00720	0.09120	
0.00588	0.00800	0.09920	
0.00604	0.00480	0.10400	
0.00633	0.01440	0.11840	
0.00678	0.03600	0.15440	15 th percentile
0.00694	0.02160	0.17600	
0.00913	0.00480	0.18080	
0.00958	0.01200	0.19280	
0.00974	0.00720	0.20000	
0.01224	0.00960	0.20960	
0.01271	0.02880	0.23840	
0.01316	0.01440	0.25280	
0.01366	0.00960	0.26240	
0.01374	0.02400	0.28640	
0.01421	0.07200	0.35840	
0.01427	0.01440	0.37280	
0.01456	0.04320	0.41600	
0.01466	0.03600	0.45200	
0.01474	0.04320	0.49520	
0.01516	0.02400	0.51920	50 th percentile
0.01519	0.02160	0.54080	
0.01569	0.01440	0.55520	
0.01606	0.10800	0.66320	
0.01659	0.06480	0.72800	
0.01736	0.01440	0.74240	
0.01886	0.03600	0.77840	

(Continued)

Table G1-8 (Concluded)

$\nu(0.2)$	$P[\nu(0.2)]$	$\Sigma P[\nu(0.2)]$	
0.01939	0.02160	0.80000	
0.03576	0.00320	0.80320	
0.03623	0.00960	0.81280	
0.03668	0.00480	0.81760	
0.03718	0.00320	0.82080	
0.03808	0.01440	0.83520	
0.04026	0.00800	0.84320	
0.04073	0.02400	0.86720	85 th percentile
0.04088	0.00480	0.87200	
0.04118	0.01200	0.88400	
0.04168	0.00800	0.89200	
0.04186	0.00480	0.89680	
0.04233	0.01440	0.91120	
0.04258	0.03600	0.94720	
0.04278	0.00720	0.95440	95 th percentile
0.04328	0.00480	0.95920	
0.04418	0.02160	0.98080	
0.04538	0.01200	0.99280	
0.04698	0.00720	1.00000	

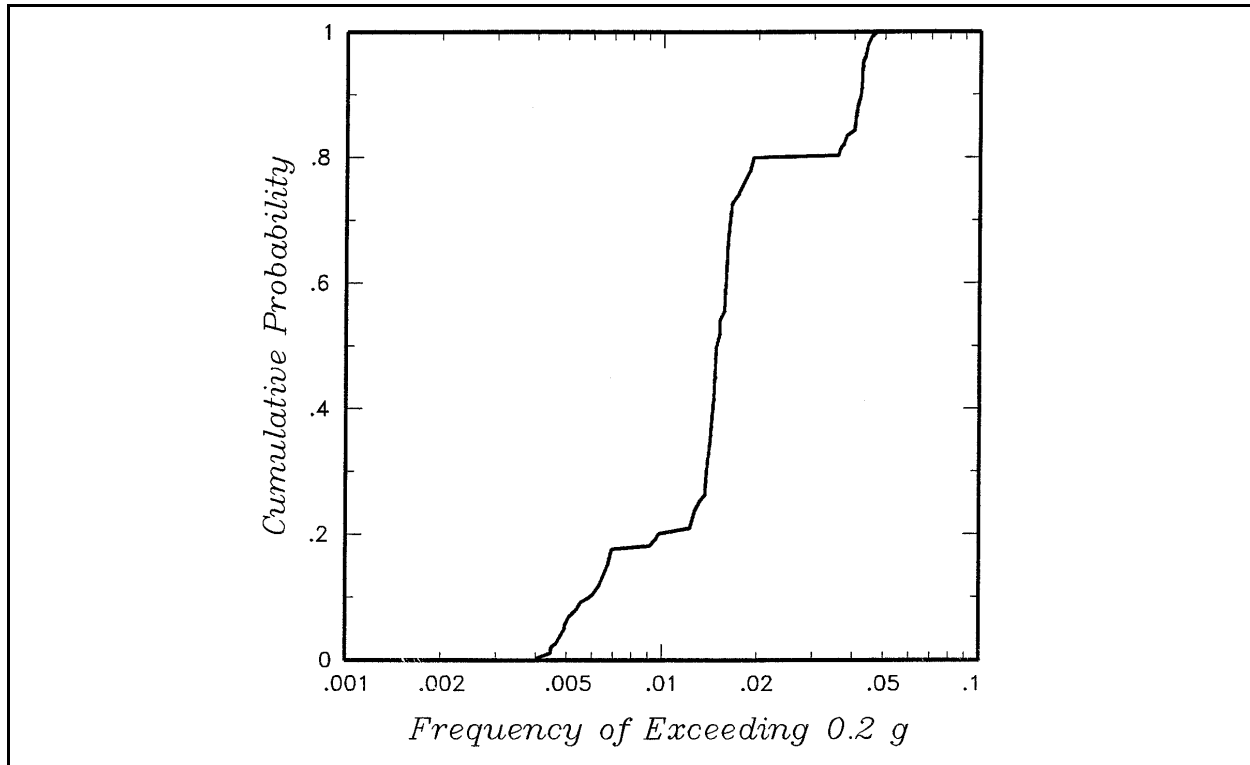


Figure G1-5. Exceedance frequency probability distribution

Section II
Example 2

Probabilistic Seismic Hazard Analysis for Rock Site in San Francisco Bay Area

G2-1. Introduction

The site location is shown in Figure G2-1 relative to the locations of active faults in the San Francisco Bay area. For this site, equal hazard response spectra of rock motions were developed and compared with deterministic response spectra for maximum credible earthquakes.

G2-2. Seismic Source Characterization

The site is located approximately 21 km east of the San Andreas fault and 7 km west of the Hayward fault, as shown in Figure G2-1. The seismic sources, including discrete faults and area sources, are shown in Figure G2-2. The corridors shown around the faults are for analyzing the seismicity that is likely associated with the faults. For each fault, cumulative earthquake recurrence based on seismicity was plotted and compared with earthquake recurrence based on geologic slip rate data for the fault. For the slip-rate-based recurrence assessments, two magnitude distribution models were initially used: exponential model and characteristic model. Comparisons of recurrence estimated for each model with seismicity were made. Examples of these comparisons for the San Andreas fault and Hayward fault are shown in Figures G2-3 and G2-4, respectively. These comparisons and comparisons for other faults indicate that the characteristic magnitude distribution used in conjunction with fault slip rate data provided recurrence characterizations in good agreement with seismicity data. On the other hand, the exponential magnitude distribution used with fault slip rate data resulted in recurrence rates that exceeded the rates from seismicity data. From these comparisons and comparisons for the other faults, it was concluded that the fault-specific recurrence was appropriately modeled using the characteristic magnitude distribution model. This model was used for all the fault-specific sources. Recurrence on the area sources was modeled using both the exponential magnitude distribution and seismicity data and both the exponential and characteristic magnitude distributions and tectonic data on plate convergence rates in the San Francisco Bay area. For the entire central bay area, a comparison was made between the recurrence predicted by the adopted recurrence models and the observed seismicity. This comparison is shown in Figure G2-5. The faults contribute much more to the regional recurrence than do the area sources. Because the fault recurrence is modeled using geologic slip-rate data, the comparison in Figure G2-5 indicates good agreement between seismicity and geologic data in defining the regional rate of earthquake activity. Figure G2-6 illustrates the generic logic tree for seismic source characterization used for the probabilistic seismic hazard analysis (PSHA). As shown, alternative hypotheses and parameter values were incorporated for segmentation, maximum rupture length (influencing maximum earthquake magnitude), maximum magnitude estimate correlations, recurrence approach (alternatives of using seismicity data and tectonic convergence rate data for source zones), recurrence rates and b-values, and magnitude distribution model for recurrence assessments (characteristic for faults and characteristic and exponential for area sources).

G2-3. Ground Motion Attenuation Characterization

Three different sets of rock ground motion attenuation relationships for response spectral acceleration at different periods of vibration (5 percent damping) as well as for peak acceleration were utilized. Median values for these relationships (for magnitudes 5, 6, and 7) are illustrated in Figure G2-7 for peak acceleration and spectral acceleration at two periods of vibration. Each set of these relationships also has its associated model of uncertainty (dispersion) around the median curves. The dispersion relationships for the preferred attenuation model (designated Caltrans 1991 in Figure G2-7) are summarized in Table G2-1.

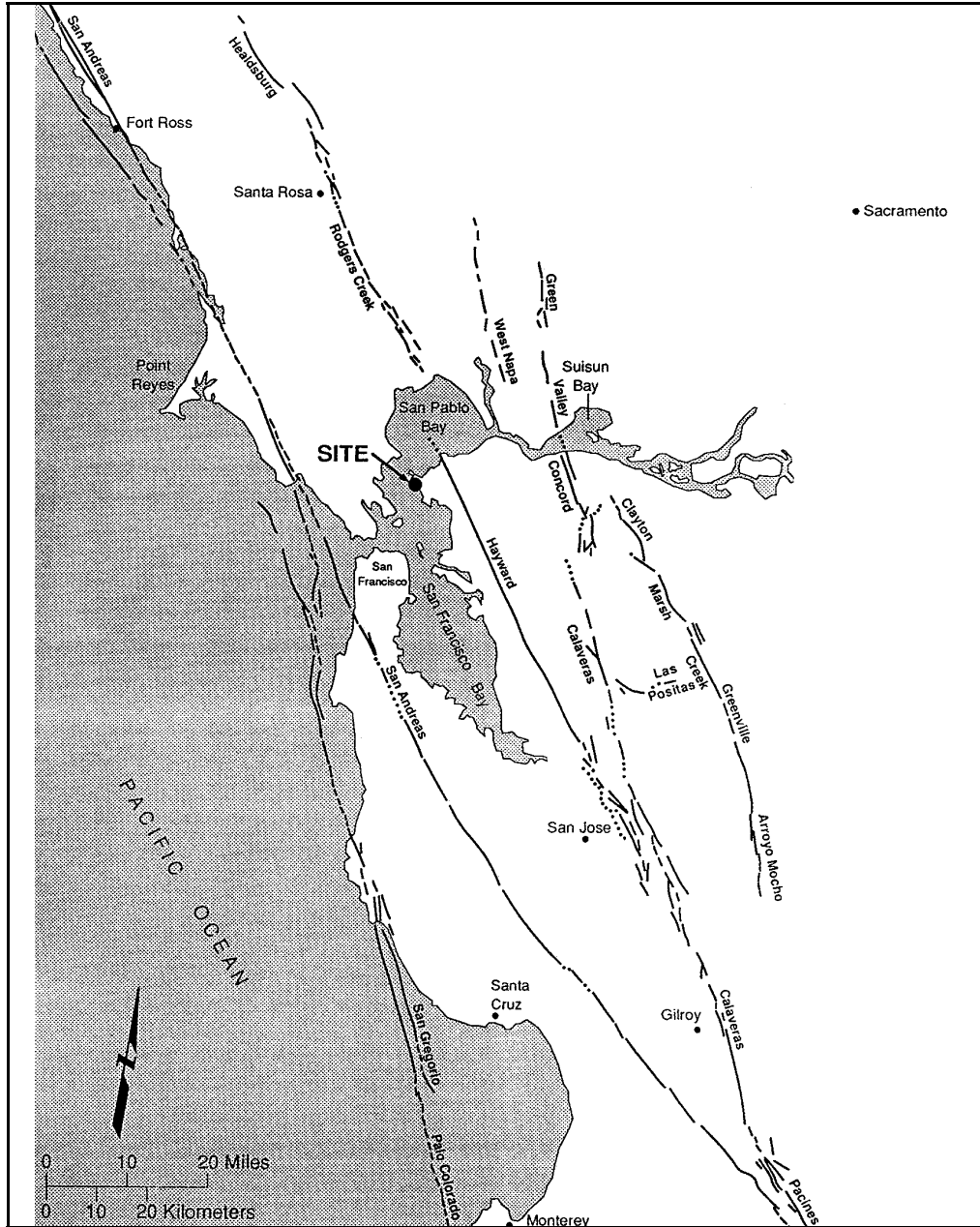


Figure G2-1. Regional active fault map

(The attenuation model designated Caltrans 1991 is the relationship of Sadigh et al. 1993.) This model predicts increasing dispersion for decreasing magnitude and increasing period of vibration, based on analysis of ground motion data. The three sets of attenuation relationships form three additional branches that are added to the logic tree in Figure G2-6.

G2-4. PSHA Results

Typical results of the PSHA are illustrated in Figure G2-8 in terms of the hazard curves obtained for peak acceleration and response spectral acceleration at two periods of vibration. The distribution about the

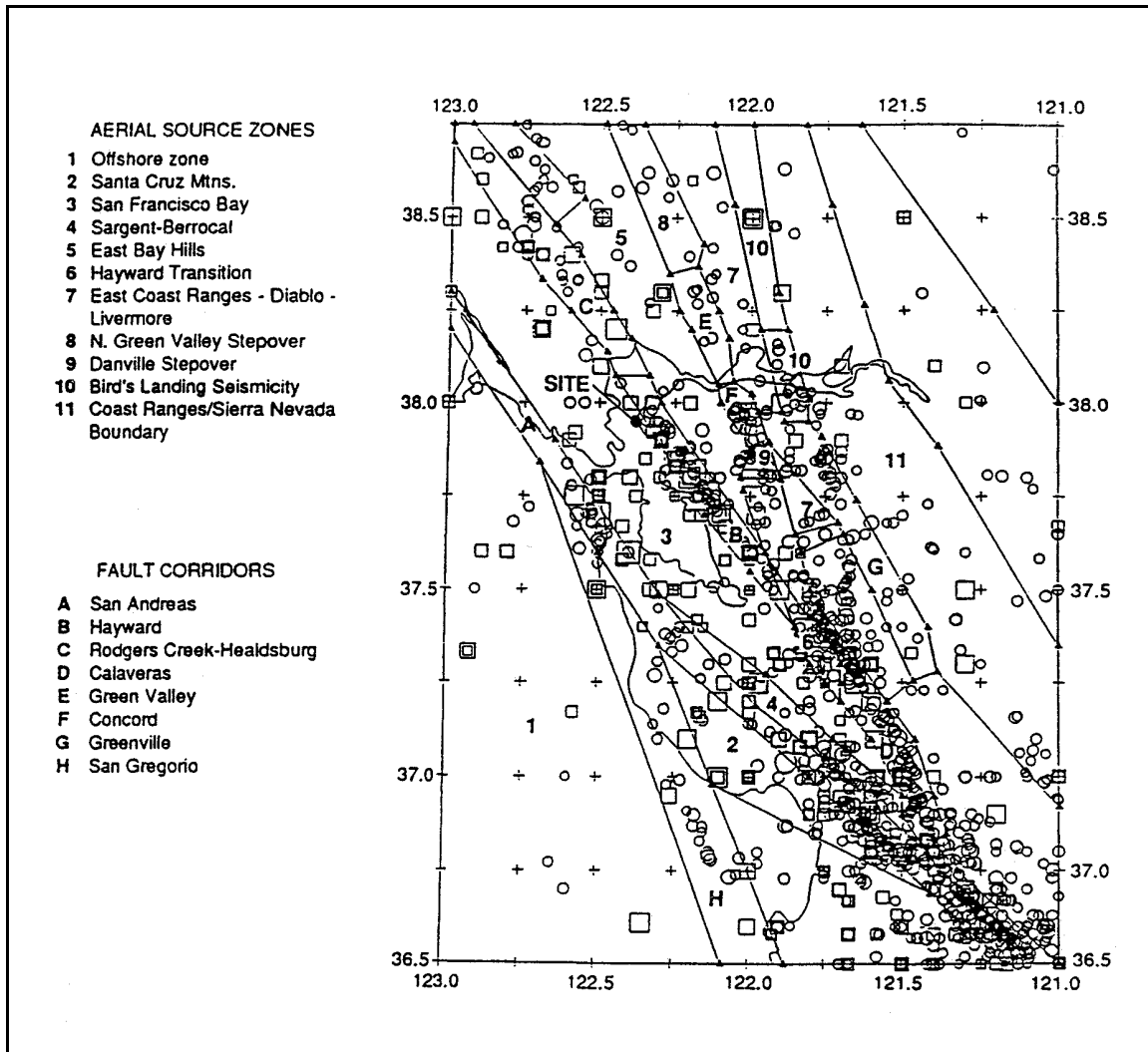


Figure G2-2. Map of the San Francisco Bay area showing independent earthquakes, fault corridors, and areal source zones. Fault corridors define the area within which seismicity is assumed to be related to fault-specific sources

mean hazard curves represents the uncertainty in seismic source characterization and ground motion attenuation characterization modeled in the logic tree. Figure G2-9 shows the contributions of different seismic sources to the hazard (sources are shown in Figures G2-1 and G2-2). As shown, the Hayward fault, which is closest to the site, dominates the hazard for peak ground acceleration (PGA) and response spectral values at low periods of vibration, but the San Andreas fault contribution increases with increasing vibrational period (reflecting the potential for larger magnitude earthquakes on the San Andreas fault than on the Hayward fault and the relatively greater influence of magnitude on long-period motions than on short-period motions). Magnitude contributions to the mean hazard curves are illustrated in Figure G2-10. The contributions of higher magnitudes increase both with increasing period of vibration and with increasing return period (RP). Analyses of two of the components of the seismic hazard model that contribute to the uncertainty in the hazard curves are illustrated in Figures G2-11 and G2-12. From Figure G2-11, it can be seen that much of the uncertainty in the hazard curves is associated with uncertainties as to the appropriate attenuation relationship. By comparison, Figure G2-12 indicates that the uncertainty associated with different models of fault segmentation for the San Andreas fault is

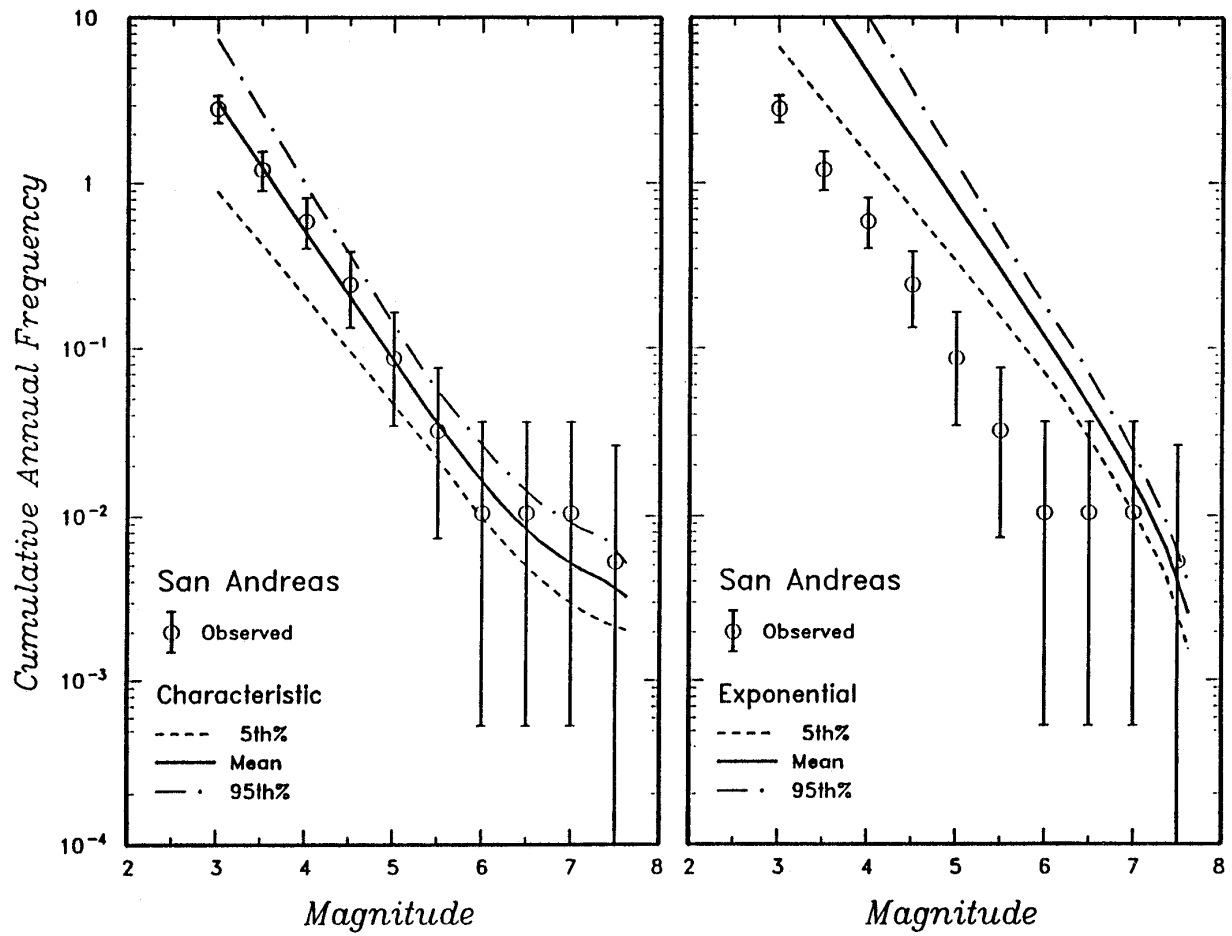


Figure G2-3. Comparison of recurrence rates developed from independent seismicity and from fault slip rates for the San Andreas fault. Predicted recurrence rates are shown for the characteristic earthquake and exponential magnitude distribution models

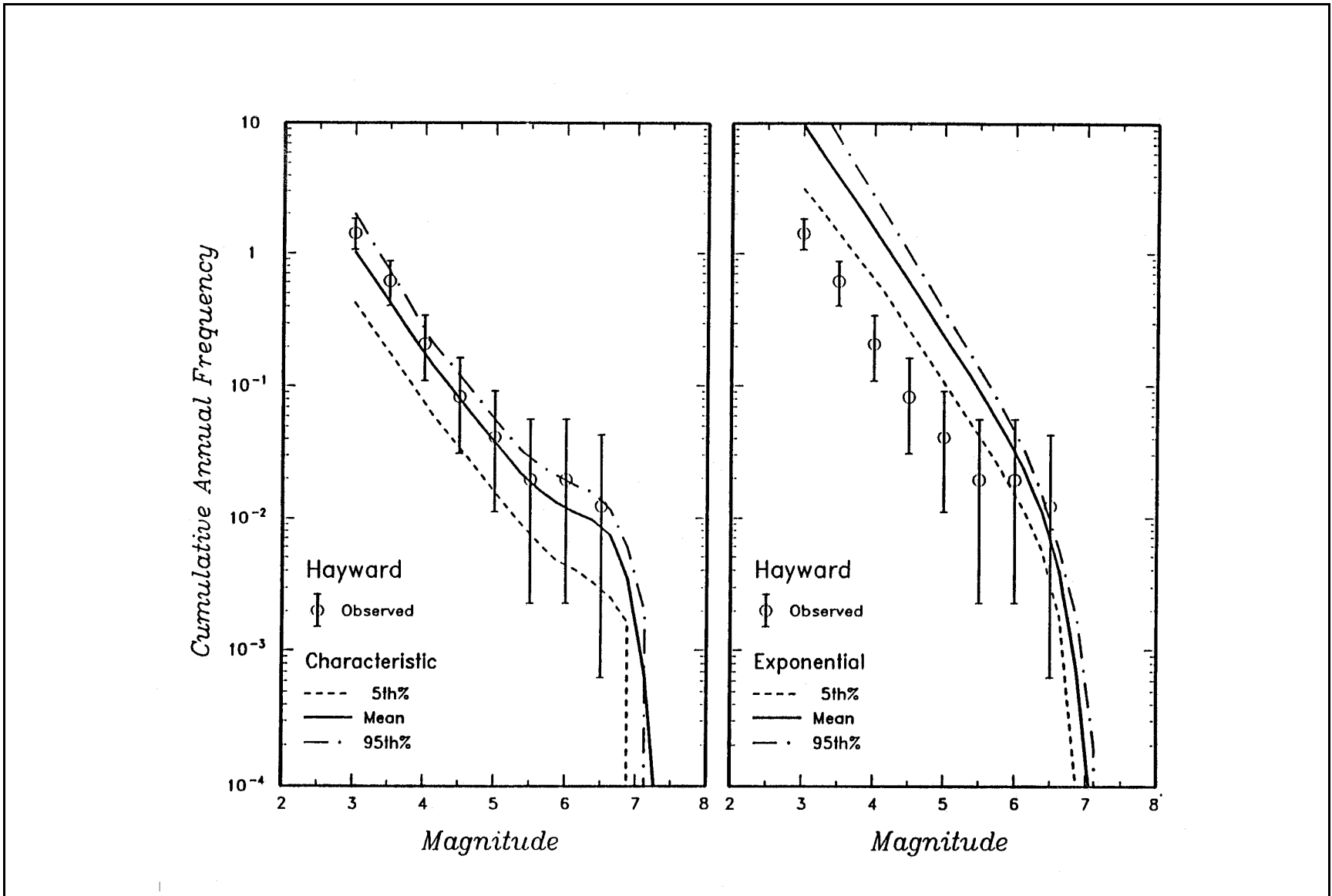


Figure G2-4. Comparison of recurrence rates developed from independent seismicity and from fault slip rates for the Hayward fault. Predicted recurrence rates are shown for the characteristic earthquake and exponential magnitude distribution models

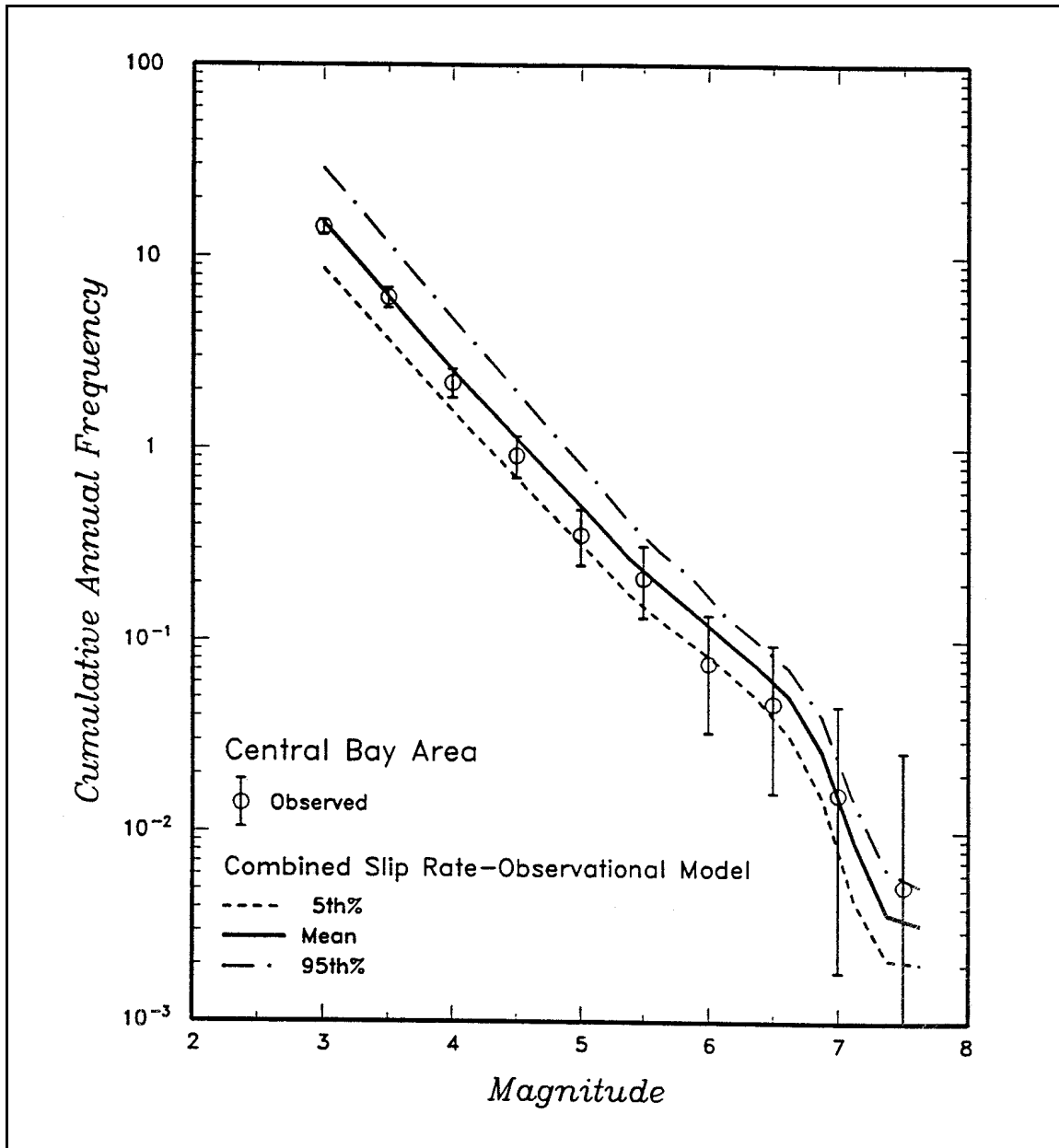


Figure G2-5. Comparison of modeled recurrence and seismicity for the central bay area

relatively small, particularly at lower frequencies of exceedance. Equal hazard response spectra (expressed in the form of tripartite plots) constructed from the mean hazard results are shown in Figure G2-13 for return periods varying from 100 to 2,000 years.

G2-5. Comparison of Probabilistic and Deterministic Results

Deterministic response spectra estimates for the site were also developed for maximum credible earthquakes (MCEs) on the San Andreas fault (MCE of moment magnitude M_w 8) and the Hayward fault (MCE of M_w 7.25), assumed to occur on the portion of the faults closest to the site. Both median and 84th percentile response spectra were developed using the preferred set of attenuation relationships. In

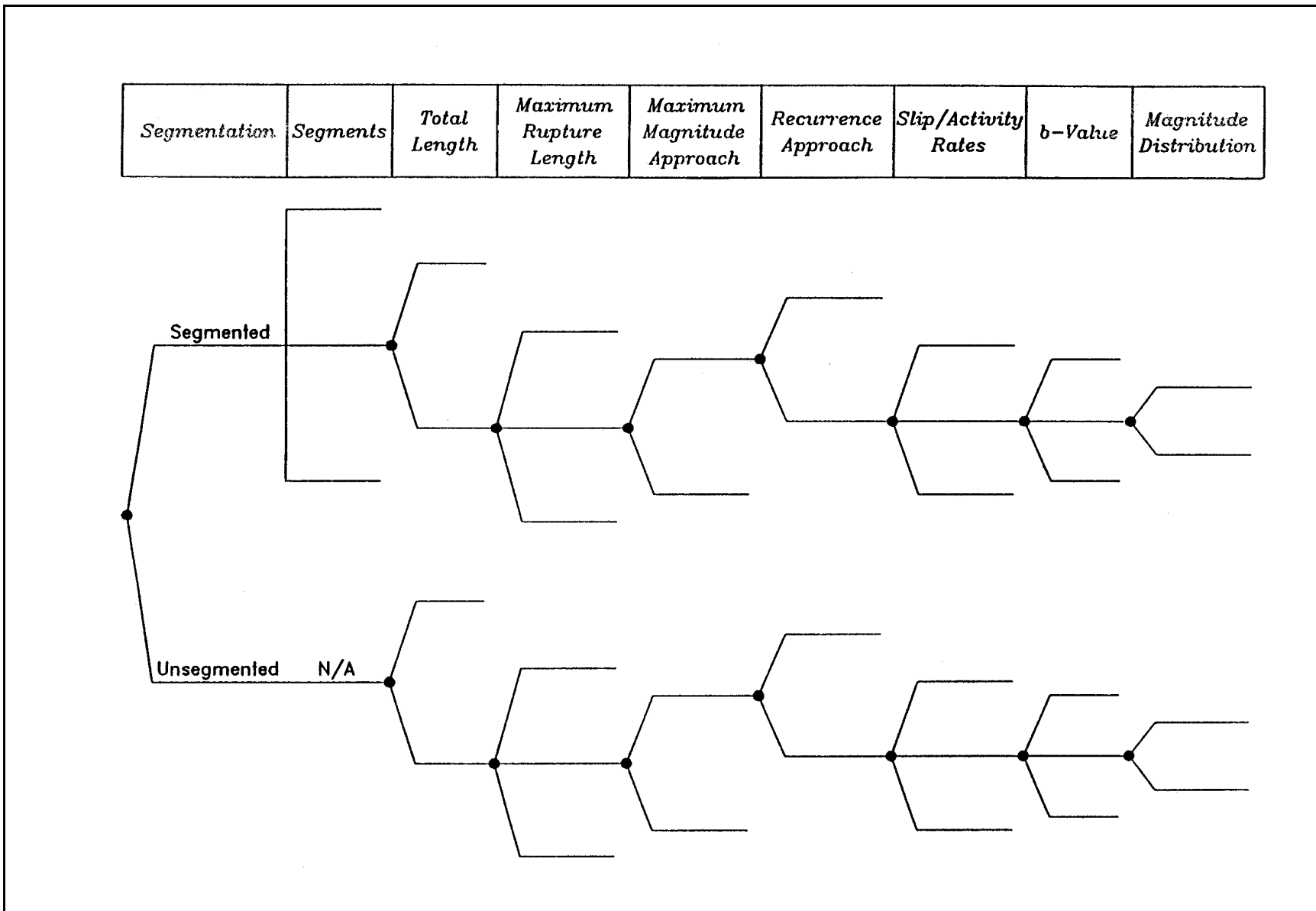


Figure G2-6. Generic logic tree used in this study to characterize seismic sources for PSHA

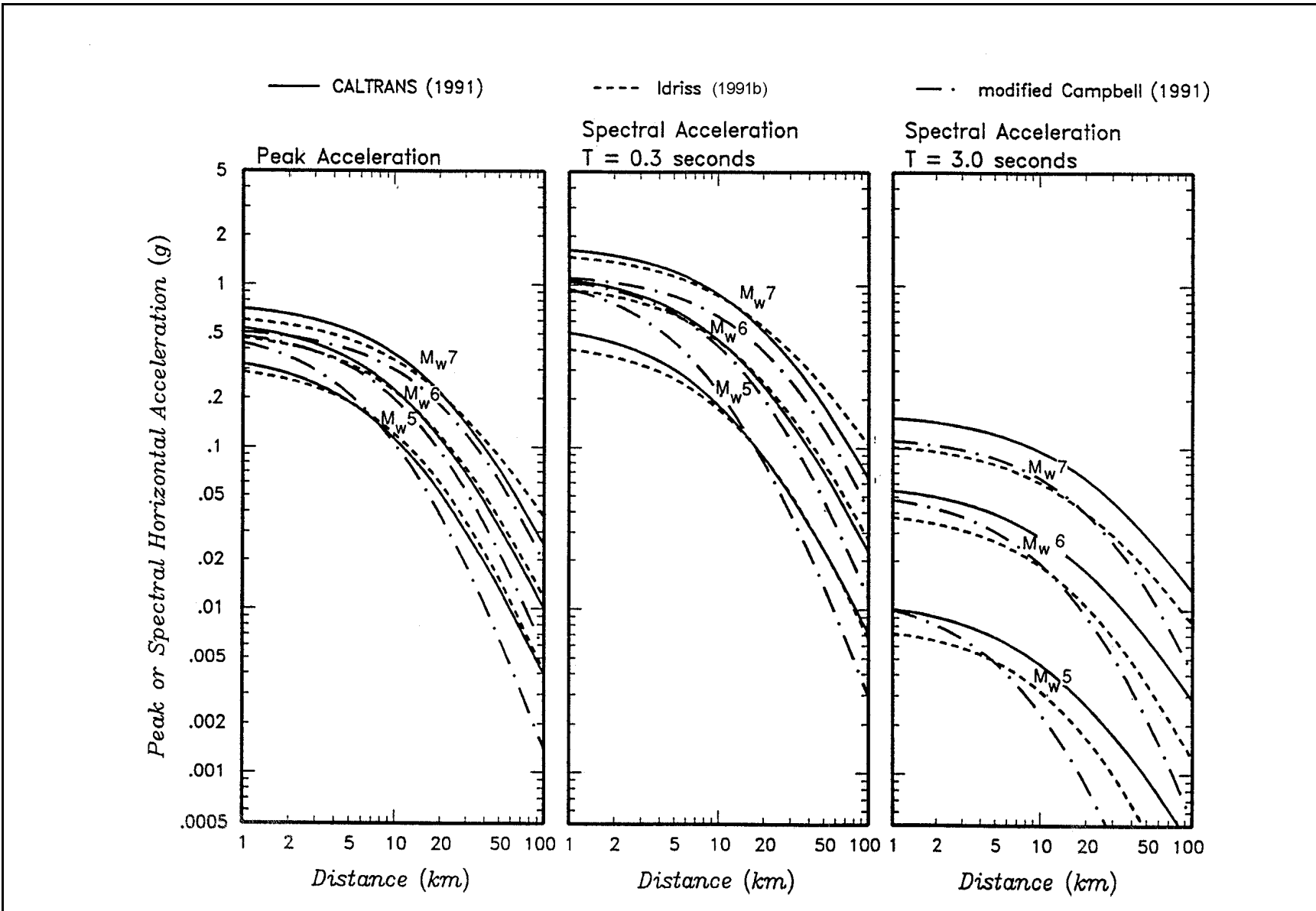


Figure G2-7. Ground motion attenuation relationships

Table G2-1
Dispersion Relationships for Horizontal Rock Motion

Ground Motion Parameter	Period (sec)	Sigma ($\ln y$)
Peak ground acceleration (g)	--	1.39 - 0.14*M; 0.38 for M > = 7.25
Response spectra acceleration (g)	0.05	1.39 - 0.14*M; 0.38 for M > = 7.25
	0.07	1.40 - 0.14*M; 0.39 for M > = 7.25
	0.09	1.40 - 0.14*M; 0.39 for M > = 7.25
	0.10	1.41 - 0.14*M; 0.40 for M > = 7.25
	0.12	1.41 - 0.14*M; 0.40 for M > = 7.25
	0.14	1.42 - 0.14*M; 0.41 for M > = 7.25
	0.15	1.42 - 0.14*M; 0.41 for M > = 7.25
	0.17	1.42 - 0.14*M; 0.41 for M > = 7.25
	0.20	1.43 - 0.14*M; 0.42 for M > = 7.25
	0.24	1.44 - 0.14*M; 0.43 for M > = 7.25
	0.30	1.45 - 0.14*M; 0.44 for M > = 7.25
	0.40	1.48 - 0.14*M; 0.47 for M > = 7.25
	0.50	1.50 - 0.14*M; 0.49 for M > = 7.25
	0.75	1.52 - 0.14*M; 0.51 for M > = 7.25
1.00	1.53 - 0.14*M; 0.52 for M > = 7.25	
> 1.00	1.53 - 0.14*M; 0.52 for M > = 7.25	

Note: Sigma ($\ln y$) is the standard deviation of the natural logarithm of the respective ground motion parameter y . M is earthquake moment magnitude.

Figure G2-14, the deterministic spectra are compared with the equal hazard spectra. It may be noted that in terms of response spectral amplitudes, the Hayward MCE 84th percentile governs over the San Andreas MCE except at periods greater than about 3 sec, and the Hayward MCE spectrum is approximately at the level of the 1000- to 2000-year return period equal hazard spectrum through the period range. Because it was desired for this site to establish an MCE as a design earthquake and to have a return period of about 1000 to 2000 years associated with the design ground motions, it was decided to select the 84th percentile spectrum for the Hayward MCE as the design response spectrum.

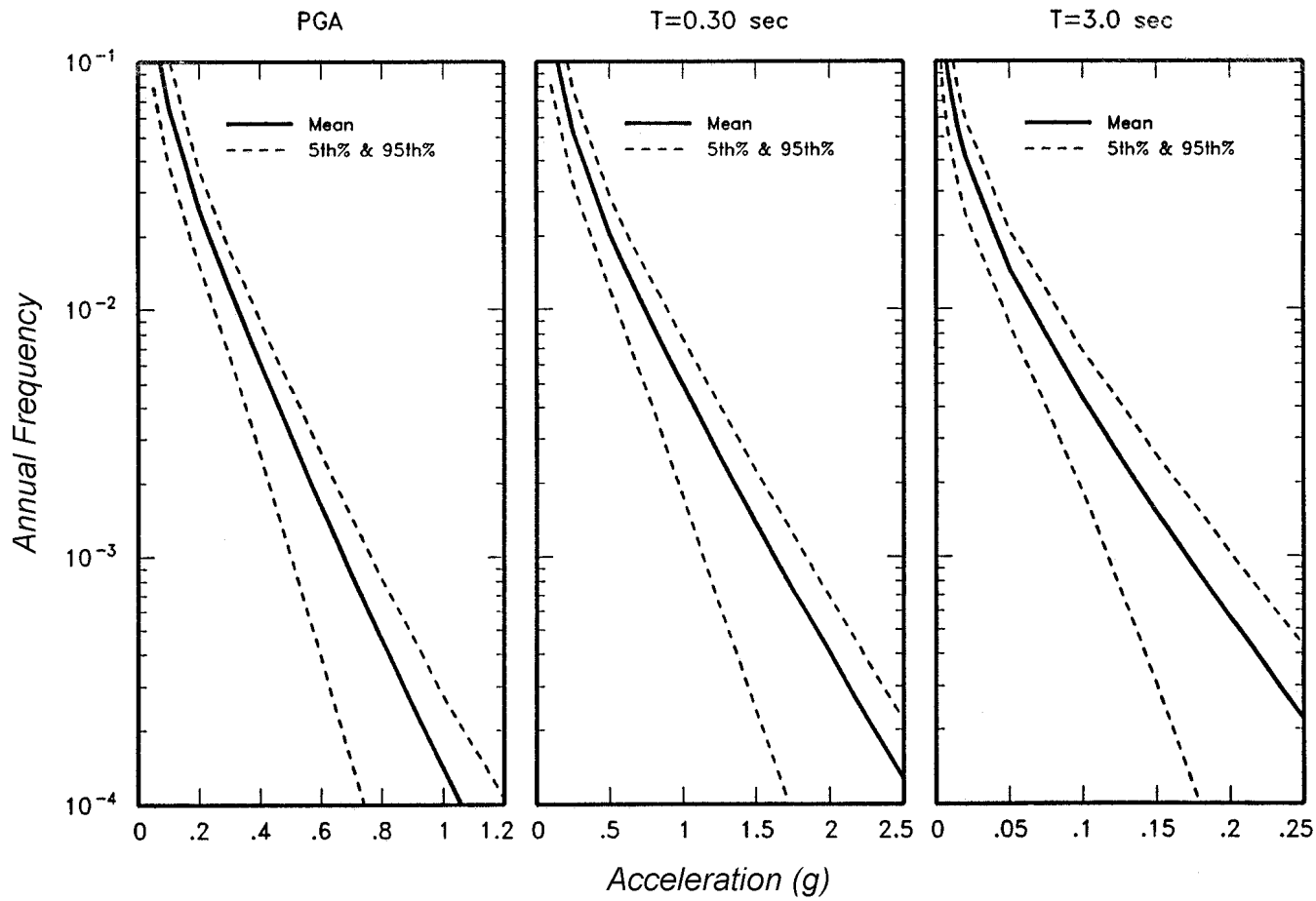


Figure G2-8. Mean, 5th, and 95th percentile hazard curves for the site for peak acceleration and 5 percent-damped spectral accelerations at periods of 0.3 and 3.0 sec

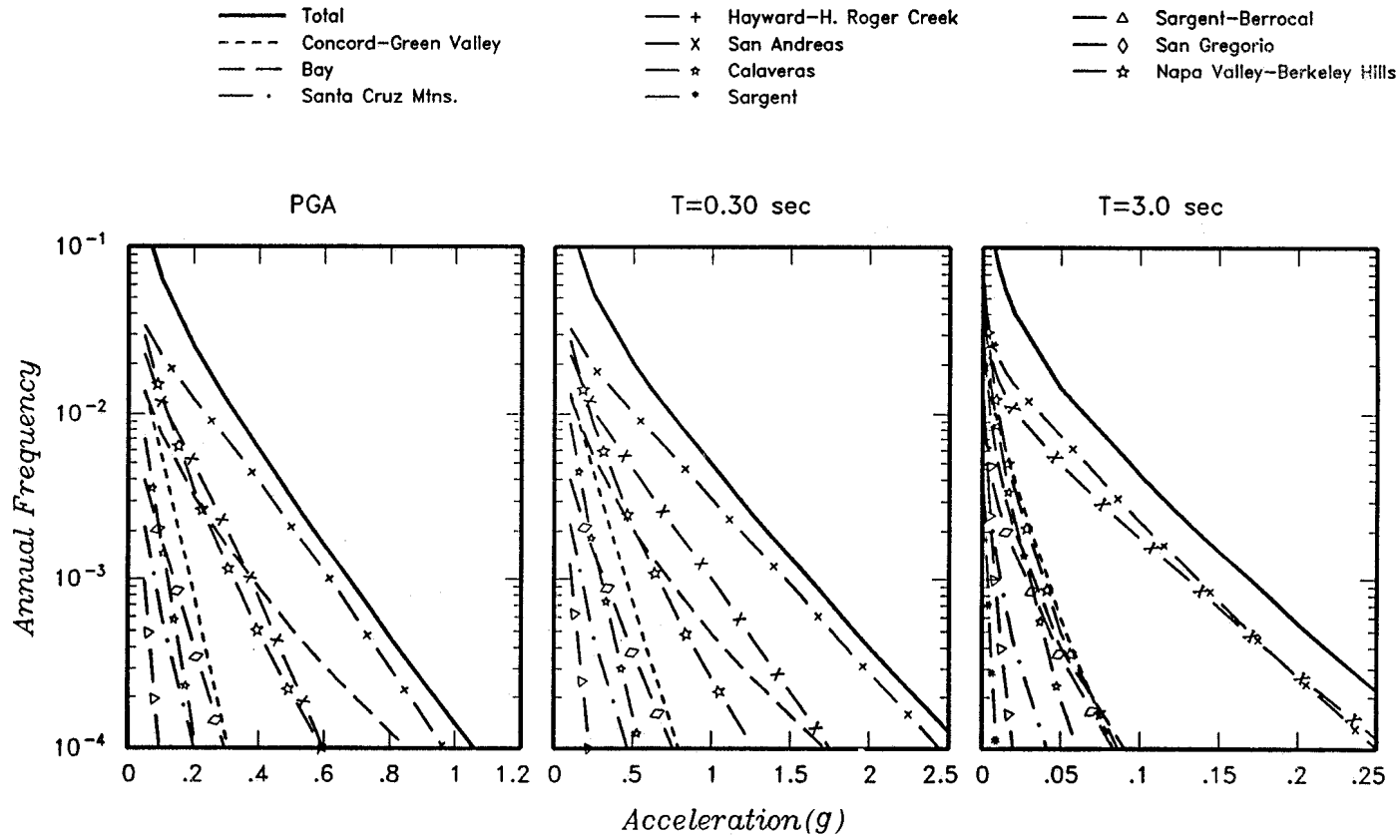
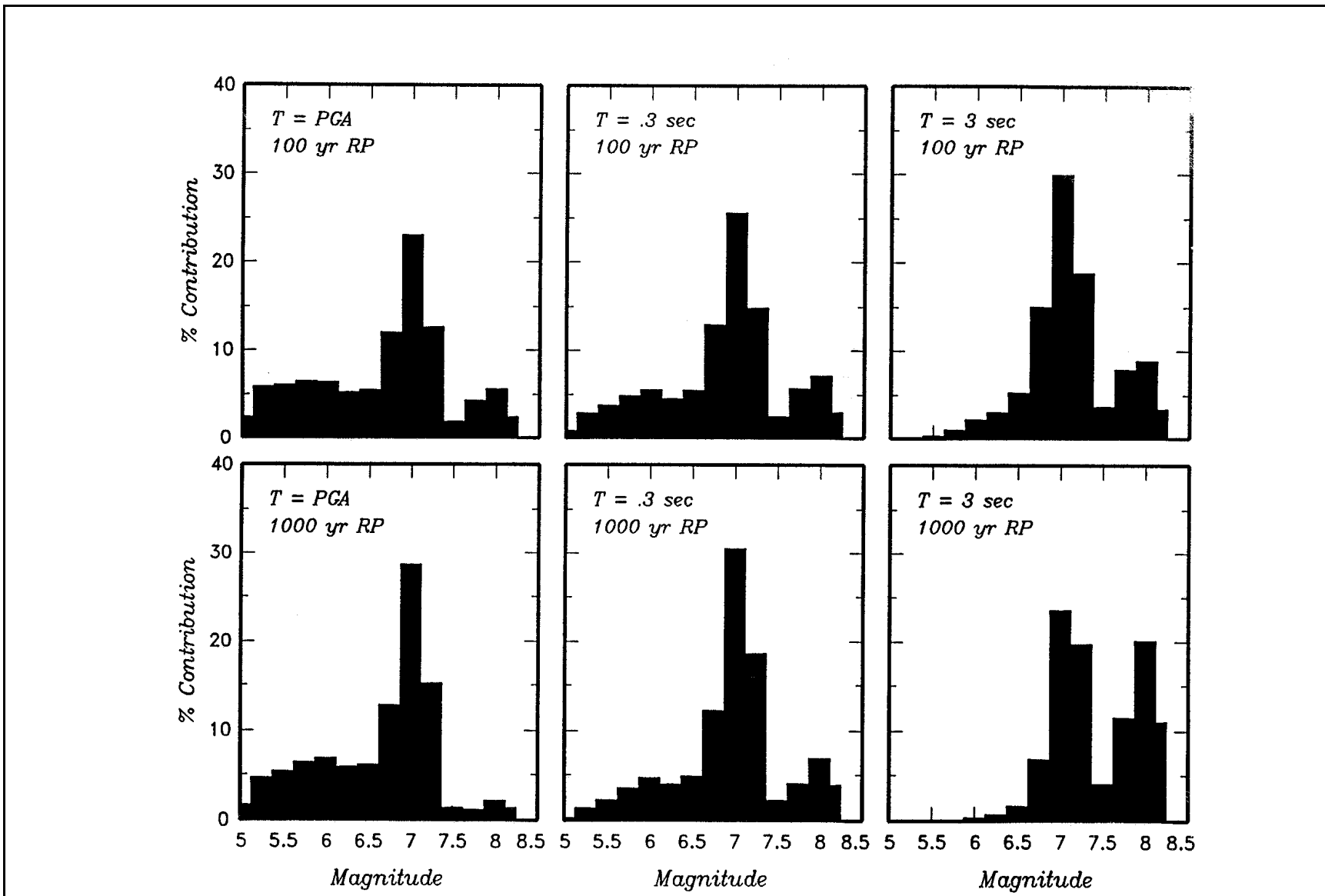


Figure G2-9. Contributions of various sources to mean hazard at the site. Shown are results for peak acceleration and 5 percent-damped spectral accelerations at periods of 0.3 and 3.0 sec



G-29 Figure G2-10. Contributions of events in various magnitude intervals to the mean hazard at the site. Shown are results for peak acceleration and 5 percent-damped spectral accelerations at periods of 0.3 and 3.0 sec

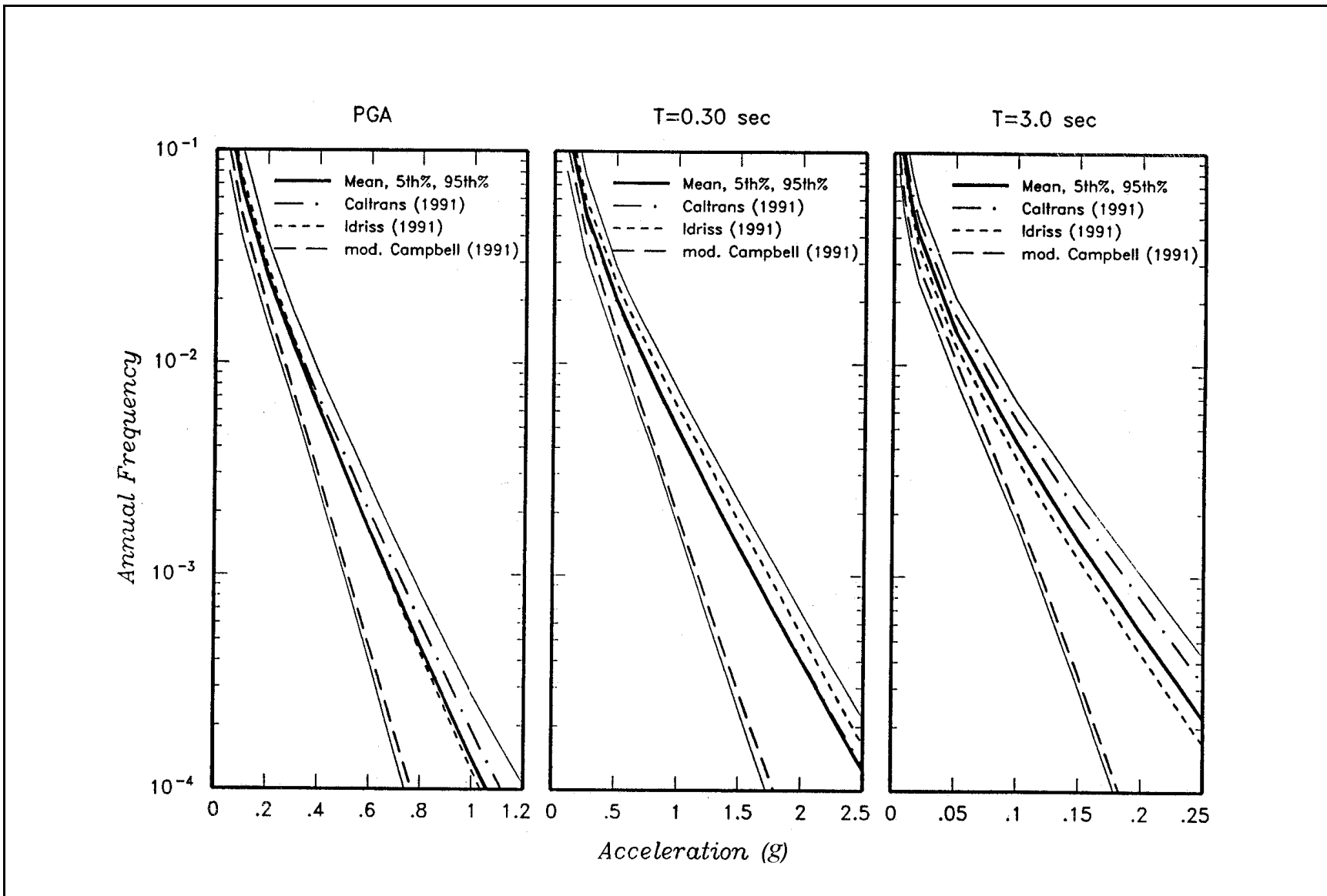
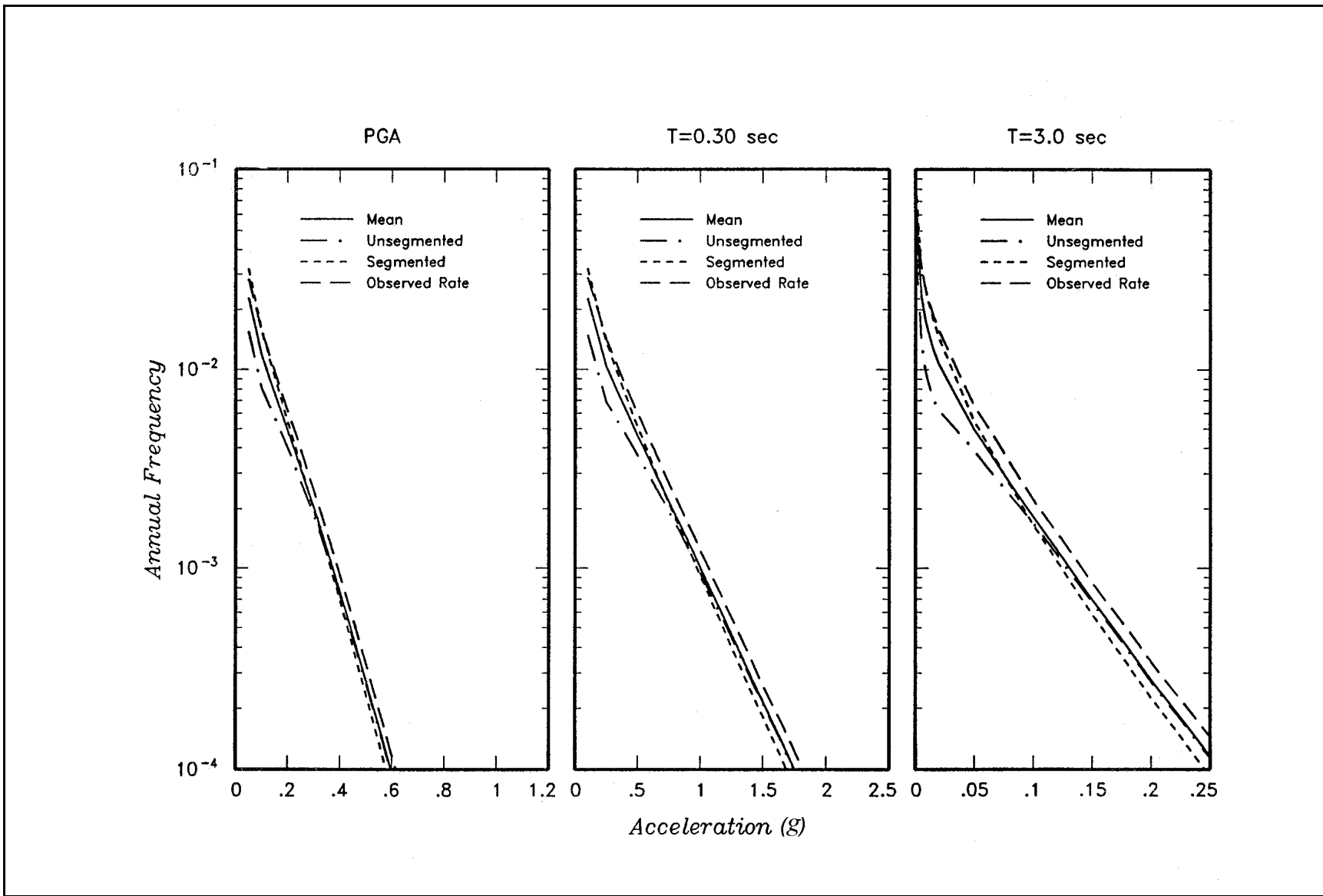


Figure G2-11. Sensitivity of mean hazard at the site to the choice of attenuation model. Shown are results for peak acceleration and 5 percent-damped spectral accelerations at periods of 0.3 and 3.0 sec



G-31

Figure G2-12. Sensitivity of mean hazard at the site to the choice of segmentation model for the San Andreas fault. Shown are results for peak acceleration and 5 percent-damped spectral accelerations at periods of 0.3 and 3.0 sec

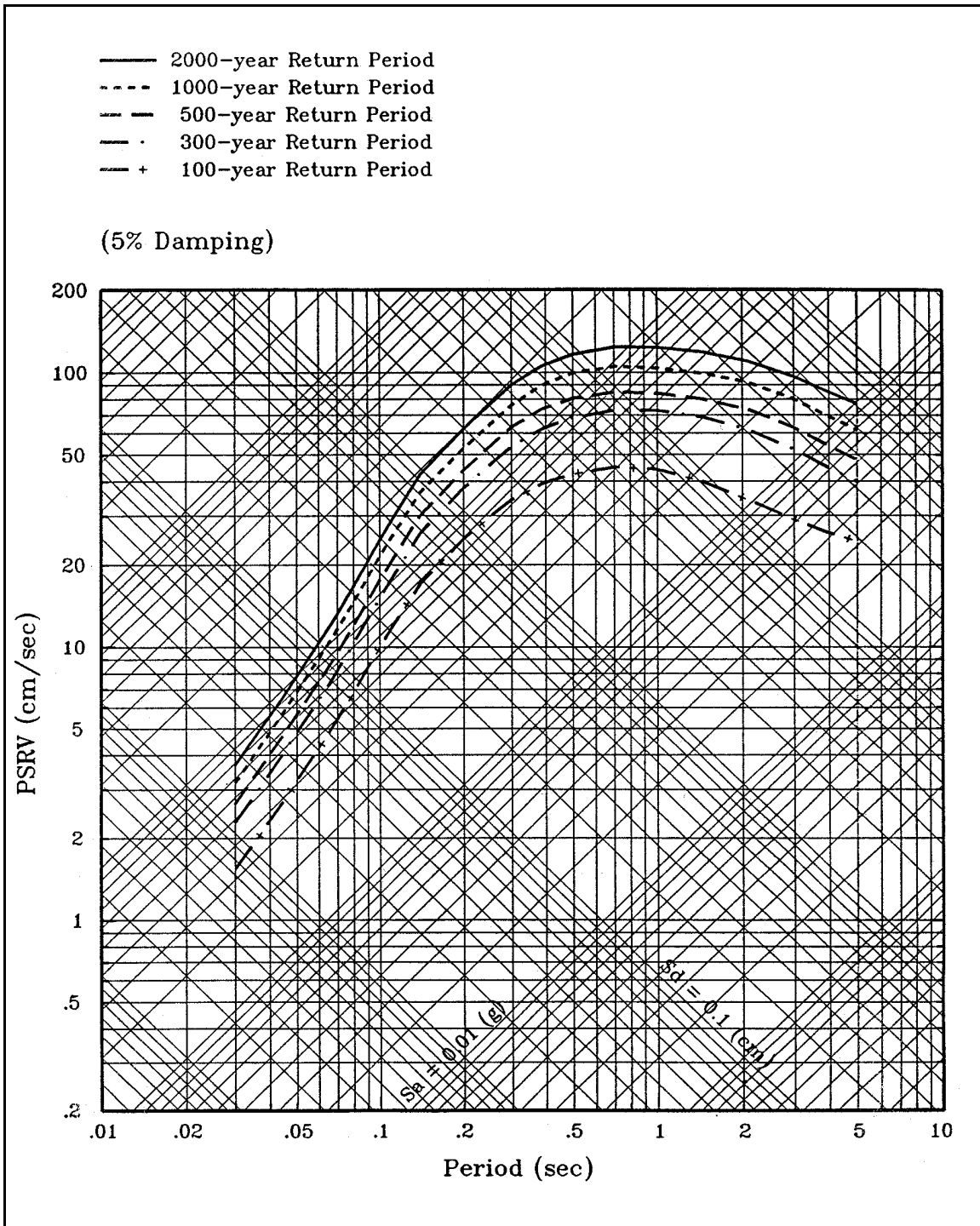


Figure G2-13. Equal-hazard pseudo-relative velocity (PSRV) response spectra for the site (5 percent damping)

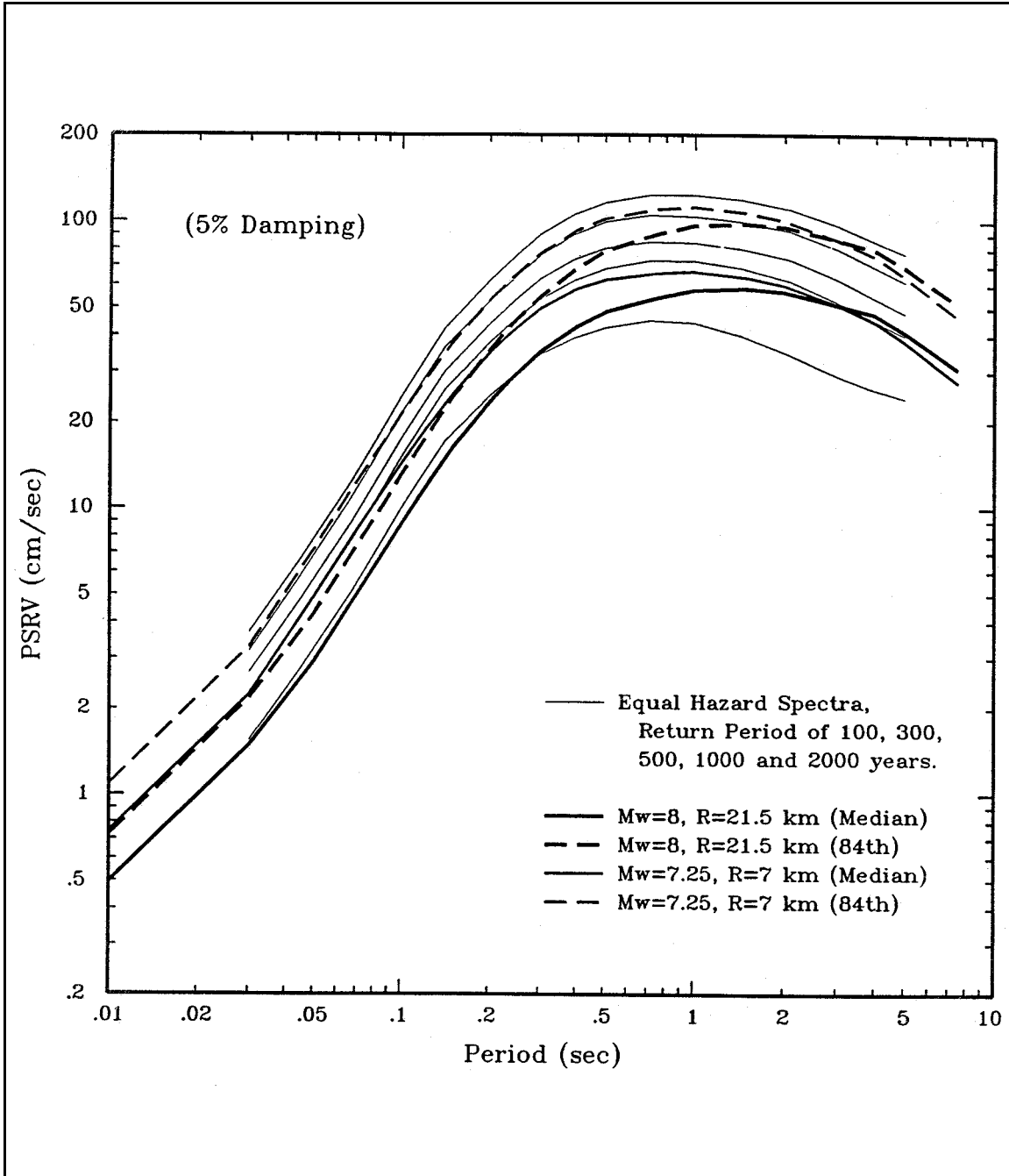


Figure G2-14. Comparison of the deterministic response spectra with equal hazard spectra for the site

Section III
Example 3
Soil Site in Arkansas

G3-1. Introduction

The site location, shown in Figure G3-1, is in southeast Arkansas near the Mississippi River. For this site, equal hazard response spectra of top-of-soil ground motions were developed and compared with deterministic response spectra for maximum credible earthquakes (MCE).

G3-2. Seismic Source Characterization

The seismic source zones identified for the study are shown in Figure G3-1 along with seismicity epicenters. These zones were developed as a synthesis of results presented in two comprehensive studies of seismic hazard in the eastern United States by the Electric Power Research Institute (EPRI) (1987) and the Lawrence Livermore National Laboratory (Bernreuter et al. 1989), as well as subsequent generalized evaluations by Johnston and Nava (1990) and Mitchell et al. (1991). The site is located in the Ouachita fold belt seismic zone, a region of low seismicity. North of and close to the site is the low-seismicity Southern Reelfoot rift seismic zone, while farther north (180 km from the site) is the relatively high seismicity New Madrid seismic zone, which was the source of the 1811-1812 New Madrid earthquake sequence. On the basis of analysis of historical seismicity, earthquake recurrence relationships were developed for the various seismic source zones. The historical seismicity for the New Madrid seismic zone is shown in Figure G3-2 along with a fitted recurrence curve having an exponential magnitude distribution. Also shown in Figure G3-2 is the inferred recurrence of large-magnitude earthquakes from paleoseismic data. Since the evidence from paleoseismic data is somewhat equivocal, two recurrence relationships were used for the New Madrid seismic zone. One consisted of the exponential model fitted to the seismicity and extrapolated to the maximum magnitude (m_b , approximately 7.5) for this source zone; the other consisted of a characteristic magnitude model that fits the moderate-magnitude seismicity data yet also fits the paleoseismic data for the occurrence of large earthquakes. The two recurrence relationships used are shown by the upper and lower curves in Figure G3-3. An exponential magnitude distribution fitting historical seismicity was used to model recurrence for the other seismic source zones. Seismicity rates for the Ouachita fold belt source zone are illustrated in Figure G3-4. The modeling of uncertainty in the seismic source characterization is shown in the logic tree in Figure G3-5. For all sources, two methods, equally weighted, were used to analyze completeness in the seismicity catalog. Figure G3-5 elaborates on the modeling of the Ouachita fold belt seismic source. As shown, it was modeled as both a single zone (the entire source) and two zones roughly separated by the Mississippi River, since the region to the east appears to have lower seismicity than the region to the west (Figure G3-4). These models were given equal weight. To account for uncertainty in maximum magnitude, two values were used, weighted as shown. The wide range in modeled recurrence rates and b-values reflects the limited amount of seismicity data.

G3-3. Ground Motion Attenuation Characterization

a. Ground motion attenuation relationships were selected to estimate peak ground acceleration and response spectral values at the ground surface at the site, which is a deep-soil site. Two sets of relationships were selected. The first set was that developed by Boore and Joyner (1991) for deep-soil-site ground motions in the eastern United States. The second set consisted of a modification of the Boore and Joyner (1991) relationships. The modified attenuation relationships were developed by conducting

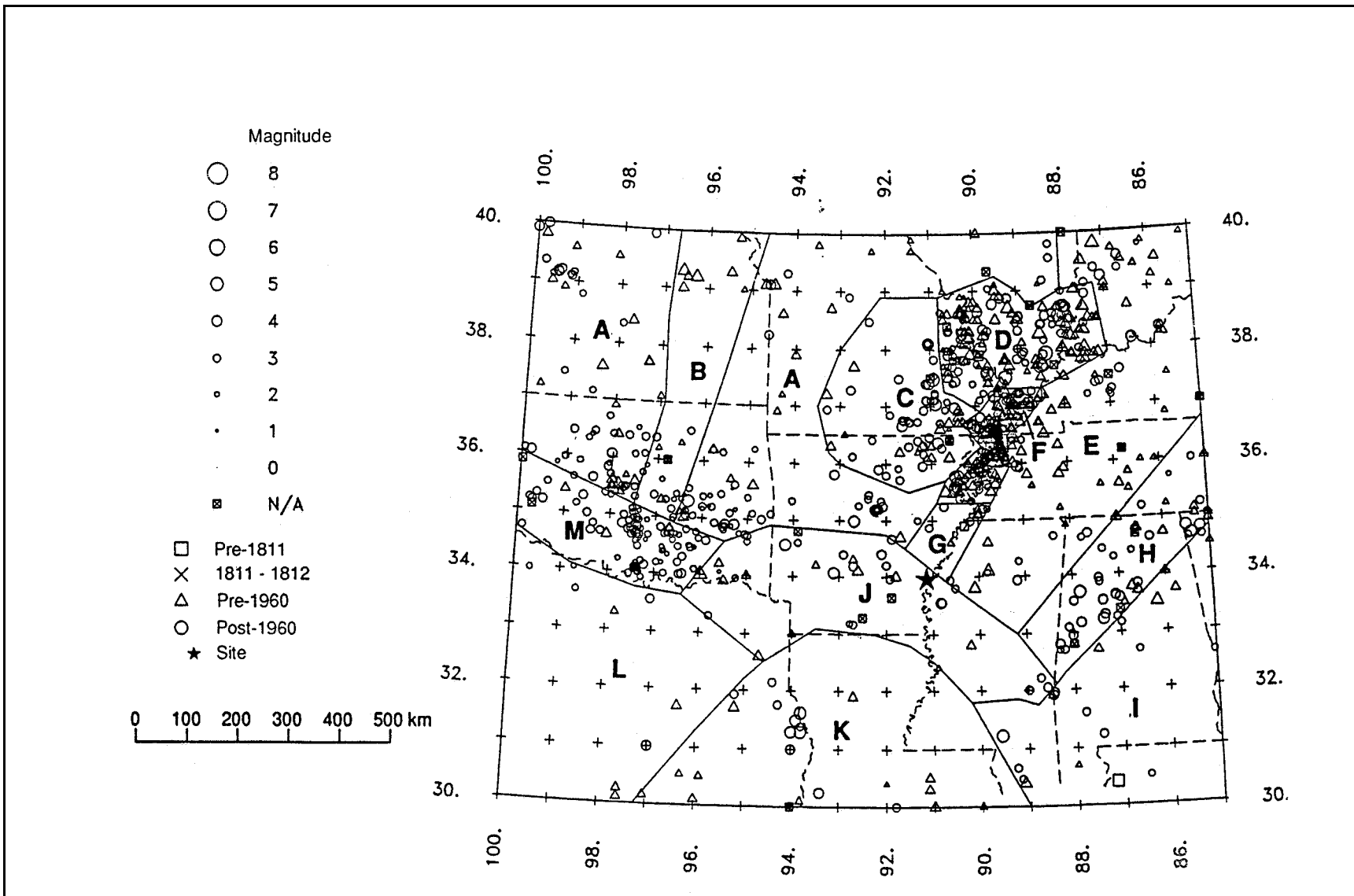


Figure G3-1. Historical seismicity and seismic source zones for the south-central United States. A - Great Plains, B - Nemaha ridge, C - Ozark uplift, D - St. Louis-Wabash, E - South-central, F - New Madrid seismic zone/Reelfoot rift complex, G - Southern Reelfoot rift, H - New York-Alabama lineament, I - Eastern Piedmont/Mesozoic basins, J - Ouachita fold belt, K - Southern Gulf Coast, L - New Mexico-Texas, M - Oklahoma aulacogen

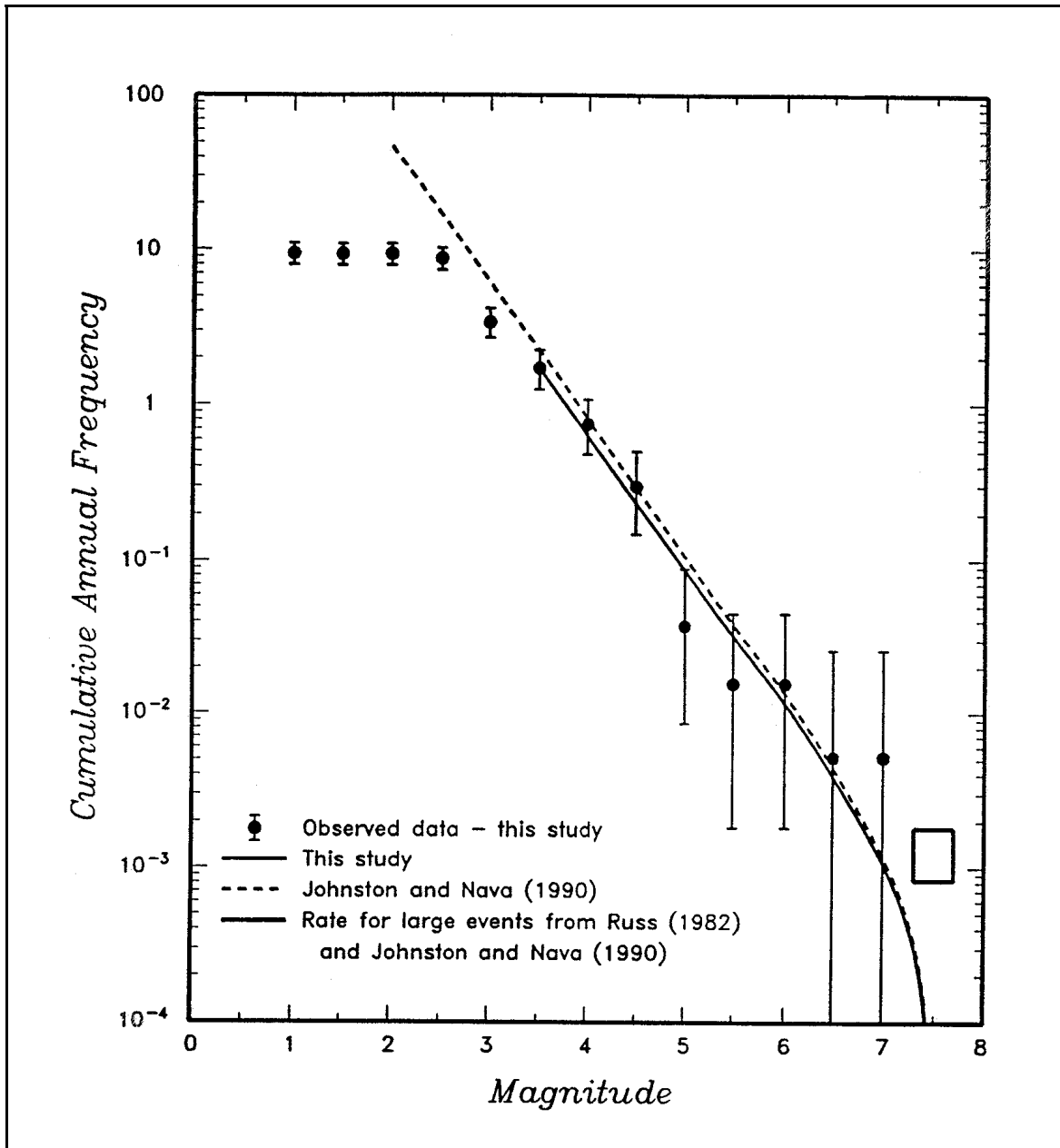


Figure G3-2. Earthquake recurrence relationships for New Madrid source zone. Box at lower right is inferred rate for large-magnitude events from paleoseismic data

site-specific theoretical (numerical) modeling of seismic wave propagation and site response using the Band-Limited White Noise/Random Vibration Theory (BLWN/RVT) approach for estimating rock motions combined with a local equivalent-linear site response analysis. The method is described by Silva and Lee (1987), Silva (1989), and Silva et al. (1989). The soil profile and crustal structure for the site vicinity were modeled for this analysis.

b. The two sets of attenuation relationships are shown in Figure G3-6 for peak ground acceleration and response spectral accelerations at two periods of vibration. These two sets of attenuation relationships, equally weighted, comprise additional branches on the logic tree shown in Figure G3-5.

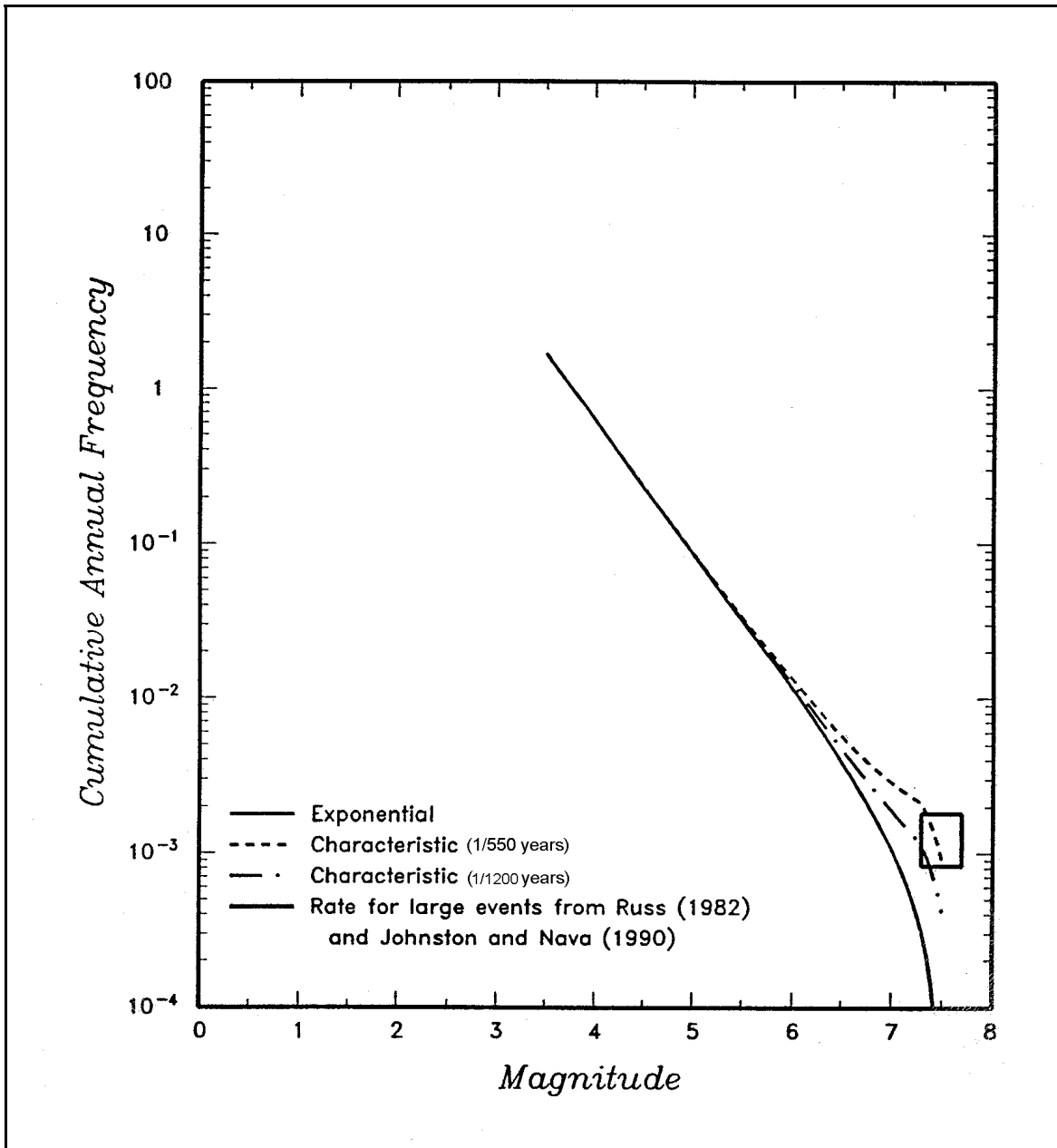


Figure G3-3. Recurrence relationships used to model New Madrid seismicity

G3-4. PSHA Results

Hazard curves obtained from the analysis for peak ground acceleration and response spectral accelerations for three periods of vibration are shown in Figure G3-7. The bands around the mean curves reflect the uncertainty in input parameters as incorporated in the logic tree. Contributions of different seismic sources to the hazard are shown in Figure G3-8. The hazard is dominated by the New Madrid seismic zone because its rate of earthquake occurrence is much higher than the other seismic zones. From the hazard curve results for a number of periods of vibration, equal hazard response spectra were constructed. These response spectra are shown in Figure G3-9 for return periods varying from 100 to 5000 years.

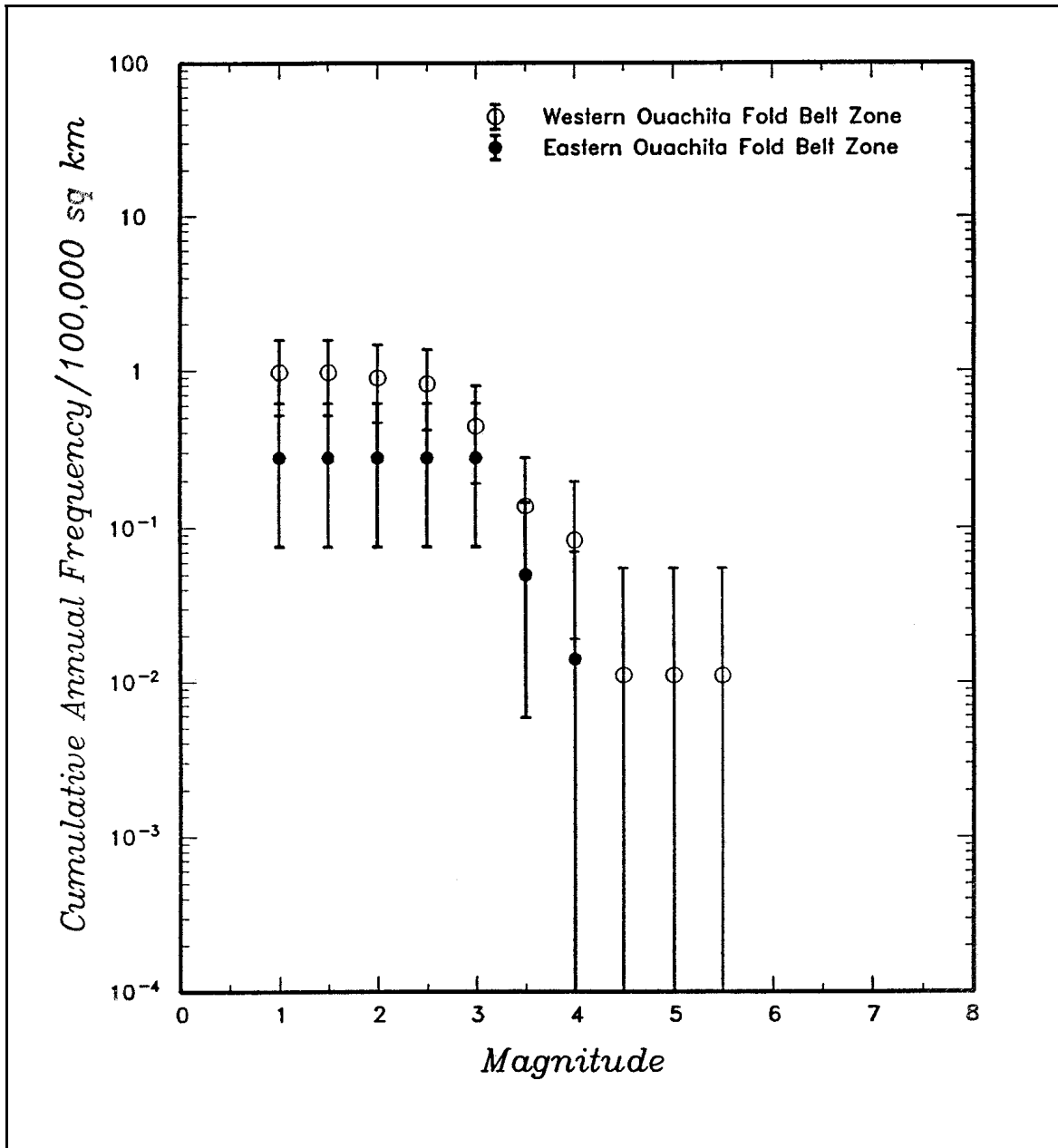


Figure G3-4. Cumulative earthquake frequencies for the western and eastern portions of the Ouachita fold belt source zone

G3-5. Comparison of Deterministic and Probabilistic Results

a. The equal hazard response spectra are compared in Figure G3-10 with deterministic estimates of response spectra for an MCE (magnitude m_b 7.5) occurring on the New Madrid seismic zone at the closest approach to the site (180 km). As shown, the median and mean spectra for the MCE are associated with return periods generally in the range of 1000 to 5000 years, whereas the 84th percentile spectrum for the MCE is associated with a return period greater than 5000 years. The equal hazard spectra were also compared with spectra deterministically estimated for the Ouachita fold belt seismic

<i>Attenuation Model</i>	<i>Catalog Completeness Method</i>	<i>Sources</i>	<i>Zone Configuration</i>	<i>Maximum Magnitude</i>	<i>Recurrence Rate</i>	<i>b-value</i>	<i>Recurrence Model</i>
--------------------------	------------------------------------	----------------	---------------------------	--------------------------	------------------------	----------------	-------------------------

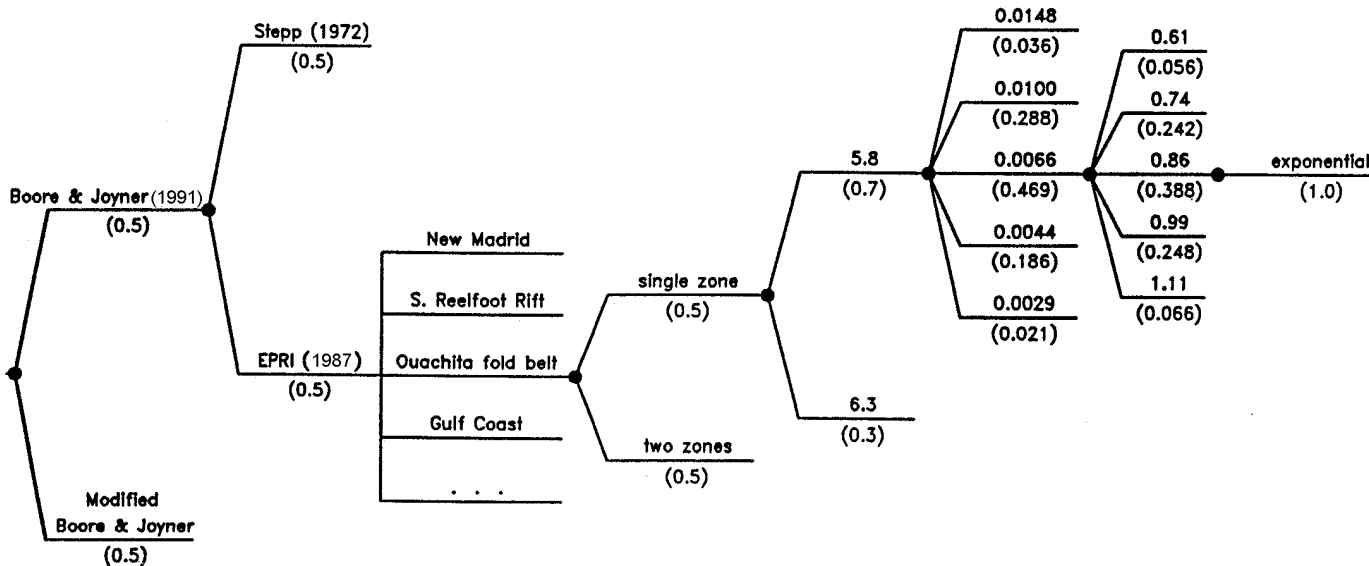


Figure G3-5. Logic tree used to model input parameter uncertainty for probabilistic seismic hazard analysis

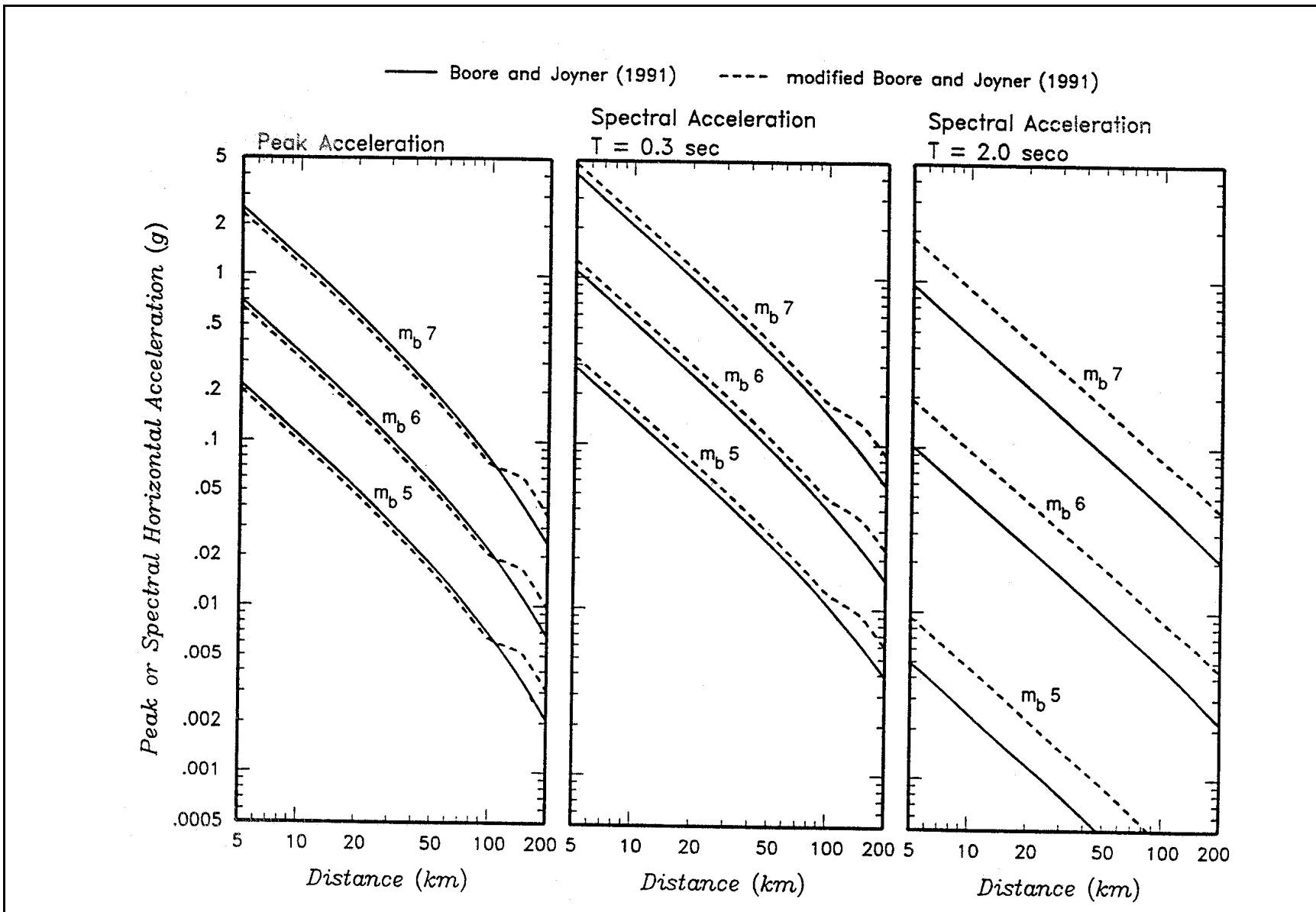


Figure G3-6. Attenuation relationships

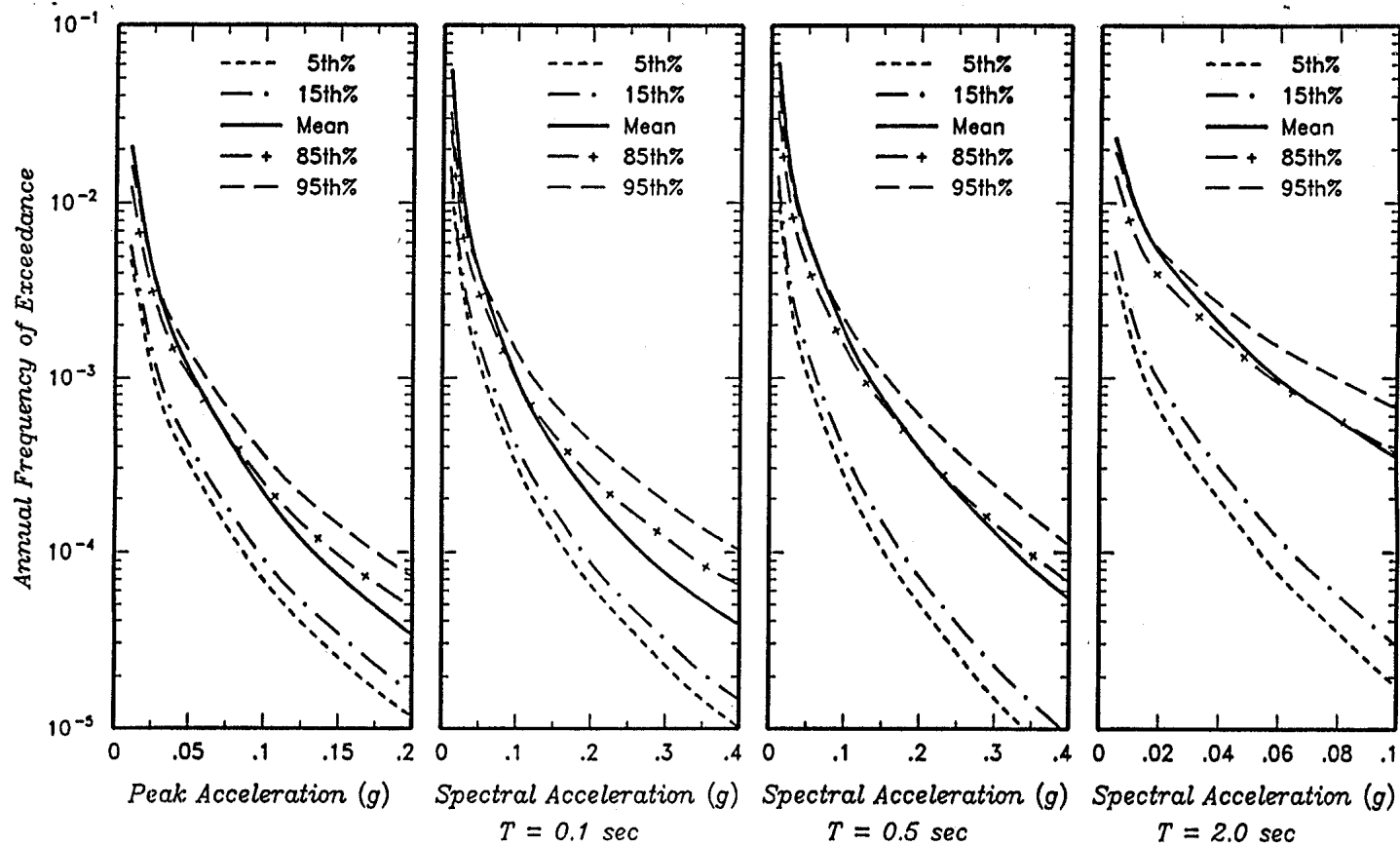


Figure G3-7. Computed hazard curves for peak acceleration and 5 percent-damped spectral accelerations at periods of 0.1, 0.5, and 2.0 sec. Shown are the mean hazard curves and the 5th, 15th, 85th, and 95th percentile hazard curves developed from the distributions of the input parameters

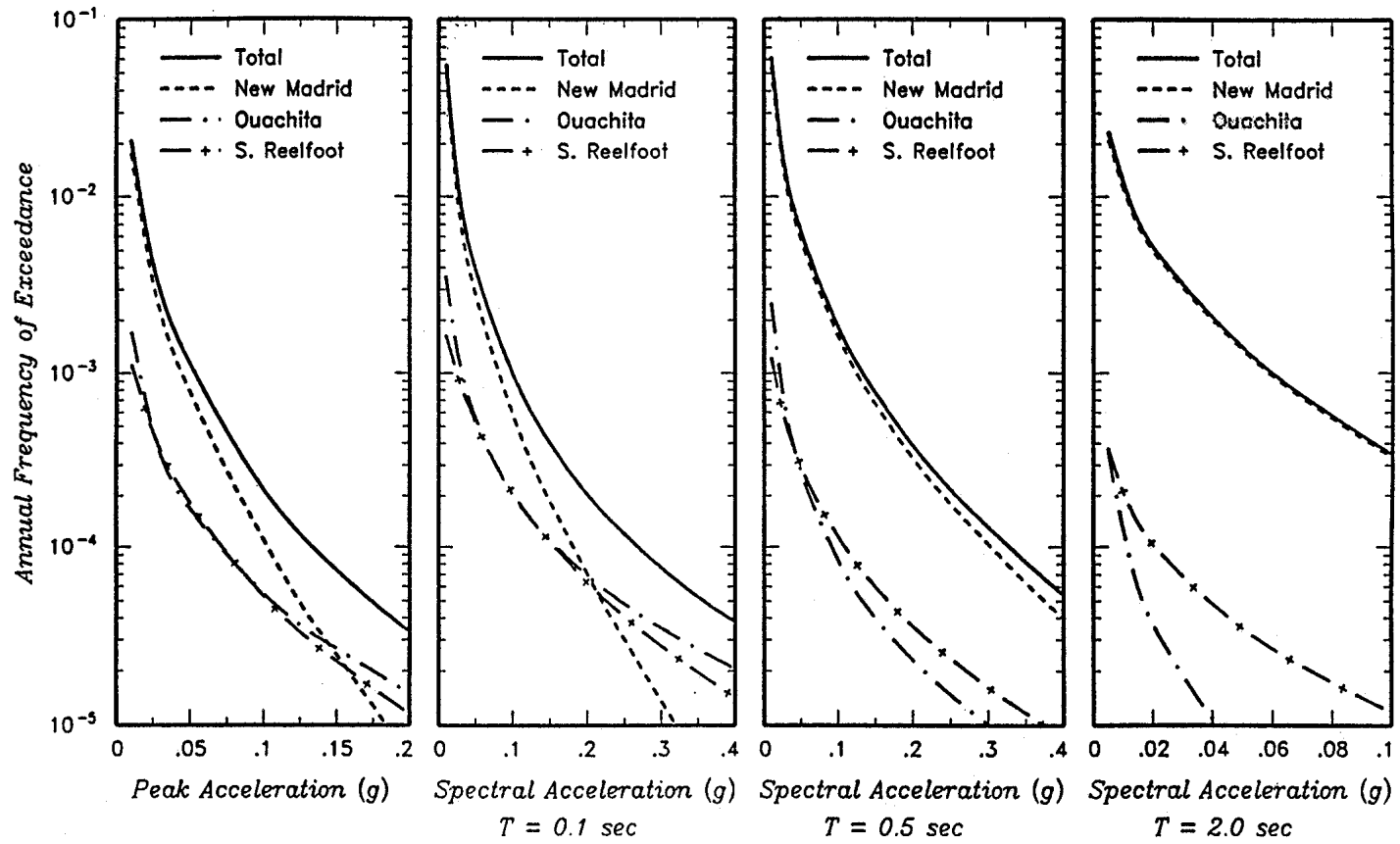


Figure G3-8. Contributions of the main seismic sources to the total mean hazard

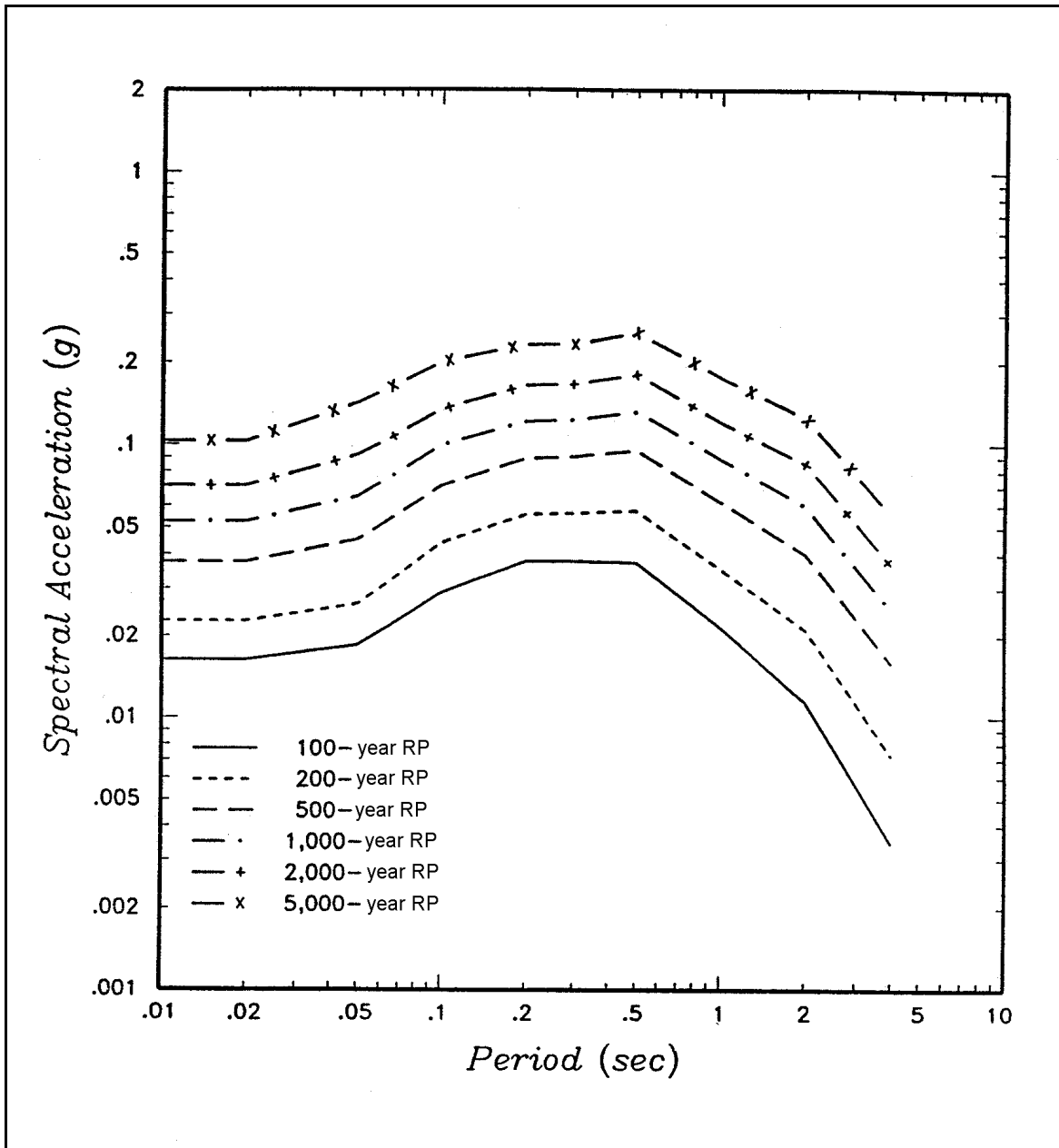


Figure G3-9. Equal-hazard spectra (5 percent damping) for return periods of 100, 200, 500, 1000, 2000, and 5000 years

zone (MCE m_b 5.8) and Reelfoot rift seismic zone (MCE m_b 6.8). In the case of the Ouachita fold belt, a source-to-site distance of 15 km was assumed, which provides an estimate consistent with a statistical random earthquake analysis for a 25-km radius around the site (see Appendix D for description of random earthquake analysis methodology). In the case of the Reelfoot rift seismic zone, the earthquake was assumed to occur at the closest approach of the zone to the site (20 km). The deterministic versus probabilistic comparisons for these two sources are shown in Figures G3-11 and G3-12. For the Ouachita fold belt, ground motions corresponding to the mean estimate were selected. As shown in Figure G3-11, at periods of vibration less than 0.7 sec, these ground motions have a return period longer than 5000 years. For the Reelfoot rift seismic zone, it was assessed that the deterministic event was

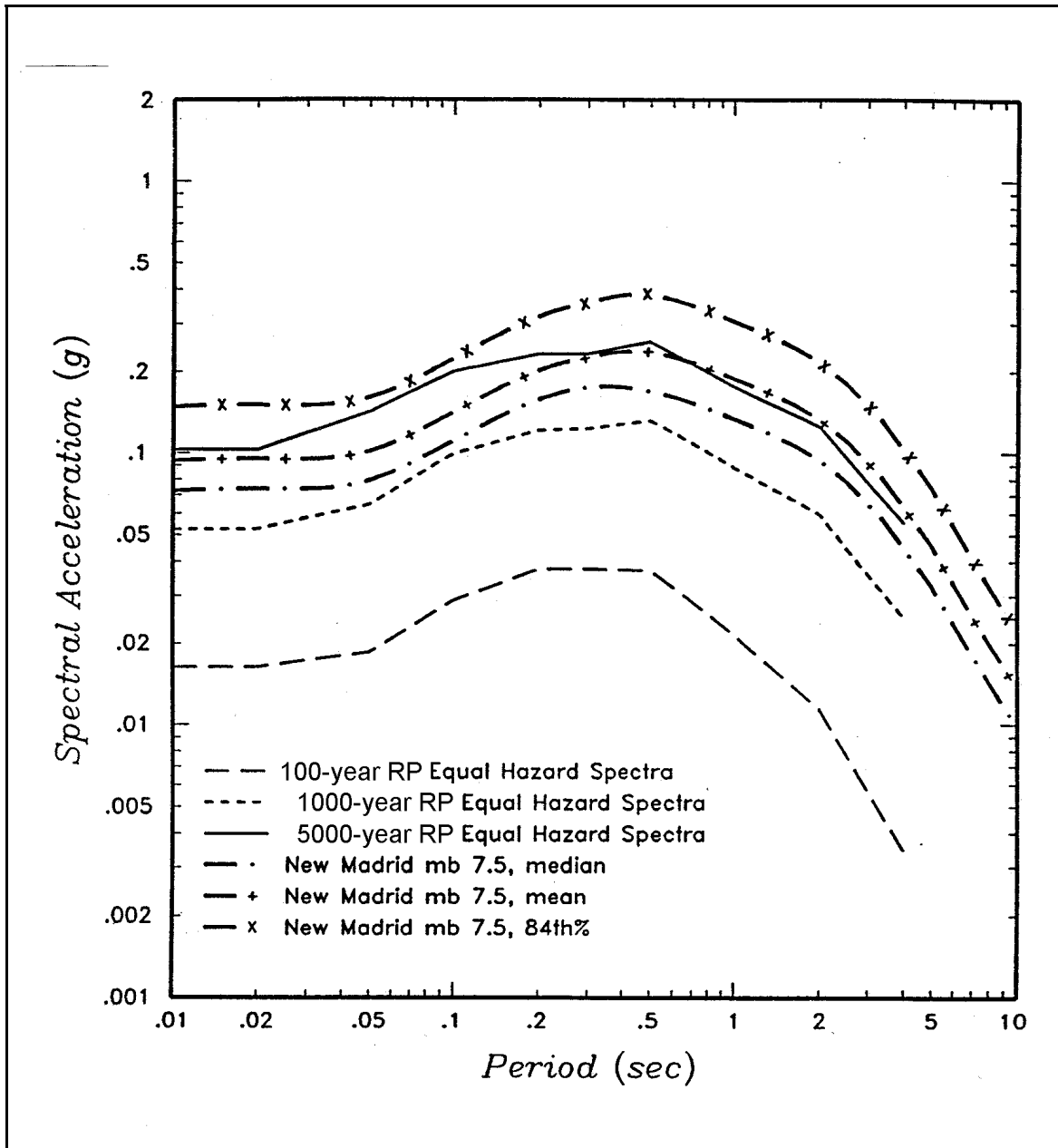


Figure G3-10. Comparison of deterministic ground motion spectra for the New Madrid seismic zone with the equal-hazard spectra from Figure G3-9 (5 percent damping)

sufficiently unlikely (ground motions in Figure G3-12 have return periods much longer than 5000 years) that it would be overly conservative to include this event as an MCE.

b. For this project, the following four design response spectra were selected from the probabilistic and deterministic results:

(1) Operating basis earthquake (OBE), having a 50 percent chance of exceedance in 100 years (corresponding return period of 144 years), which is defined by an equal hazard response spectrum for a 144-year return period.

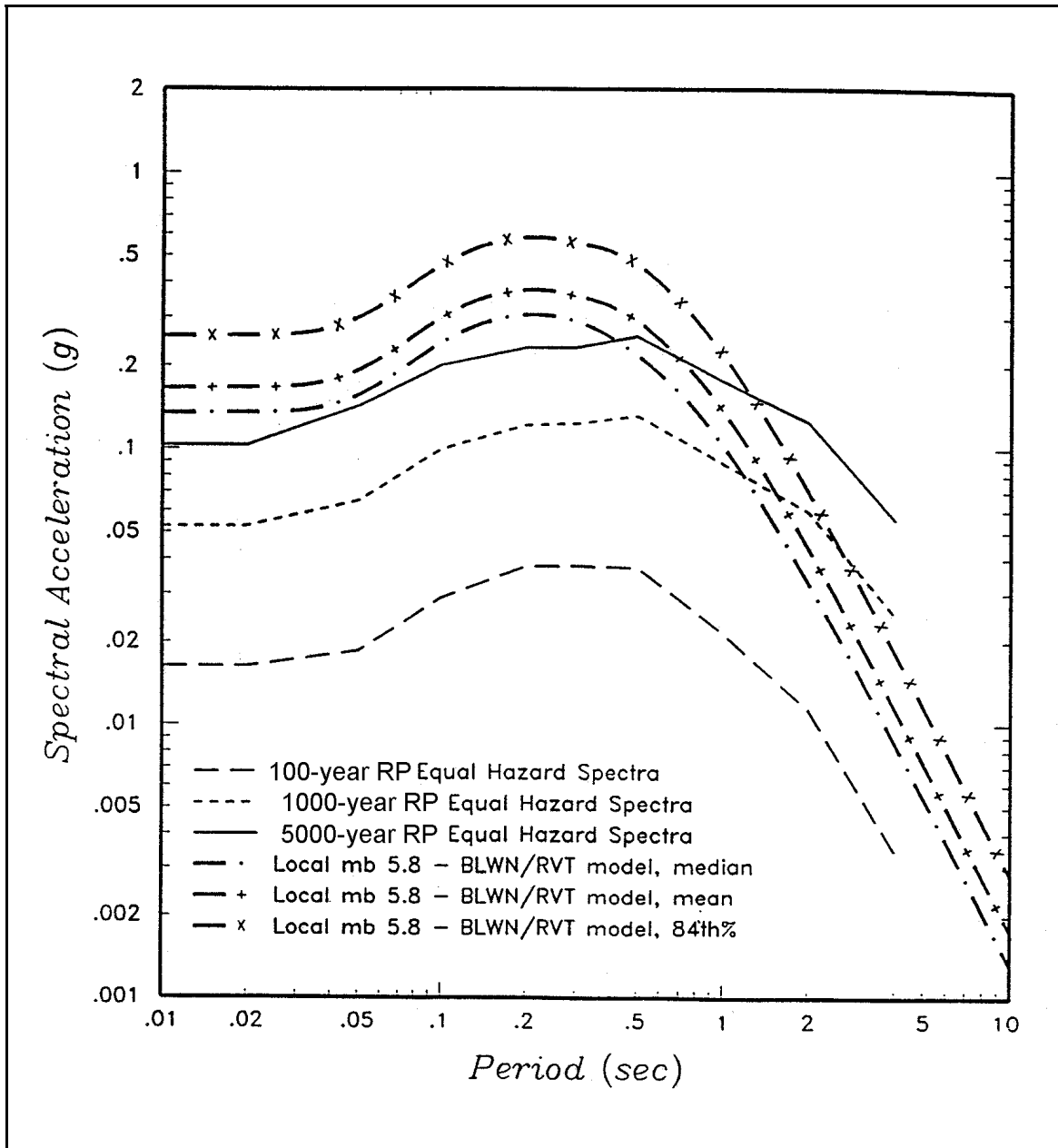


Figure G3-11. Comparison of deterministic ground motion spectra for the Ouachita fold belt source zone with the equal-hazard spectra from Figure G3-9 (5 percent damping)

(2) MDE having a 10 percent probability of exceedance in 100 years (corresponding return period of 950 years), which is defined by an equal hazard response spectrum for a 950-year return period.

(3) Maximum design earthquake (MDE) taken as the MCE on the New Madrid seismic zone at the closest approach to the site, defined by a mean response spectrum for the MCE as described in *a* above.

(4) MDE taken as the MCE on the Ouachita fold belt seismic zone at a 15-km distance from the site, defined by a mean response spectrum for the MCE as described in *a* above.

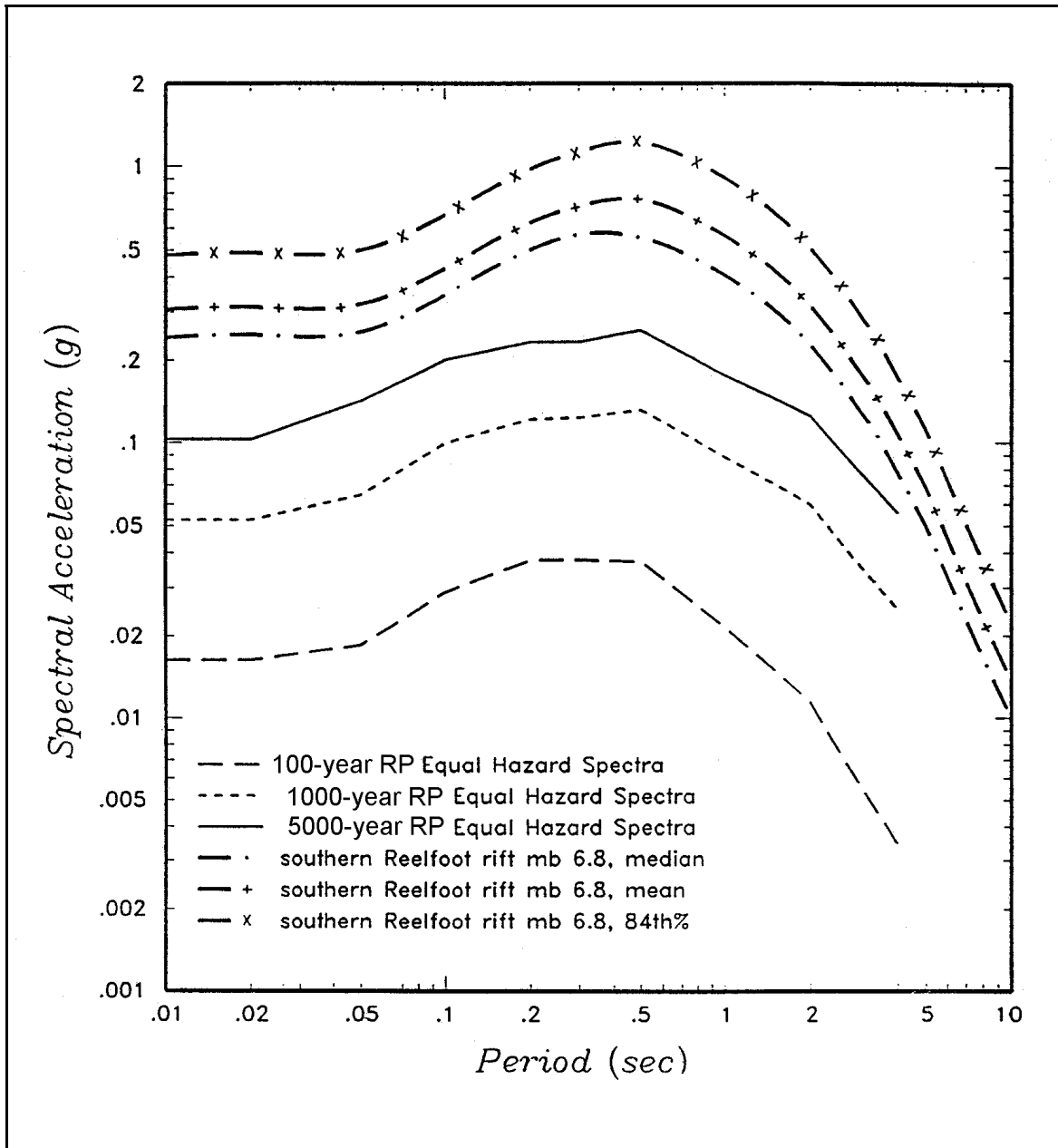


Figure G3-12. Comparison of deterministic ground motion spectra for the southern Reelfoot rift source zone with the equal-hazard spectra from Figure G3-9 (5 percent damping)

The OBE and MDE response spectra are shown in Figures G3-13 and G3-14, respectively. Figure G3-14 also compares the MDE with the spectra obtained using the effective PGA mapped for the site region and the spectral shapes defined in ATC 3-06 (Applied Technology Council 1978) or by the National Earthquake Hazards Reduction Program provisions (Building Seismic Safety Council 1994).

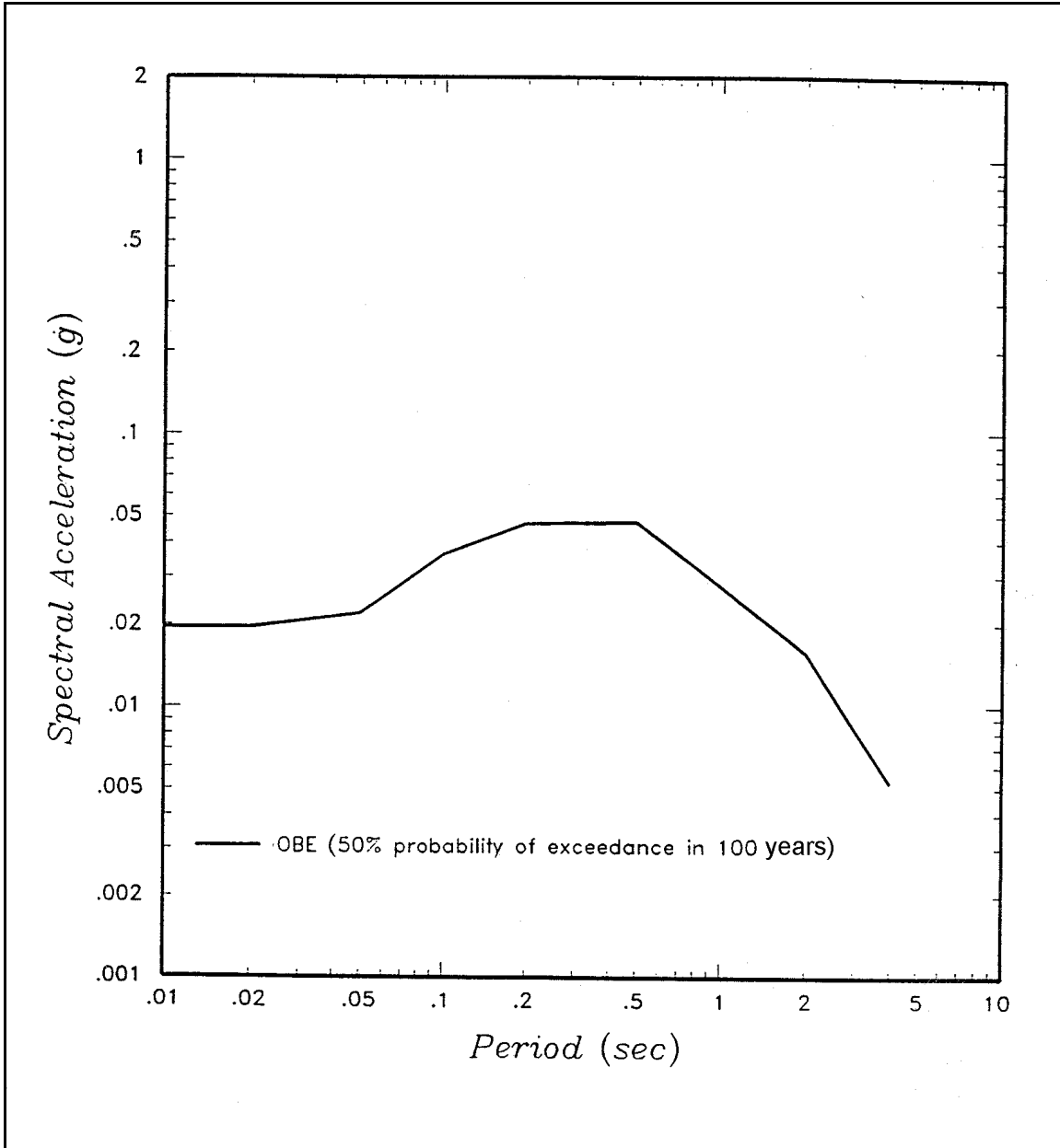


Figure G3-13. OBE spectrum (5 percent damping)

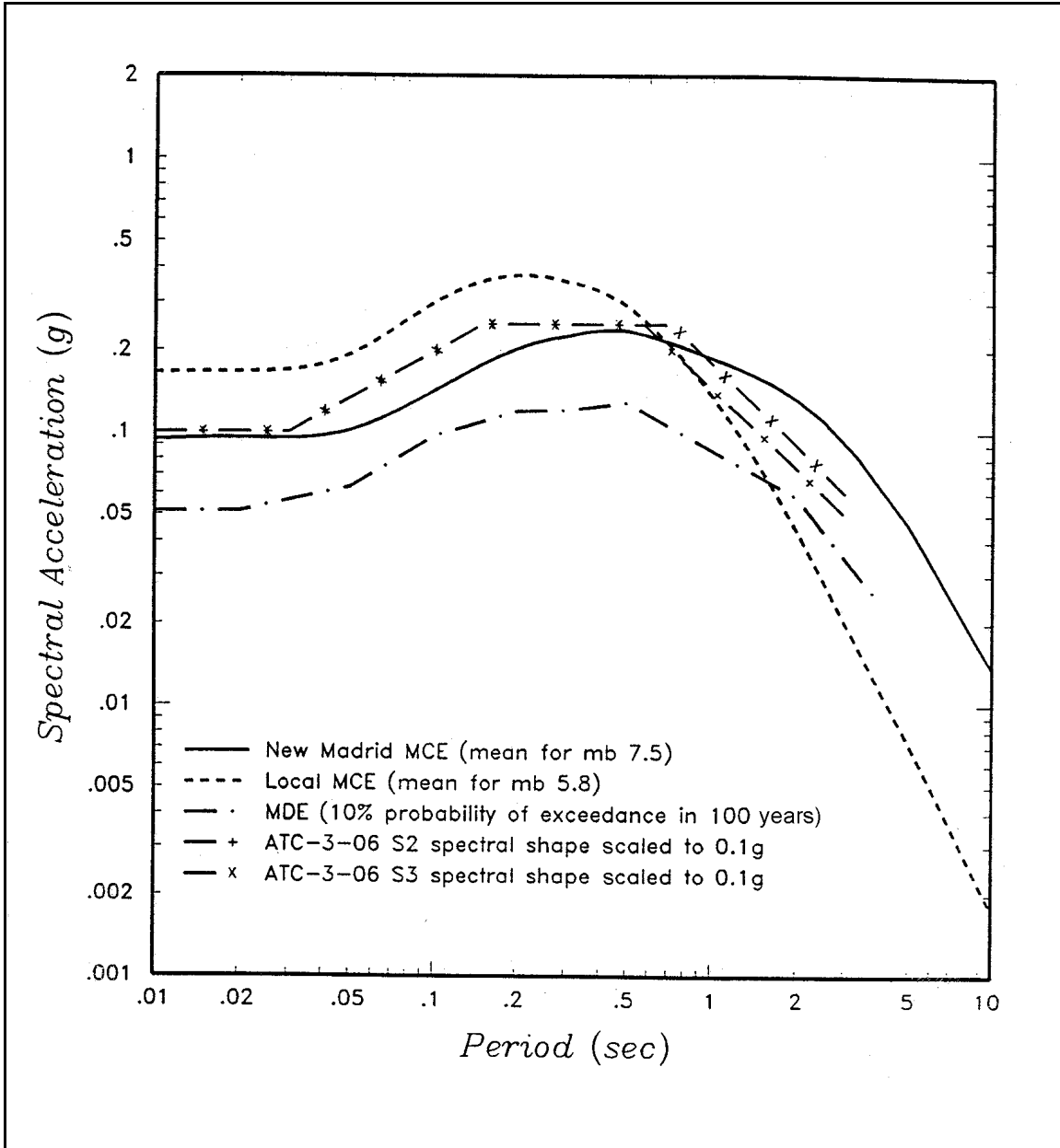


Figure G3-14. MDE spectra (5 percent damping)

Section IV
Example 4
Rock Site in Illinois

G4-1. Introduction

The site location, shown in Figure G4-1, is in southern Illinois on the Ohio River. For this site, equal-hazard response spectra of rock motions were developed for the MDE and OBE. The equal-hazard spectra are compared with deterministic response spectra for the MCE.

G4-2. Seismic Source Characterization

The dominant source zone for this site is the Iapetan Continental Rifts source zone (ICR), which represents an interconnected system of partially developed and failed continental rifts that lie within the midcontinent region of the United States. This zone includes the New Madrid source zone (NSZ), where the large 1811 and 1812 earthquakes occurred. The extent of ICR is shown by the heavy line in Figure G4-1 along with source zones outside ICR and the historical seismicity. Modeling of earthquake recurrence within the dominant ICR can be summarized as follows:

a. The recurrence rate for large (1811-1812 type) earthquakes in NSZ is modeled based on paleoseismic evidence. As shown in Figure G4-2, the paleoseismic-determined rate of these earthquakes exceeds the rate of large earthquakes predicted from the historical seismicity.

b. The recurrence rate for smaller earthquakes in ICR is determined by the historical seismicity. Two basic models are used within a logic tree framework for defining subzones for characterizing recurrence within ICR: a seismicity-based model (given a weight of 0.25) and a geology-based model (given a weight of 0.75). The seismicity-based model divides ICR into cells of one-half degree latitude and longitude and calculates recurrence rates based on the historical seismicity in the cell. Different degrees of smoothing of seismicity rates and b-values among adjacent cells are accomplished using the methodology developed by EPRI (1987). In the geology-based model, Zone ICR is divided into subzones as indicated in Figure G4-1. Different combinations of subzones are defined in a logic tree approach. The possible combinations are controlled in part by the presence or absence of four possible tectonic boundaries within the ICR (Figure G4-1) and the assessed likelihood that these features represent fundamental boundaries that control the distribution, rate, and maximum magnitudes of seismicity. The logic tree for weights assigned to these boundaries is shown in Figure G4-3. Thirty alternative subzonations (not shown herein) of ICR result from the logic tree of Figure G4-3. Within each subzone of each alternative, seismicity rates are determined based on the seismicity within the subzone and assuming the rate is uniform within the subzone.

Probabilistic distributions of maximum earthquake magnitudes are also part of the source model logic tree. These probabilistic distributions were determined using the methodology developed by EPRI (Johnston et al. 1994). This methodology used worldwide databases to assess maximum earthquake magnitudes in stable continental regions (like the eastern United States) where active faults have not been identified and therefore maximum magnitude cannot be estimated on the basis of fault dimensions (as is done in the western United States). However, for the New Madrid zone, maximum earthquake magnitudes were estimated on the basis of both estimated rupture models by Johnston (1996) and Gomberg and Ellis (1994) and correlations of magnitude with rupture dimensions; and estimates of magnitudes of the 1811-1812 earthquakes by Johnston (1996).

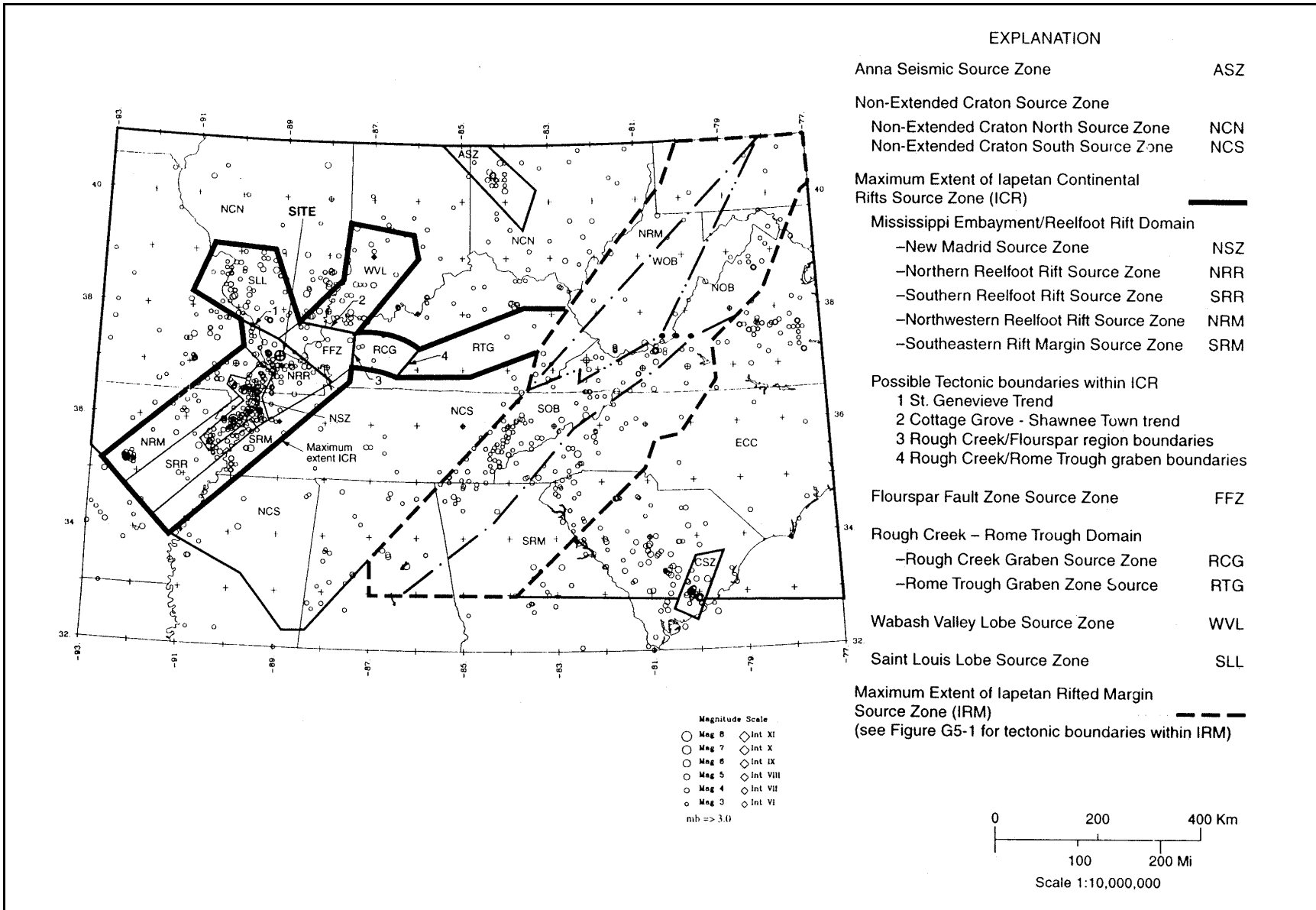


Figure G4-1. Seismic source zonation model of central and southeastern United States, rock site in Illinois

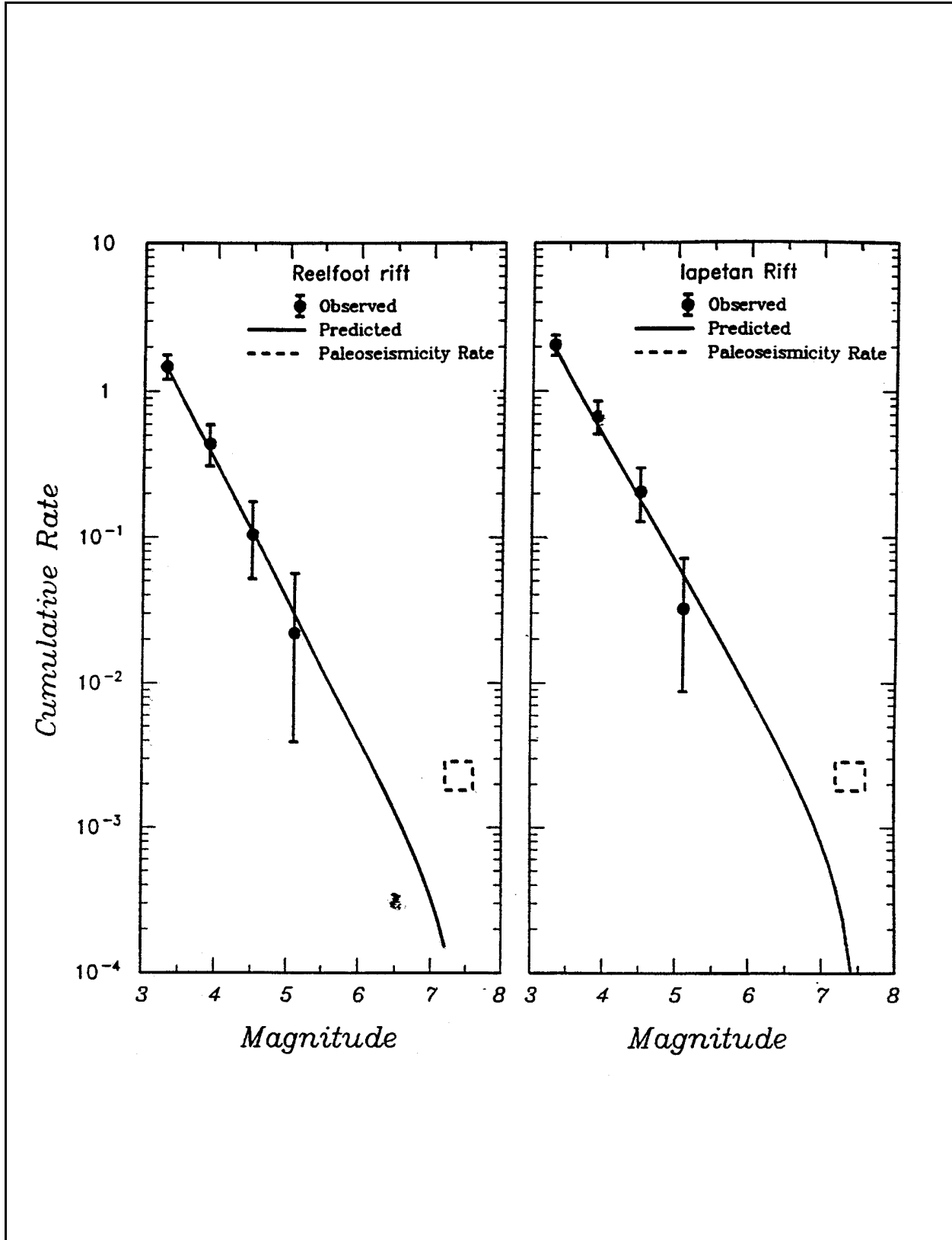


Figure G4-2. Comparison of historical and paleoseismic recurrence estimates for the Reelfoot Rift and Iapetan Rift seismic zone

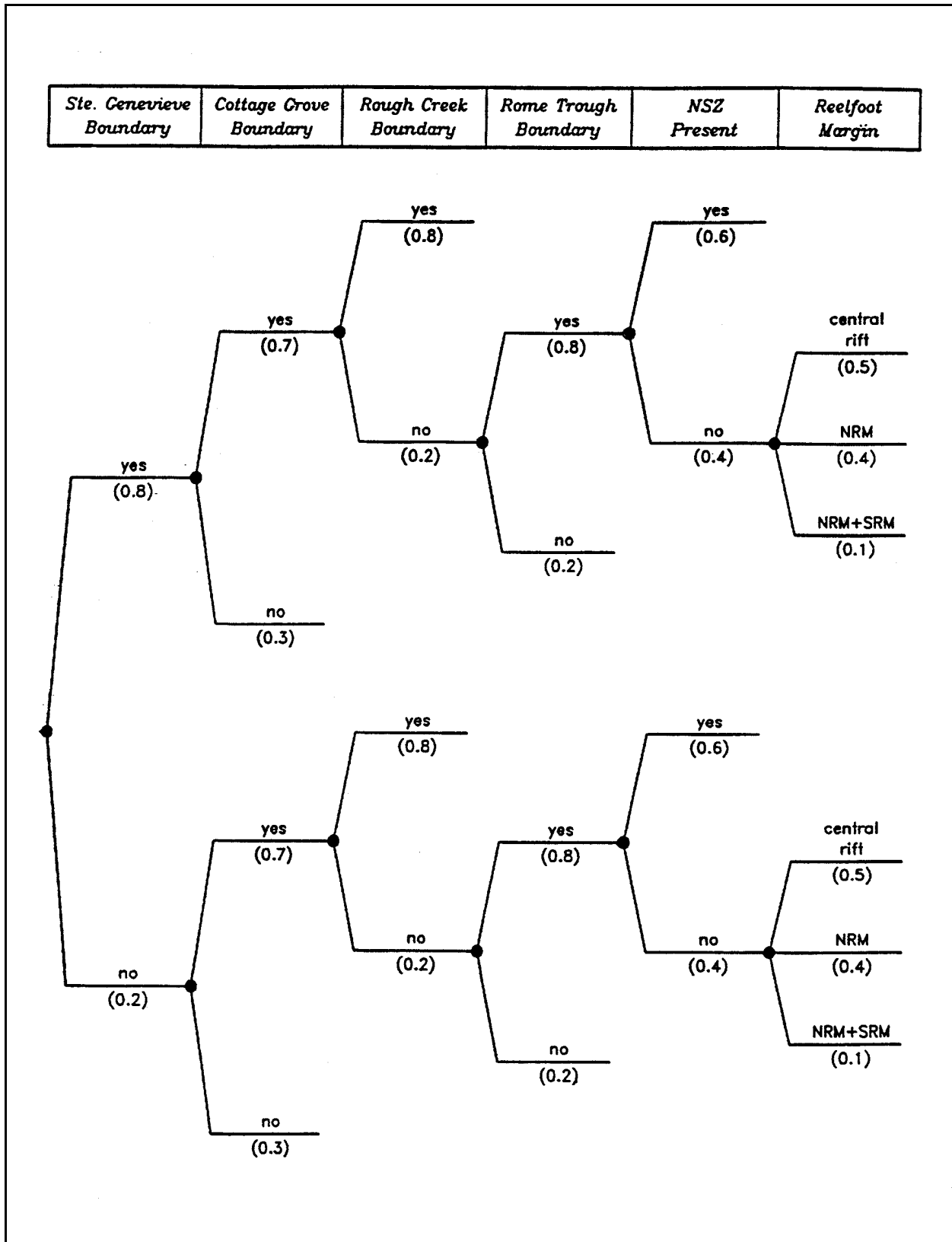


Figure G4-3. Logic tree showing relative weights assigned to boundaries separating potential subzones of the Iapetan Rift seismic zone

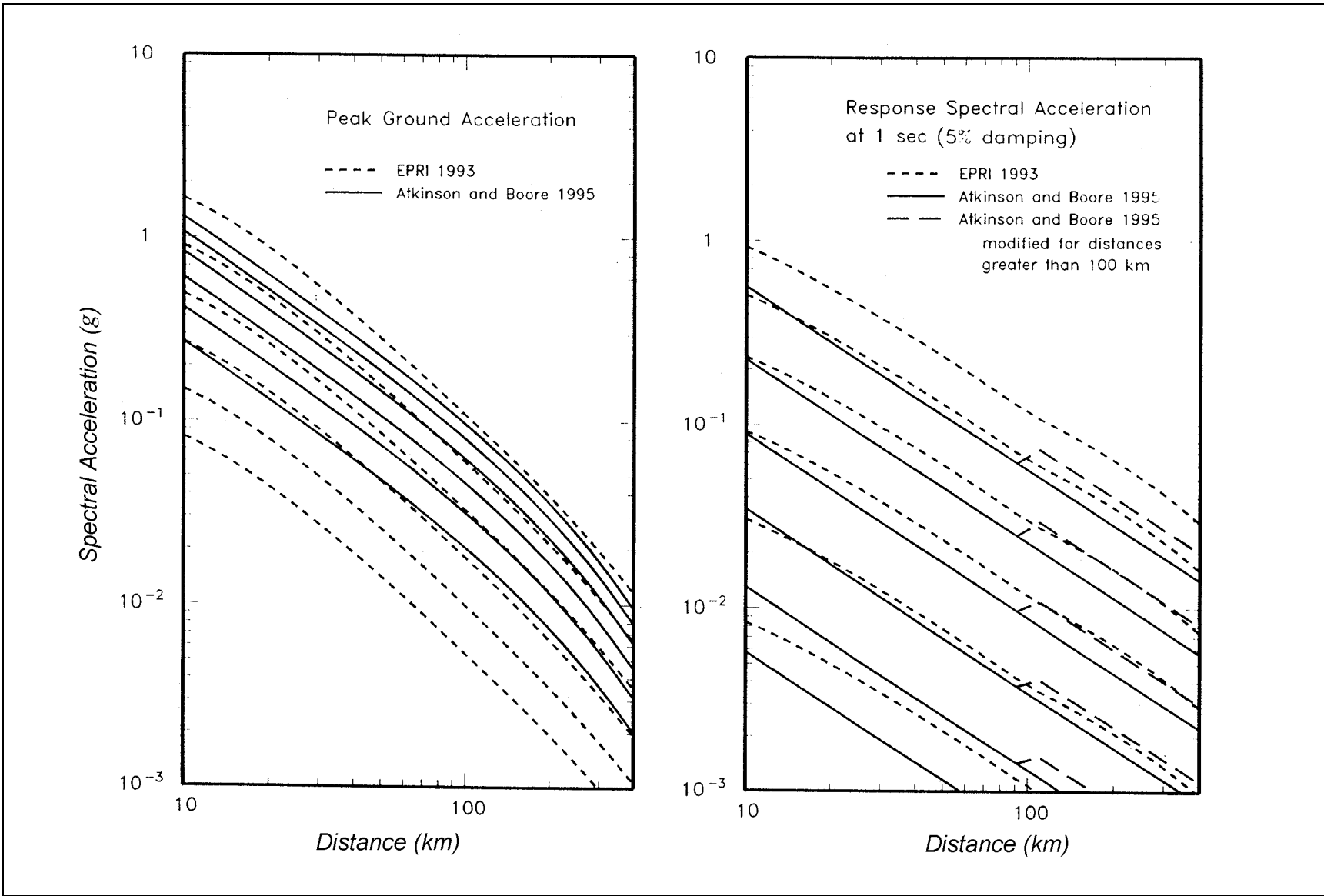


Figure G4-4. Attenuation curves of Atkinson and Boore (1995) and EPRI (1993) for peak ground acceleration and response spectral acceleration at 1.0-sec period. Note: Lowest curve for each relationship is for m_b 5.0; highest curve, for m_b 7.5

G4-3. Ground Motion Attenuation Characterization

a. It was desired to estimate ground motions on rock at the site. Two attenuation relationships applicable to hard rock in the eastern United States for horizontal peak ground acceleration and response spectral accelerations of ground motions at different periods of vibration were used. The relationships are those of EPRI (1993) (later published as Toro, Abrahamson, and Schneider 1997, see Tables 3-1 and 3-3, main text) and Atkinson and Boore (1995) (later published as Atkinson and Boore 1997, see Tables 3-1 and 3-3, main text).

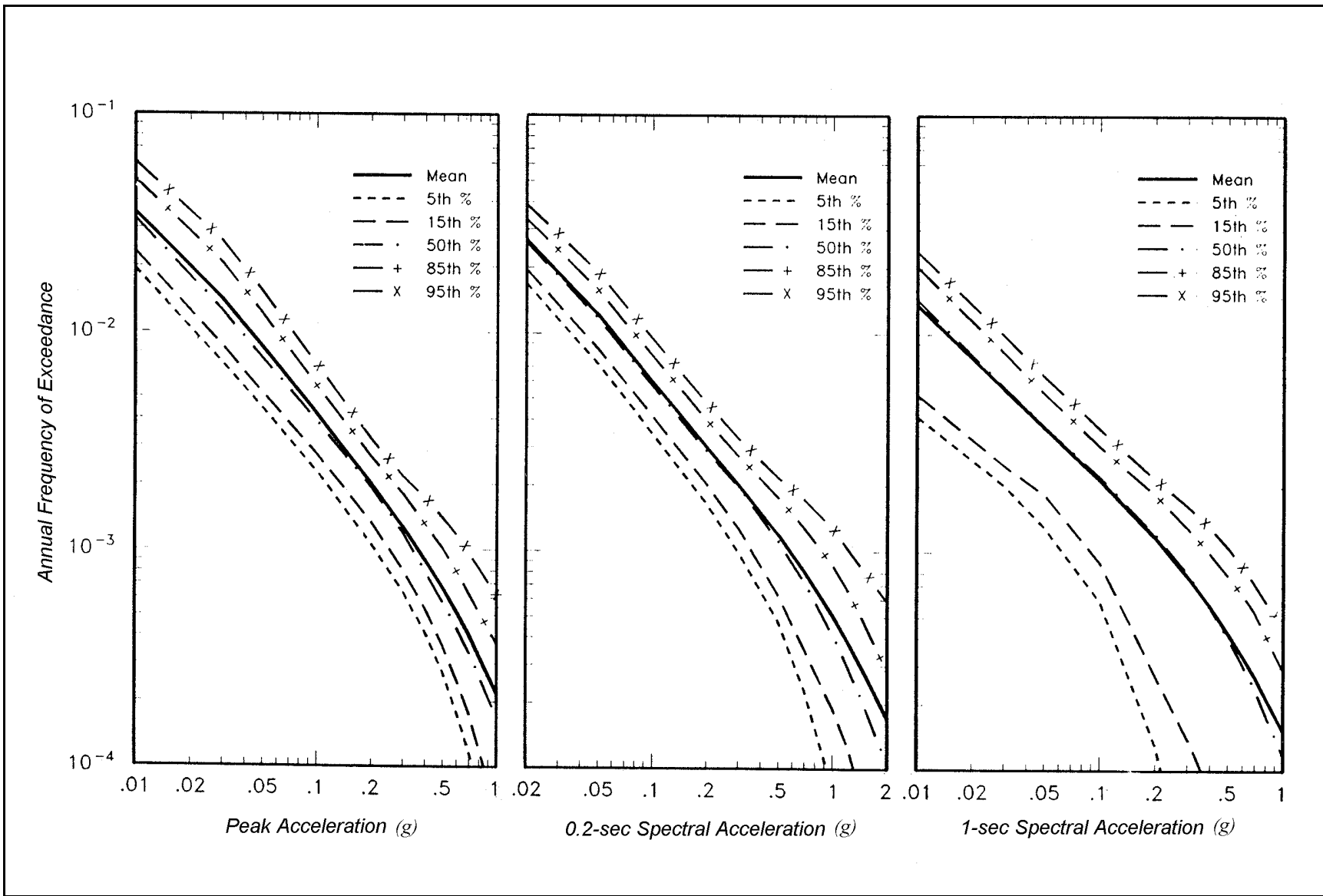
b. The relationship for response spectral acceleration of EPRI extends to periods as long as 1 sec, and that of Atkinson and Boore extends to a period of 2 sec. The EPRI relationship was extrapolated to a period of 2 sec. This was accomplished by extrapolating the coefficients of the attenuation relationship and examining the reasonableness of the resulting spectral prediction. The smooth quadratic form of the relationship of Atkinson and Boore (1995) underestimates their simulations of longer period ground motions at distances beyond 100 km. Therefore, their relationships were modified at periods greater than 0.5 sec to result in ground motion estimates closer to the simulation results.

c. Plots of the attenuation relationships of EPRI (1993) and Atkinson and Boore (1995) for peak ground acceleration and response spectral accelerations at 1.0 sec are presented in Figure G4-4. The modifications to the 1-sec motion at distances greater than 100 km can be seen in the figure. The plots in Figure G4-4 clearly indicate the distinctive differences between the two eastern United States attenuation relationships: the Atkinson and Boore (1995) relationships result in higher spectral values than those of EPRI (1993) for peak ground acceleration and for short-period response spectral accelerations (less than about 0.2-sec period), but lower values than those of EPRI (1993) at longer periods.

d. In the hazard analysis, the relationship of EPRI (1993) was given a higher weight (0.67) than that of Atkinson and Boore (1995) (0.33). The reason for this judgment was that the EPRI (1993) relationship resulted from an EPRI study that involved input from a number of ground motion experts and thus could be viewed as having achieved a certain degree of consensus regarding the model. The practical effect of higher weighting on the EPRI (1993) model is to increase longer period ground motions and reduce short-period ground motions.

G4-4. PSHA Results

Hazard curves obtained from the analysis for peak ground acceleration and response spectral acceleration at two periods of vibration are shown in Figure G4-5. The uncertainty bands around the mean curves, reflecting the alternative seismic source models and attenuation relationships incorporated into the logic tree, are shown in the figure. The contributions to the hazard are almost entirely from Zone ICR. Figure G4-6 shows contributions within ICR from large New Madrid Zone earthquakes with rates defined by paleoseismic data (dashed-dotted line) and smaller earthquakes defined by seismicity (dashed line). It can be seen that the smaller earthquakes dominate hazard at higher frequencies (probabilities) of exceedance and the larger, 1811-1812-type earthquakes dominate at lower frequencies (probabilities) of exceedance. Figure G4-7 compares the hazard obtained from geology-based and seismicity-based models. It can be seen that, for this site, the two modeling approaches lead to almost identical results. Equal-hazard response spectra obtained from the mean hazard results for all the periods of vibration analyzed are shown in Figure G4-8 for return periods varying from 144 to 10,000 years.



G-55

Figure G4-5. Computed hazard for peak ground acceleration and response spectral accelerations at 0.2- and 1.0-sec periods (5 percent damping total hazard curves)

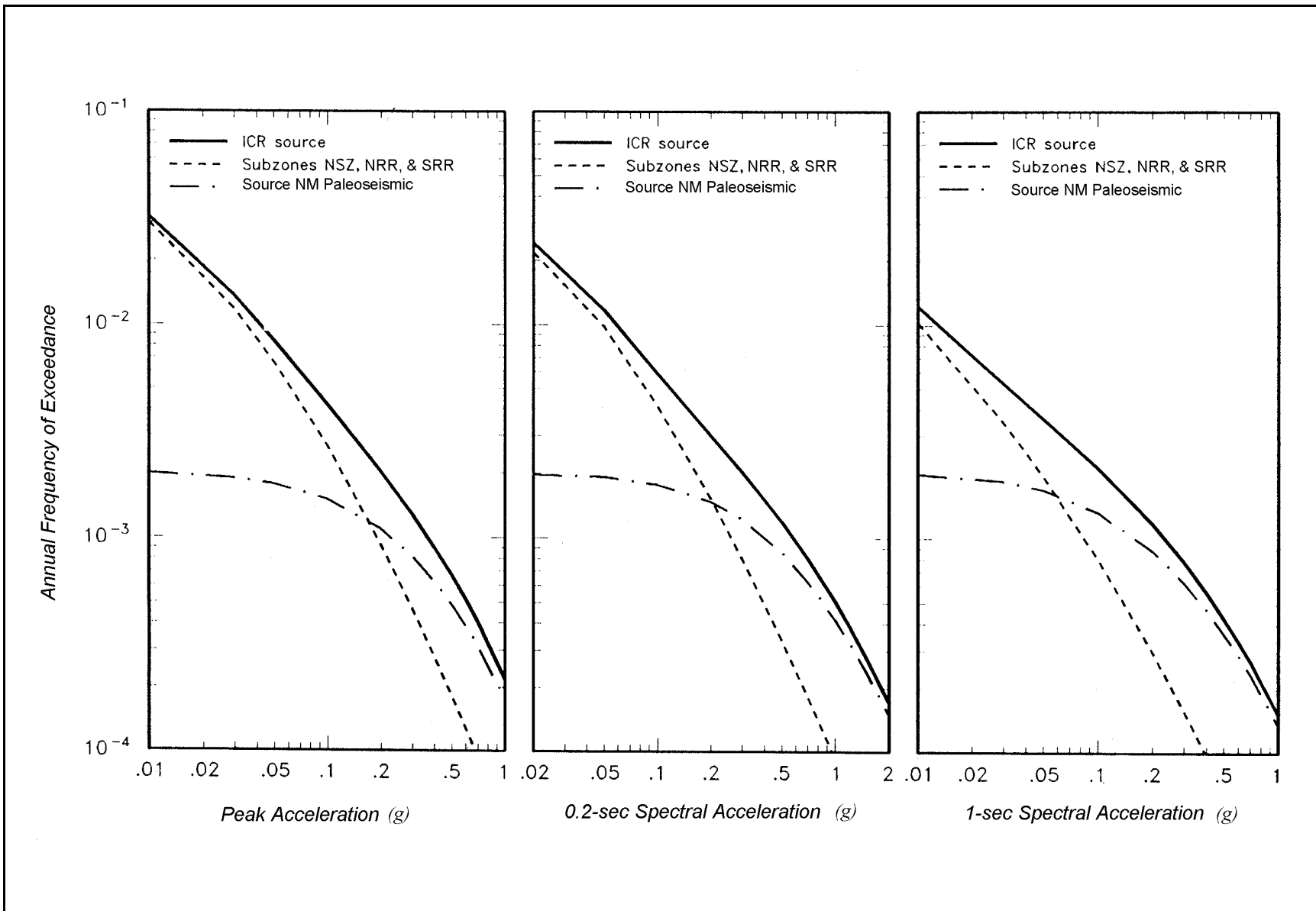


Figure G4-6. Contributions of components of the ICR source to the hazard at 5 percent damping

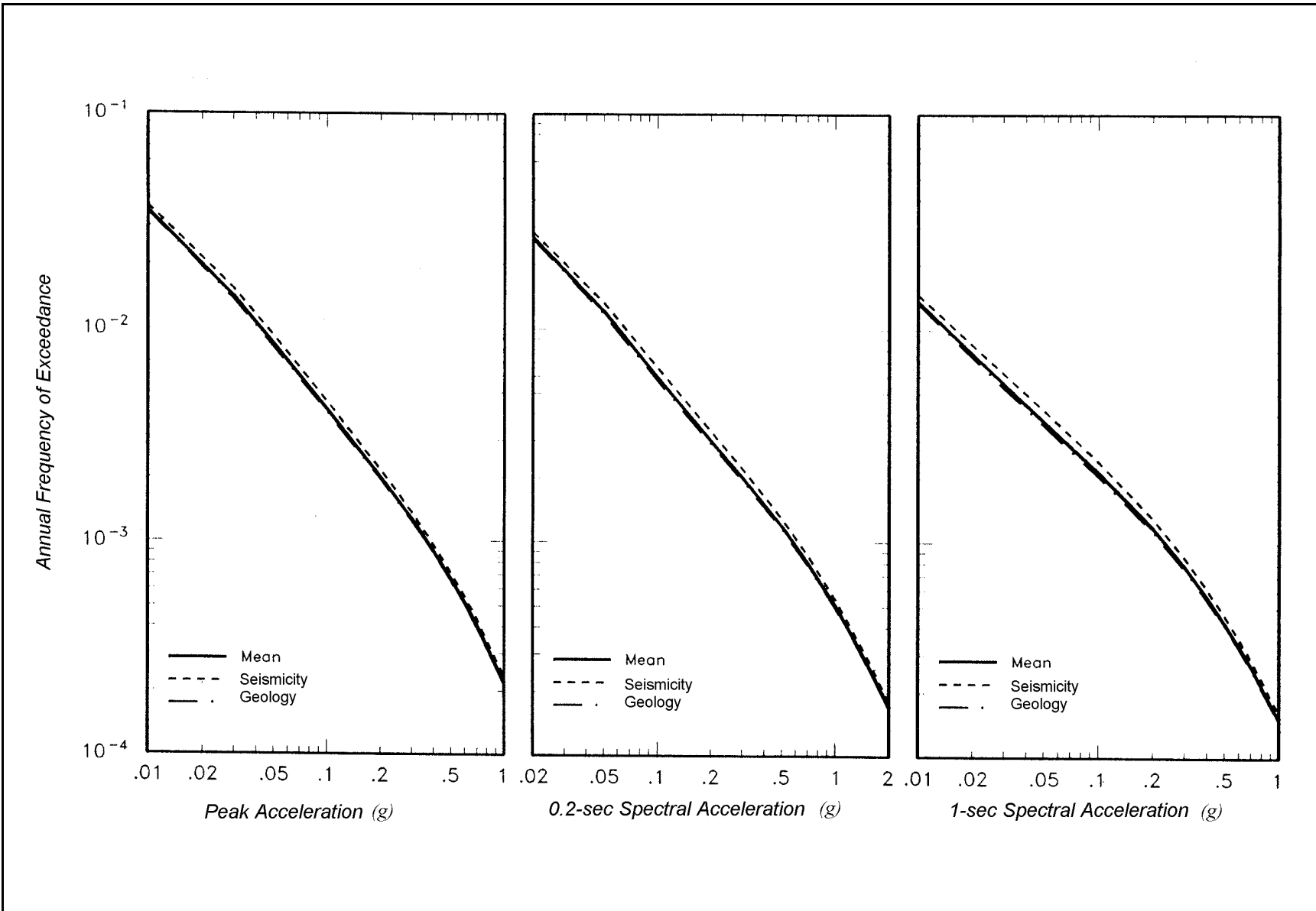


Figure G4-7. Comparisons of hazard from the geology- and seismicity-based models at 5 percent damping

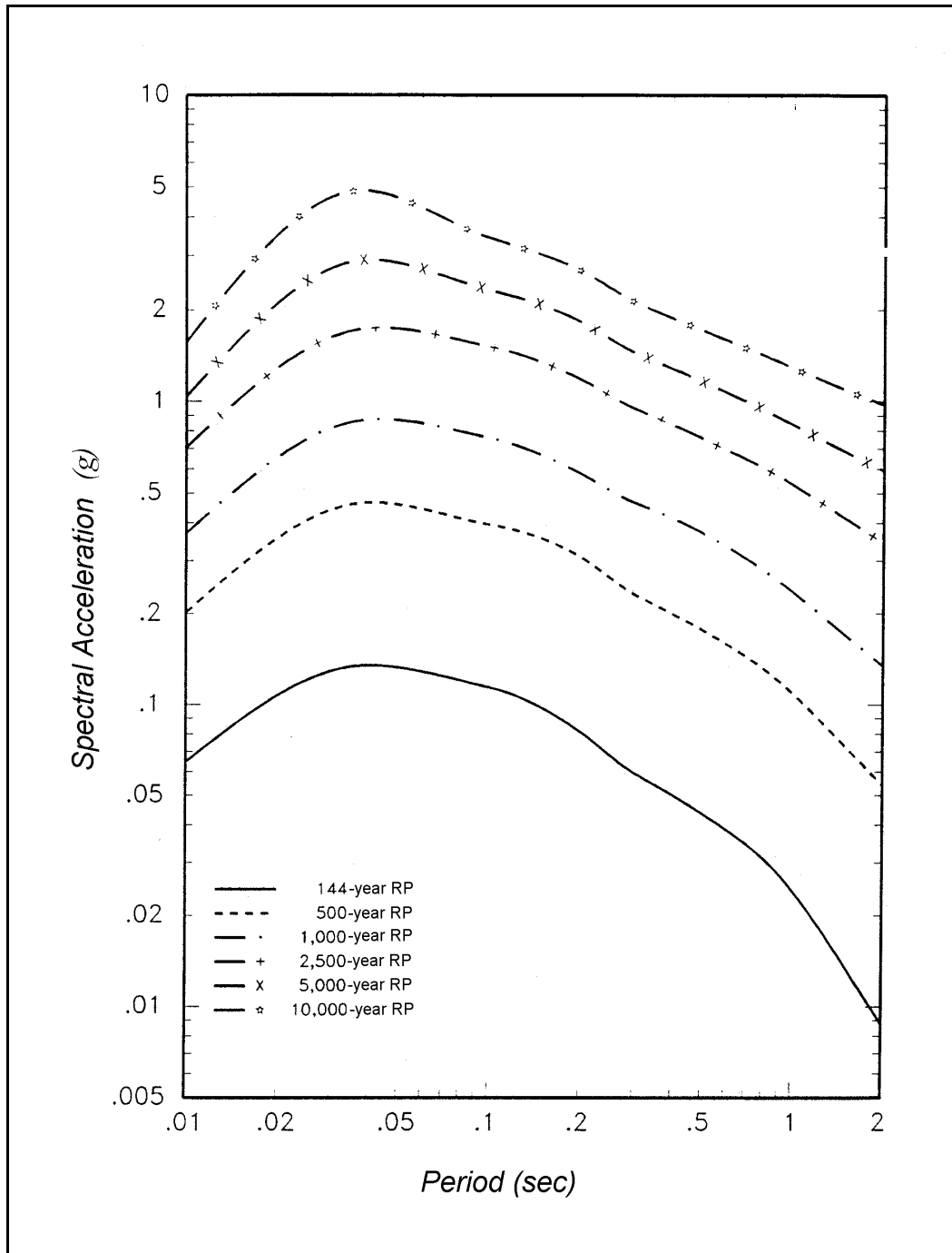


Figure G4-8. Equal-hazard response spectra (5 percent damping)

G4-5. Comparison of Deterministic and Probabilistic Results

a. The probabilistic equal-hazard spectra of rock motions at this site were compared with deterministic spectra of rock motions at the site for an MCE occurring on the closest approach of the New Madrid source. The maximum event assigned to this source ranged from m_b 7.0 to 8.0 with a mean value of m_b 7.5. The closest approach of this source to the site is 30 km. Deterministic response spectra for the

New Madrid source were computed using the attenuation models selected for the PSHA and the distribution of maximum magnitudes developed for the New Madrid source. Figure G4-9 compares median (50th percentile) and 84th percentile deterministic response spectra for this event with the equal-hazard spectra presented in Figure G4-8. The median deterministic spectrum corresponds to ground motions with a return period between 1000 and 2500 years, and the 84th percentile deterministic spectrum corresponds to ground motions with a return period of about 5000 years.

b. For this project, the equal-hazard response spectrum with a 144-year return period (50 percent probability of exceedance in 100 years) was selected as the OBE ground motion. The MDE ground motion was selected as the equal-hazard response spectrum having a 1000-year return period (approximate 10 percent probability of exceedance in 100 years).

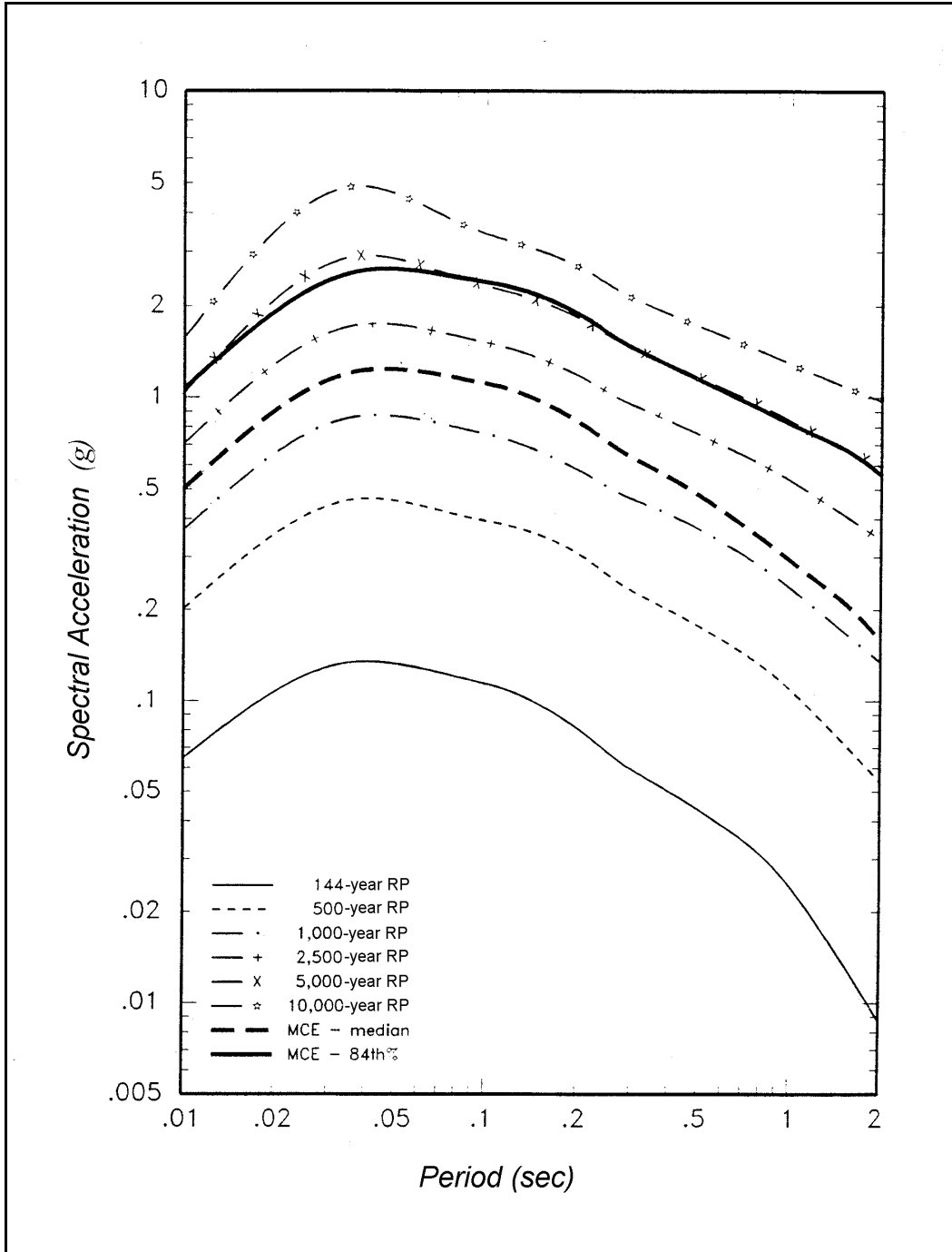


Figure G4-9. Comparison of equal-hazard and deterministic response spectra (5 percent damping)

Section V
Example 5
Rock Site in West Virginia

G5-1. Introduction

The site is located in south-central West Virginia (Figure G5-1). For this site, equal-hazard response spectra were developed for the MDE and OBE. The equal-hazard spectra are compared with the deterministic response spectrum for the MCE.

G5-2. Seismic Source Characterization

a. The site is in an area of low seismicity (Figure G5-1). Two source zones dominate the seismic hazard at the site: the ICR, which is described in Example G4; and the Iapetan Rifted Margin source zone (IRM), in which the site is located (Figure G5-1). The IRM is defined by the known or inferred presence of large normal faults formed along the passive margin of the late Proterozoic to early Paleozoic Iapetus Ocean. Compressional reactivation of favorably oriented Iapetan faults has been suggested as the causal mechanism for several seismically active regions in eastern North America. The extent of the IRM is shown by the heavy black line in Figure G5-1. Source zones outside IRM and ICR are also shown in the figure.

b. Modeling of earthquake recurrence rates within source zone ICR is described in Example G4. A similar approach to recurrence modeling was taken for source zone IRM, except that paleoseismic data are not available to supplement seismicity data for IRM.

c. As was done for ICR, two basic models were used within a logic tree framework to define subzones for characterizing recurrence within IRM: a seismicity-based model (given a weight of 0.25) and a geology-based model (given a weight 0.75). The seismicity-based model divides IRM into cells of one-half degree latitude and longitude and calculates recurrence rates based on the historical seismicity in the cell. Different degrees of smoothing of seismicity rates and b-values among adjacent cells are accomplished using the methodology developed by EPRI (1987). In the geology-based model, Zone IRM is divided into subzones as indicated in Figure G5-1. Different combinations of subzones are defined in a logic tree approach. The possible combinations are controlled by the presence or absence of three possible tectonic boundaries within IRM (Figure G5-1) and the assessed likelihood that these features represent fundamental boundaries that control the distribution, rate, and maximum magnitudes of seismicity. The logic tree for weights assigned to these boundaries is shown in Figure G5-2. Five alternative subzonations (not shown herein) of IRM result from the logic tree of Figure G5-2. Within each subzone of each alternative, seismicity rates are determined based on the seismicity within the subzone and assuming the rate is uniform within the subzone.

d. Probabilistic distributions of maximum earthquake magnitudes are also part of the source model logic tree. These probabilistic distributions were determined using the methodology developed by EPRI (Johnston et al. 1994). As discussed in paragraph G4-2, this methodology used worldwide databases to assess maximum earthquake magnitudes in stable continental regions (like the eastern United States) where active faults have not been identified and therefore maximum magnitudes cannot be estimated on the basis of fault dimensions (as is done in the western United States).

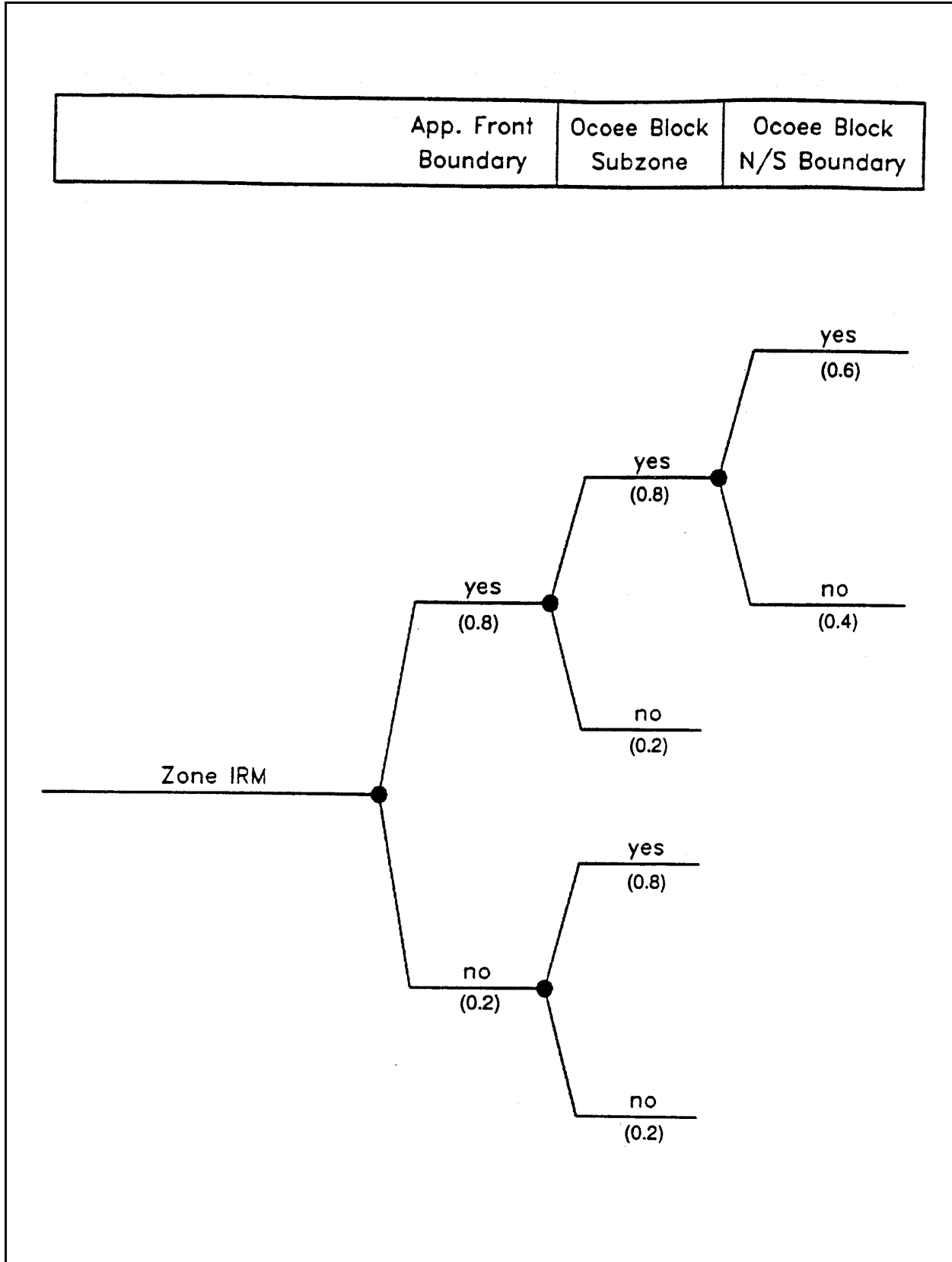


Figure G5-2. Seismic source model logic tree for Zone IRM

G5-3. Ground Motion Attenuation Characterization

It was desired to estimate ground motions on rock at the site. Two attenuation relationships applicable to hard rock in the eastern United States for horizontal peak ground acceleration and response spectral acceleration of ground motions at different periods of vibration were used. These relationships are the same as those used for Example G4, including the relative weighting given to the relationships. The relationships are described in Section G4-3 and illustrated in Figure G4-4. An adjustment to these relationships was made to account for somewhat softer rock at the site than the hard rock applicable to the attenuation relationships. The adjustment was made by analyzing the rock crustal structure using the stochastic ground motion model of Boore (1983, 1986). The adjustments were a maximum spectral amplification of 1.2 times at periods greater than 0.1 sec, a maximum spectral deamplification of 0.8 time at periods less than 0.1 sec, and 1.0 at zero period (taken to be 0.01-sec period).

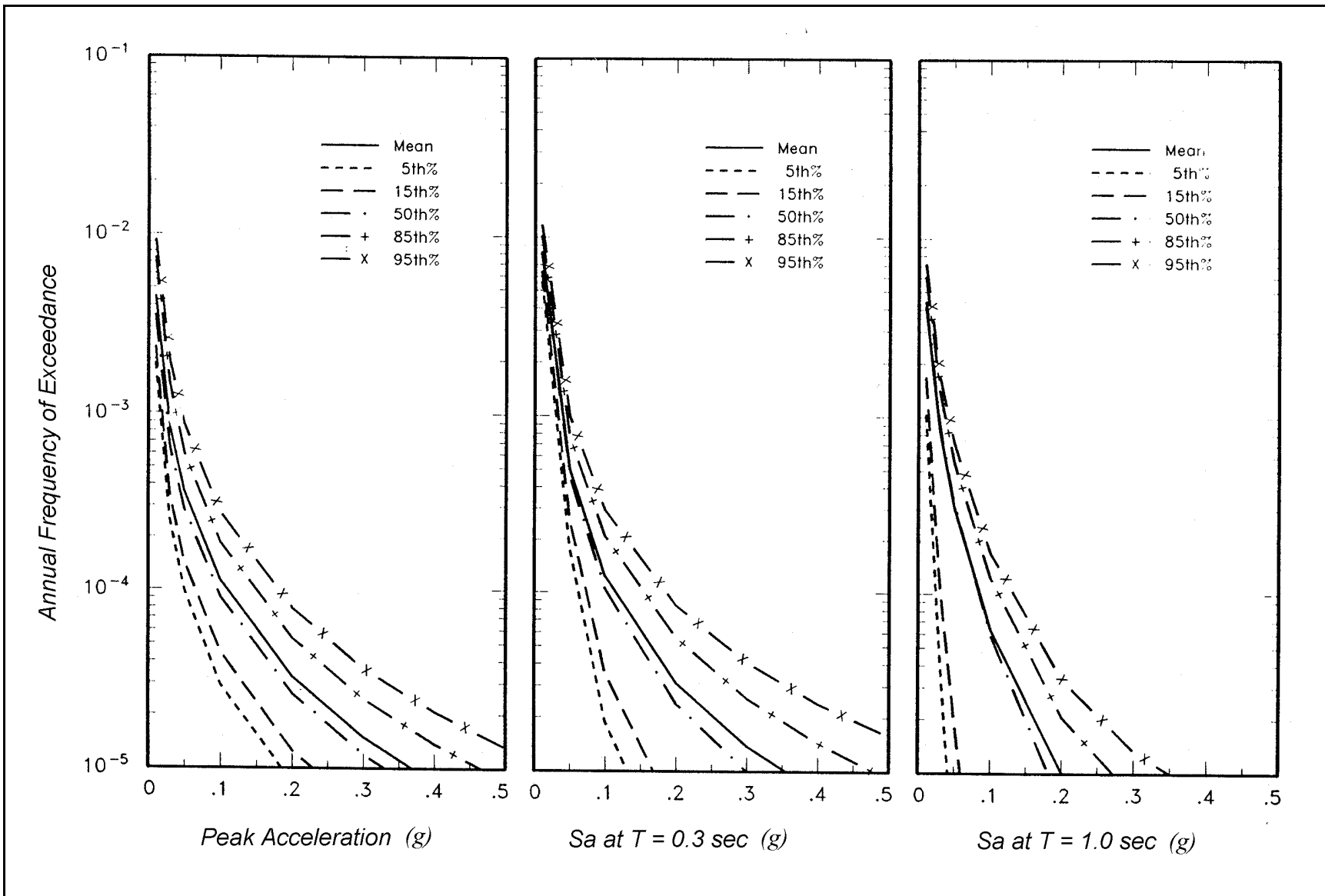
G5-4. PSHA Results

a. Hazard curves obtained from the analysis for peak ground acceleration and response spectral acceleration at two periods of vibration are shown in Figure G5-3. The uncertainty bands around the mean curves, reflecting the alternative seismic source models and attenuation relationships incorporated into the logic tree, are shown in the figure. The contributions to the hazard from different source zones for peak ground acceleration, spectral acceleration at 0.3 sec, and spectral acceleration at 1.0 sec are shown in Figure G5-4. As can be seen, for peak ground acceleration, source zone IRM dominates the hazard. With increasing period of vibration, source zone ICR contributes relatively more to the hazard and is the dominant contributor at a period of 1.0 sec. Earthquake magnitude and distance contributions to the hazard for peak ground acceleration and 1.0-sec response spectral acceleration for a return period of 1000 years are shown in Figure G5-5. For peak ground acceleration, most of the hazard comes from m_b 5 to 6 earthquakes occurring within 200 km of the site (within IRM). However, for 1.0-sec spectral acceleration, the hazard is dominated by m_b 7 to 8 earthquakes occurring at distances greater than 200 km (in the New Madrid zone). Similar to the results for Example G4, the geology-based and seismicity-based models for zone IRM give practically identical results (this result will not necessarily be obtained at other sites, however).

b. Equal-hazard response spectra obtained from the hazard results for all the periods of vibration analyzed are shown in Figure G5-6 for mean hazard results and in G5-7 for the 95th percentile of the hazard distribution (Figure G5-3). The equal-hazard spectra are relatively flat because of the long-period contribution to the hazard by source zone ICR.

G5-5. Comparison of Deterministic and Probabilistic Results

a. The probabilistic equal-hazard spectra of rock motions at the site were compared with the median deterministic spectrum of rock motions at the site for an MCE occurring within zone IRM in which the site is located. The deterministic response spectrum was determined from a statistical random earthquake analysis for the occurrence of an MCE within a radius of 25 km from the site. The distribution for the earthquake magnitude of the MCE that was developed for the PSHA was used for this analysis. The mean value of maximum magnitude from this distribution was m_b 6.3. The random earthquake analysis carried out for the site is described in paragraph D-3. Figures G5-8 and G5-9, respectively, compare the deterministic MCE response spectrum with the mean and 95th percentile equal hazard spectra. These comparisons indicate that the deterministic MCE ground motions correspond to ground motions with very long return period for periods of vibration equal to or less than about 1 sec. At periods increasingly longer than 1 sec, the return period associated with the MCE spectrum progressively decreases. This



G-65

Figure G5-3. Computed rock hazard curves for peak ground acceleration and response spectral acceleration at periods of 0.3 and 1 sec and 5 percent damping

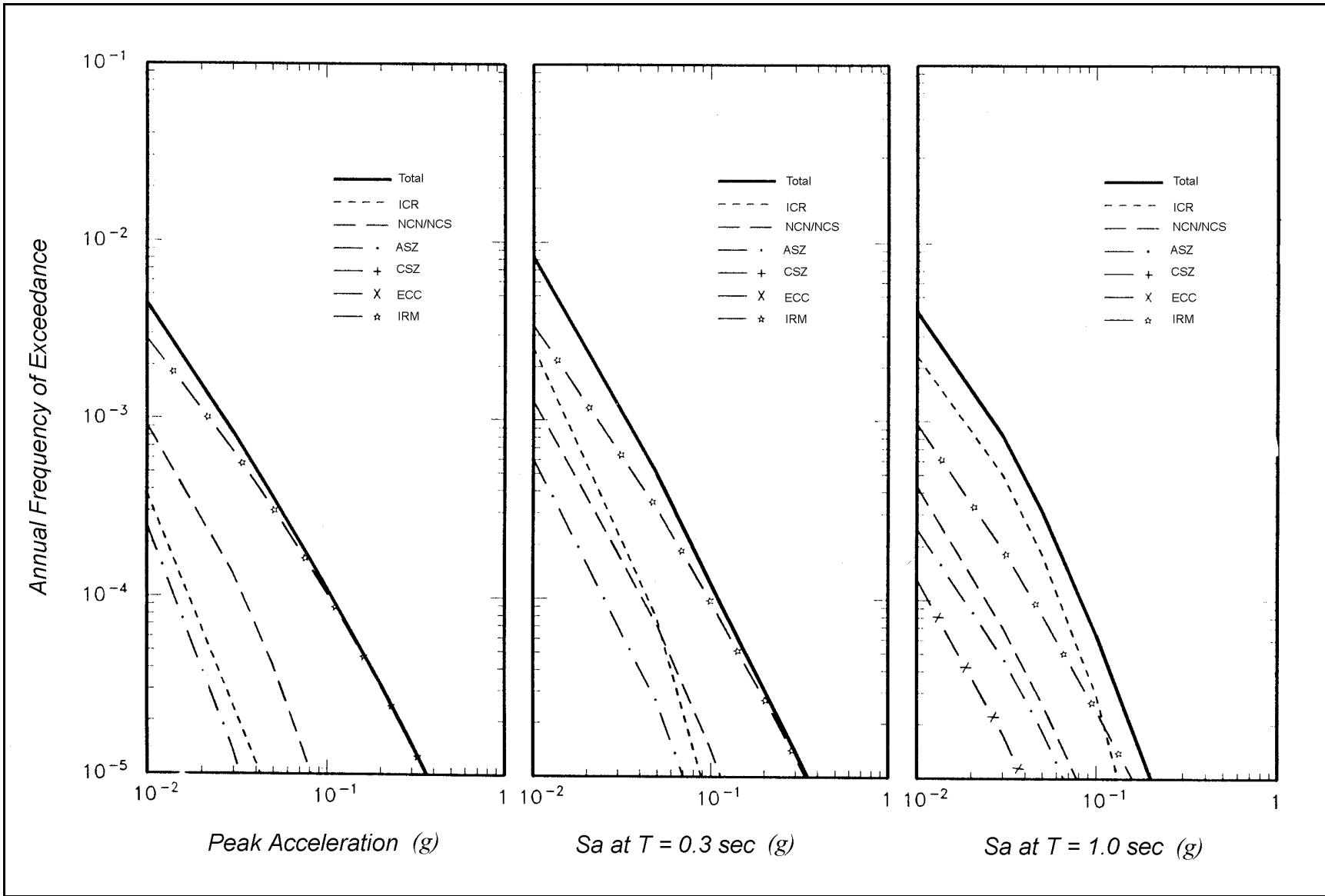


Figure G5-4. Source contributions to hazard for peak ground acceleration and spectral accelerations at periods of 0.3 and 1 sec, rock hazard curves at 5 percent damping

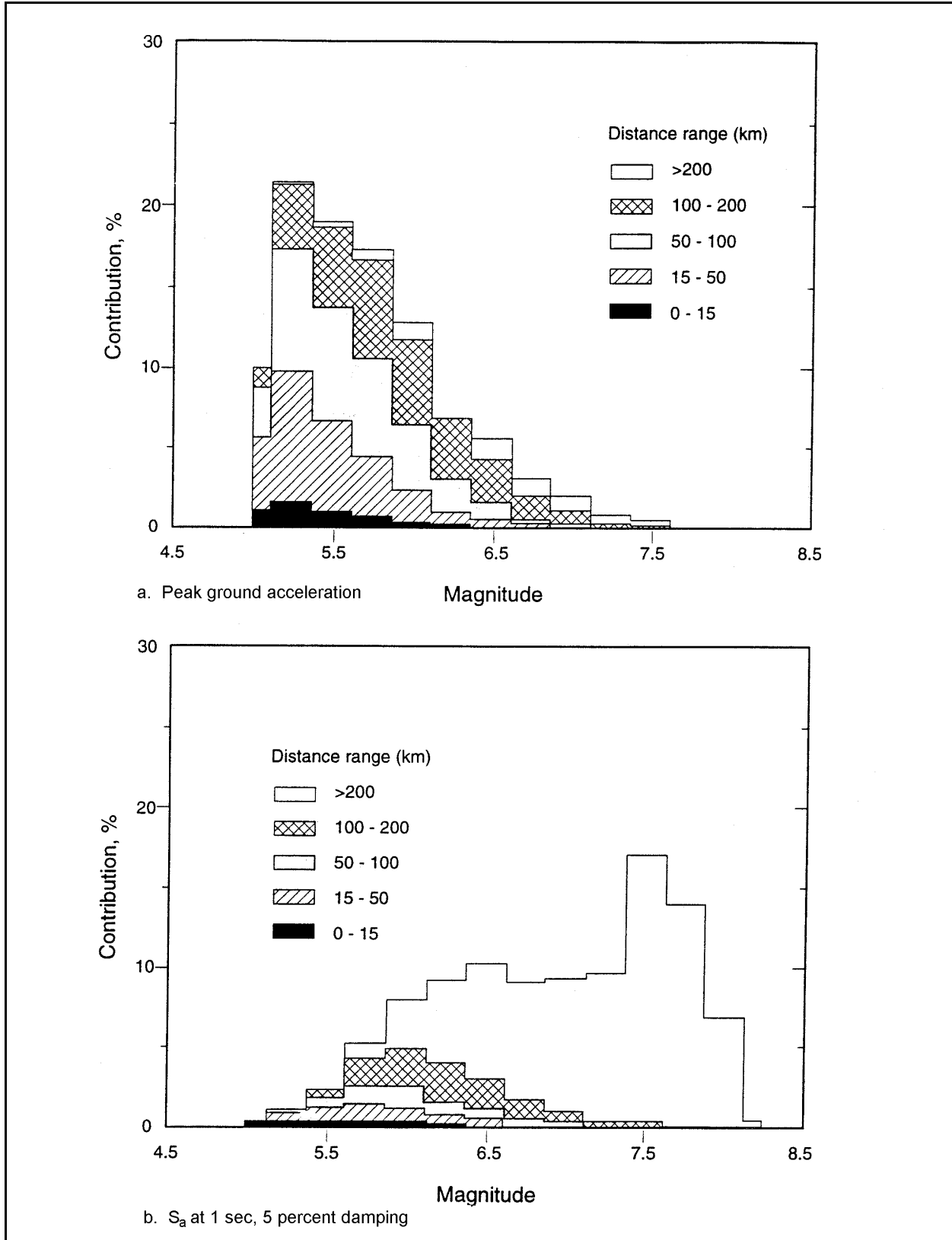


Figure G5-5. Magnitude and distance contributions to hazard for peak ground acceleration and response spectral acceleration at 1.0 sec for 1000-year return period

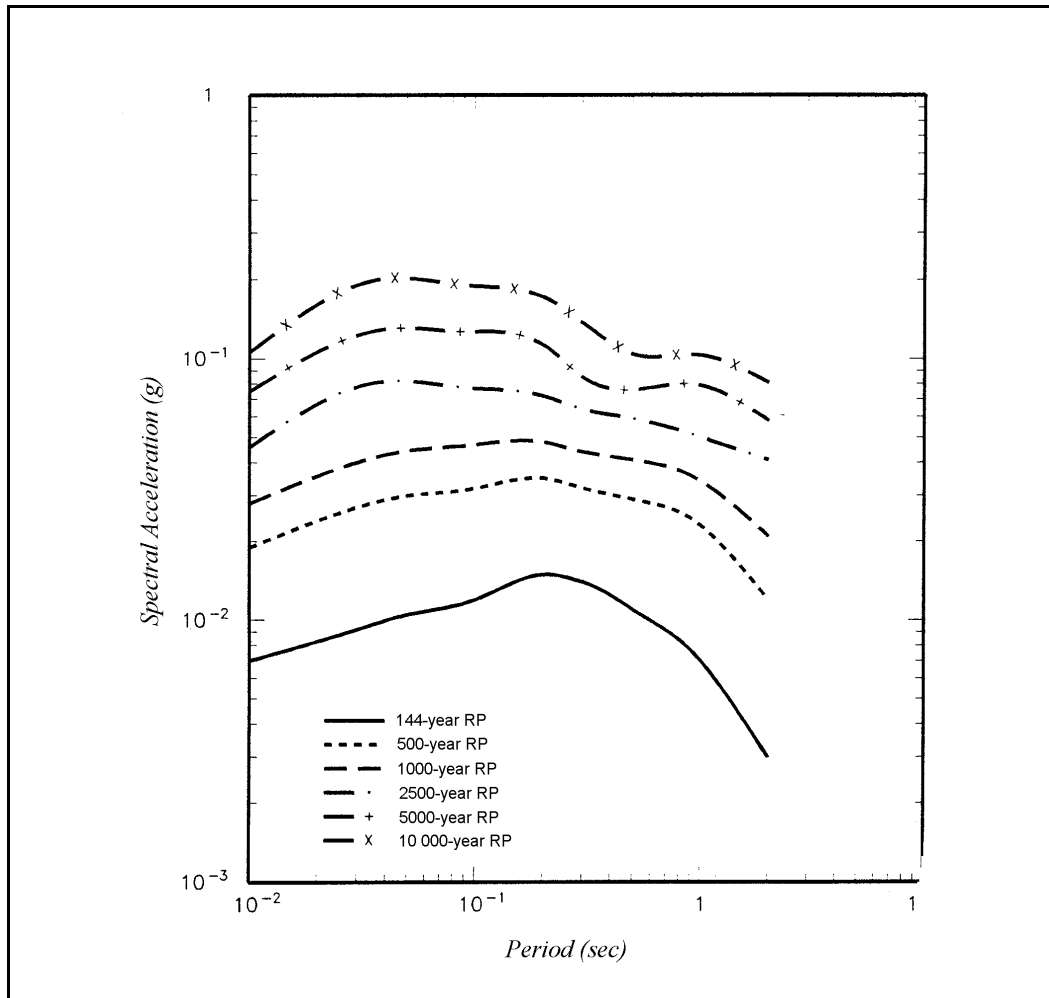


Figure G5-6. Equal-hazard response spectra, mean curves, 5 percent damping

reflects the influence of source zone ICR at long periods in the equal hazard spectrum, whereas the MCE is for the local source zone IRM.

b. The probabilistic seismic ground motion hazard at this site is quite low, reflecting the low historic seismicity in the site region. At the same time, there is considerable uncertainty in the hazard (reflecting scientific uncertainties in modeling seismic sources and ground motion attenuation), which is illustrated by the uncertainty band in hazard estimates (5th to 95th percentile) in Figure G5-3. Because of the low hazard and the uncertainty, the project team decided to adopt the 95th percentile, rather than the mean, estimates of the equal-hazard spectra as a basis for design. The equal-hazard response spectrum with a 144-year return period (50 percent probability of exceedance in 100 years) was selected as the OBE ground motion. The MDE ground motion was selected as the equal hazard response spectrum having a 1000-year return period (approximate 10 percent probability of exceedance in 100 years).

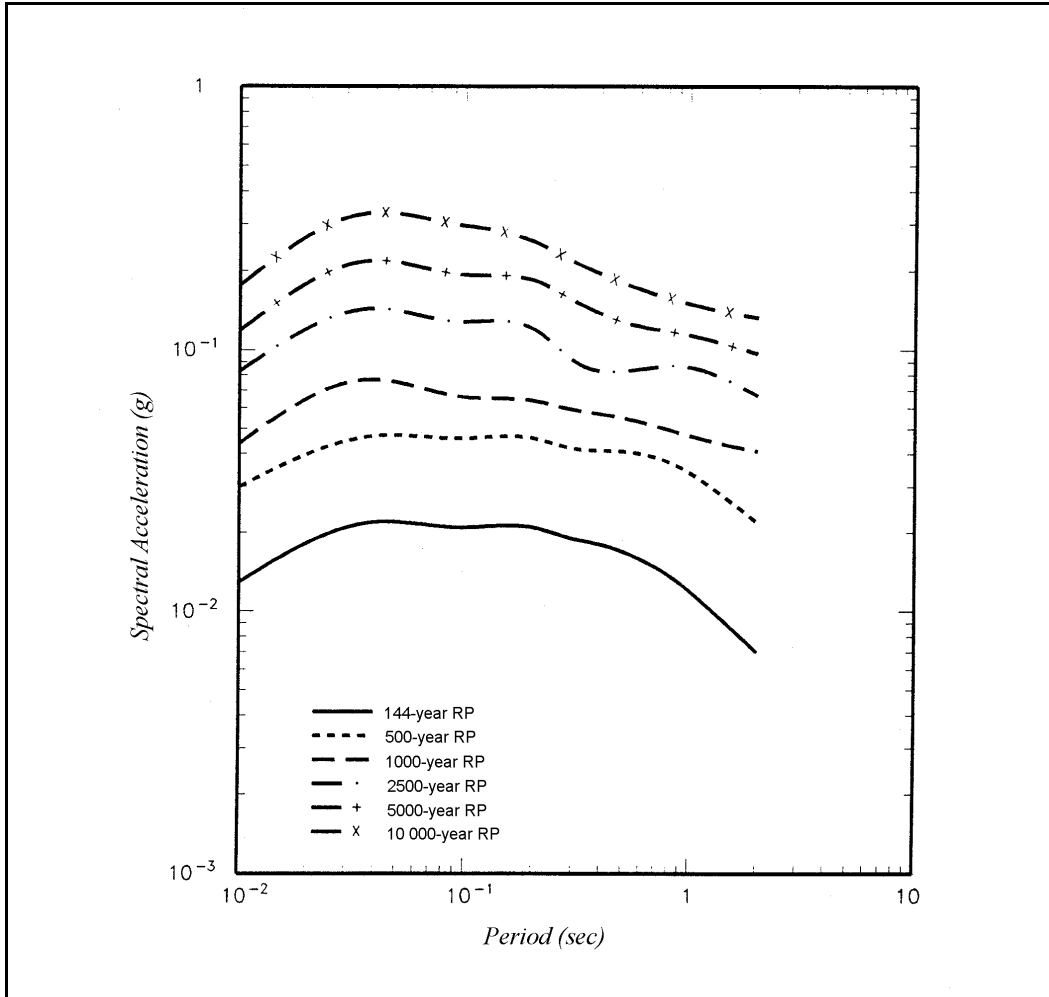


Figure G5-7. Equal-hazard response spectra, 95th percentile curves, 5 percent damping

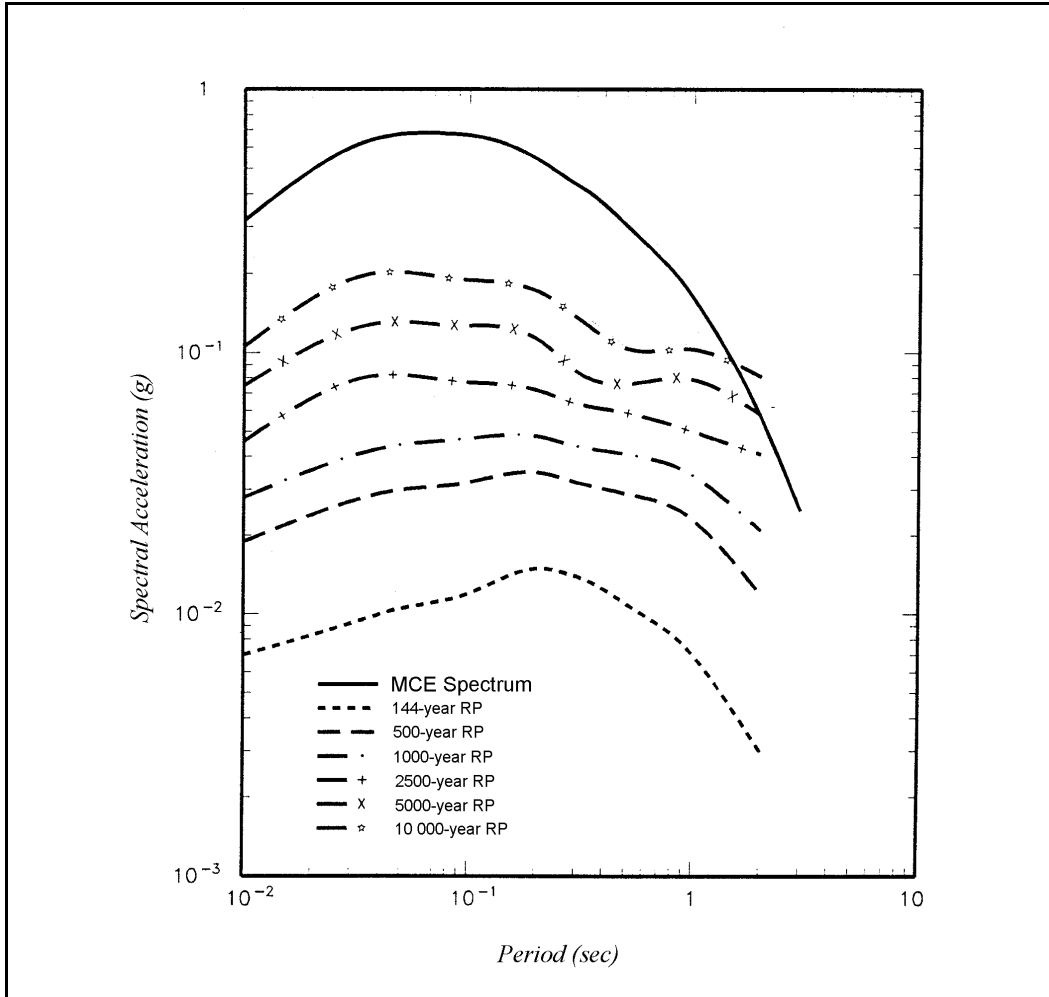


Figure G5-8. Comparison of MCE response spectrum with mean equal hazard response spectra, 5 percent damping

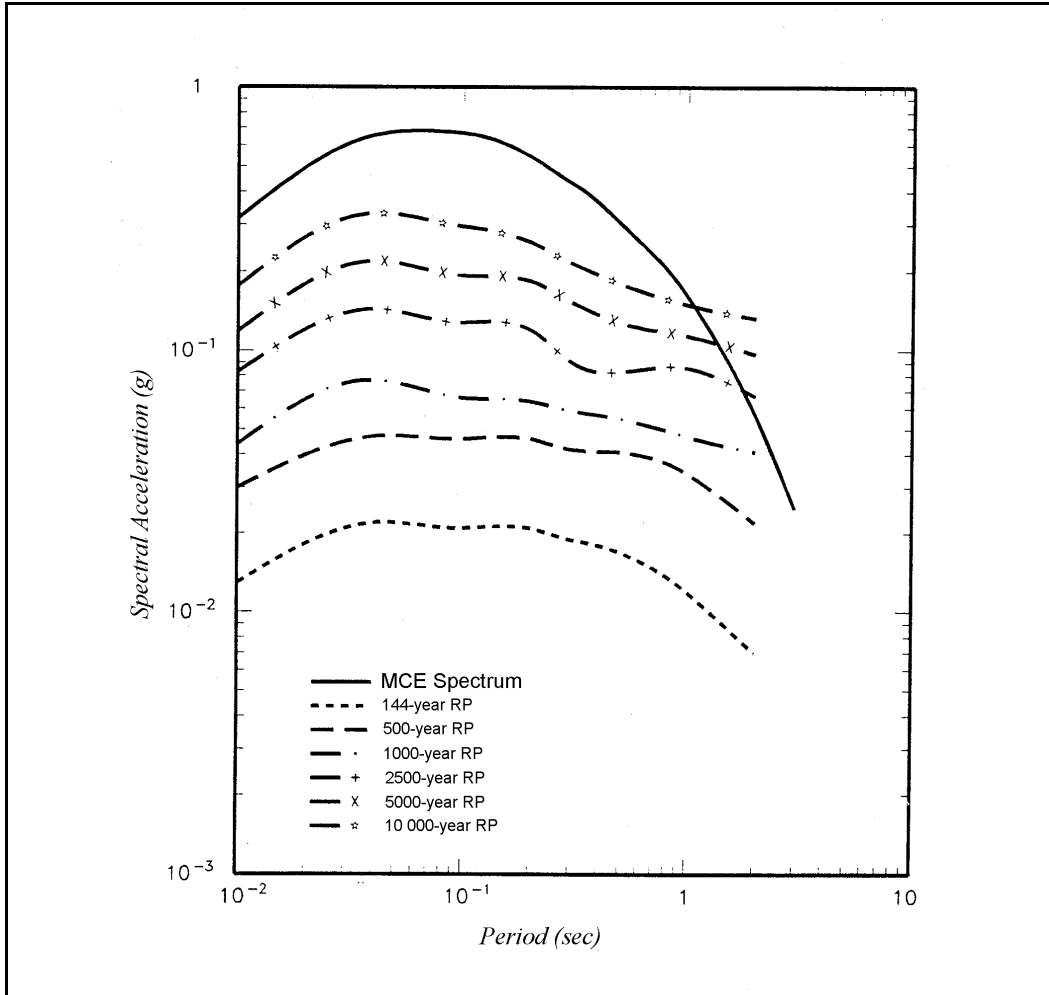


Figure G5-9. Comparison of MCE response spectrum with 95th percentile equal hazard response spectra, 5 percent damping